NASA Tech Briefs

National Aeronautics and
Space Administration

Electronic Components and Circuits

Electronic Systems

Physical Sciences

Materials

Computer Programs

Mechanics

Machinery

Fabrication Technology

Mathematics and Information Sciences

Life Sciences

97-10

October 1997

INTRODUCTION

Tech Briefs are short announcements of new technology derived from the research and development activities of the National Aeronautics and Space Administration. These Briefs emphasize information considered likely to be transferable across industrial, regional, or disciplinary lines and are issued to encourage commercial application.

Availability of NASA Tech Briefs and TSP's

Distribution of NASA Tech Briefs, a monthly periodical publication, is limited to engineers in U.S. Industry and to other domestic technology transfer agents. Requests for individual Tech Briefs or for Technical Support Packages (TSP's) announced herein should be addressed to

NASA Center for AeroSpace Information
Technology Transfer Office
800 Elkridge Landing Rd.
Linthicum Heights, MD 21090-2934
Telephone No. (301) 621-0245

Please reference the three-letter, five-digit control number located at the end of each Tech Brief. Information on NASA's Technology Utilization Program, its documents, and services is also available at the same facility.

Technology Utilization Officers and Patent Counsels are located at NASA field installations to provide technology-transfer access to industrial users. Inquiries can be made by writing to NASA field installations listed below.

Technology Utilization Officers and Patent Counsels

Ames Research Center
Technology Utilization Officer
Mail Code 223-3
Moffett Field, CA 94035

Patent Counsel
Mail Code 200-11
Moffett Field, CA 94035

Goddard Space Flight Center
Technology Utilization Officer
Mail Code 702-1
Greenbelt, MD 20771

Patent Counsel
Mail Code 204
Greenbelt, MD 20771

Lyndon B. Johnson Space Center
Technology Utilization Officer
Mail Code IC-4
Houston, TX 77058

Patent Counsel
Mail Code AL3
Houston, TX 77058

John F. Kennedy Space Center
Technology Utilization Officer
Mail Stop PT-PMO-A
Kennedy Space Center, FL 32899

Patent Counsel
Mail Code PT-PAT
Kennedy Space Center, FL 32899

Langley Research Center
Technology Utilization Officer
Mail Stop 143
Hampton, VA 23665

Patent Counsel
Mail Code 279
Hampton, VA 23665

Lewis Research Center
Technology Utilization Officer
Mail Stop 7-3
21000 Brookpark Road
Cleveland, OH 44135

Patent Counsel
Mail Code LC-LAW
21000 Brookpark Road
Cleveland, OH 44135

Jet Propulsion Laboratory
Technology Utilization Officer
Mail Stop 156-211
4800 Oak Grove Drive
Pasadena, CA 91109

NASA Resident Office-JPL
Technology Utilization Officer
Mail Stop 180-801
4800 Oak Grove Drive
Pasadena, CA 91109

Patent Counsel
Mail Code 180-801
4800 Oak Grove Drive
Pasadena, CA 91109

George C. Marshall Space Flight Center
Technology Utilization Officer
Code AT01
Marshall Space Flight Center, AL 35812

Patent Counsel
Mail Code CC01
Marshall Space Flight Center, AL 35812

John C. Stennis Space Center
Technology Utilization Officer
Code HA-30
Stennis Space Center, MS 39529

NASA Headquarters
Technology Utilization Officer
Code CU
Washington, DC 20546

Assistant General Counsel for Patent Matters
Code GP
Washington, DC 20546

Dryden Flight Research Center
Technology Utilization Officer
M/S D21-31
Bldg. 4832 Whse 7
Lilly Dr.
Edwards, CA 93523

BLANK PAGE

NASA Tech Briefs

National Aeronautics and
Space Administration

October 1997
97-10

BLANK PAGE

Electronic Components and Circuits

Hardware, Techniques, and Processes

BLANK PAGE

GaAs-JFET-Based Multiplexers for Readout of VLWIR Detectors

A prototype circuit has functioned properly at a temperature of 4 K.

NASA's Jet Propulsion Laboratory, Pasadena, California

Integrated-circuit multiplexers based on gallium arsenide junction field-effect transistors (GaAs JFETs) are undergoing development for use in reading out signals from arrays of very-long-wavelength infrared (VLWIR) detectors. To minimize thermally induced electronic noise, electromagnetic interference, and microphonics in future infrared-sensing instruments, it will be necessary to eliminate long connecting wires between infrared detectors located on cold heads and readout circuits located in warmer compartments; to do this, one must place the readout circuits in immediate contact with the infrared detectors at the detector-operating temperatures, which are typically <10 K. To be suitable for VLWIR-detector applications, readout circuits must not only be capable of operating at low temperatures but must also feature low noise, moderately low input capacitances, very low input bias currents, and low power dissipation.

The selection of GaAs-JFET-based integrated circuits for these purposes was prompted by the following considerations:

- The performances of bipolar-silicon-transistor circuits and silicon-JFET circuits at such low temperatures are severely degraded by charge-carrier freezeout. Silicon metal oxide/semiconductor field-effect transistor (MOSFET) circuits can operate at temperatures of a few K, but at these temperatures, they exhibit excessive noise and other undesired characteristics.
- Discrete GaAs JFETs had previously been found to perform well at 4 K.

N-channel GaAs JFETs and associated circuit elements designed especially for cryogenic operation can be made immune to charge-carrier freezeout. The fabrication of these devices includes the use of highly isotropic $HF:H_2O_2:H_2O$ etchants in an etch-back technique for definition of gates and isolation of mesas. The isotropy of the etch eliminates sharp edges, thereby reducing edge electric fields, with consequent reductions in gate leakage currents.

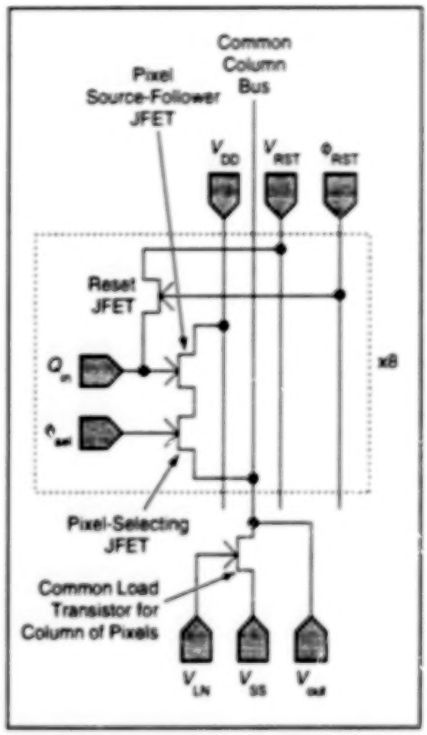

This **Abbreviated Schematic Diagram** illustrates one of eight cells, plus common column circuitry common to all eight cells, of a prototype circuit for reading out an 8 × 1 array of VLWIR detectors.

A prototype GaAs-JFET-based integrated-circuit multiplexer for readout of an 8 × 1 linear array of VLWIR detectors was designed and fabricated. Each cell of this circuit (see figure) corresponds to one pixel and its VLWIR detector. In use, the pixel marked "Q_{in}" would be connected to the VLWIR detector. As the detector integrated photogenerated electric charge, the voltage on the detector would change, and this voltage (the input voltage) would be applied to the gate of the source-follower JFET. The common load transistor at the bottom of the column would be biased at gate potential V_{LN} to form a current source. When clock potential ϕ_{sel} went high, the pixel-selecting transistor in the affected pixel would turn on, connecting the pixel source-follower JFET to the current source via the common column bus; the resultant voltage on the bus would equal the input voltage plus a fixed offset voltage. The pixel would then be reset by use of fixed reset potential V_{RST} under control by clock potential ϕ_{RST}. The foregoing process would be repeated, clocking through each of the eight pixels in turn, to sequentially read out all eight detectors.

In a preliminary test at 4 K without any detectors attached, the prototype circuit functioned properly and satisfied the requirements for low noise, low input bias current (as a result of low gate leakage), and low power dissipation. The leakage current was found to be <1 fA. When the circuit was biased at a common load current of 10 μA, the low-frequency noise was dominated by a component proportional to the reciprocal of frequency (1/*f* noise) and was of the order of 1 $\mu V/Hz^{1/2}$ at a frequency of 1 Hz.

This work was done by Thomas Cunningham and Mike Fitzsimmons of Caltech for **NASA's Jet Propulsion Laboratory**. *Further information is contained in a TSP [see page 1].*

NPO-20096

Printed-Circuit Board for Driving Multiple Actuators

Short-circuiting of one actuator does not cause the others to lose power.

NASA's Jet Propulsion Laboratory, Pasadena, California

A special-purpose printed-circuit board (PCB) holds power-conversion, digital control, and power driver circuits for driving as many as 20 actuators. The actuators can be electromechanical devices (e.g., relay switches or solenoid valves) that present inductive loads to their driver circuits.

Included on the PCB is a switching dc-to-dc power converter rated at a power level of 75 W. The power converter takes its input power from an unregulated source at a potential up to 36 V. The power converter generates output power for the actuators, regulated at 25 V. The regulated output voltage can be changed to any desired value within the capability of the converter by changing a single resistor on the PCB. The power converter includes a circuit for protection against undervoltage in the output load.

The digital control circuitry accepts digital control inputs for the actuators. Power is applied to the actuators through high-power, fast-switching actuator-driver circuits. There are 20 such driver circuits — one for each actuator. The driver circuitry includes twelve pairs of diodes

that help to suppress inductive transients in the actuators.

The power converter can withstand a momentary short circuit in its output load. A short circuit in any actuator is detected by the undervoltage-protection circuit in the power converter. Upon sensing a low voltage indicative of a short circuit, the undervoltage-protection circuit generates an input "reset" logic signal that countermands the input digital signal for the short-circuited actuator; this causes the driver circuit for the short-circuited actuator to be disabled, while the driver circuits for the remaining actuators continue to operate normally in response to their respective digital inputs.

This work was done by Thieu T. Ton and Edward H. Kopf of Caltech for **NASA's Jet Propulsion Laboratory**. *Further information is contained in a TSP [see page 1].*

In accordance with Public Law 96-517, the contractor has elected to retain title to this invention. Inquiries concerning rights for its commercial use should be addressed to

Technology Reporting Office
JPL
Mail Stop 122-116
4800 Oak Grove Drive
Pasadena, CA 91109
(818) 354-2240

Refer to NPO-20008, volume and number of this NASA Tech Briefs *issue, and the page number.*

Electronic Systems

Hardware, Techniques, and Processes

Books and Reports

BLANK PAGE

Electronic System for Teleoperation of Robotic Vehicles

Control is implemented with less complexity and at less cost than in older systems.

NASA's Jet Propulsion Laboratory, Pasadena, California

The Surface Navigation and Simulation System (SNSS) is an electronic control system for teleoperation of robots. The SNSS has been undergoing development, following an approach that involves the use of off-the-shelf electronic components and innovative control software to reduce the cost and complexity of teleoperation, both nearby and at long distance. Key components of a prototype of the SNSS are multiple linked personal-computer-based control stations and software for control of, and acquisition of data from, the robots. The prototype SNSS also includes the robots themselves; the prototype robots are small, six-wheeled vehicles equipped with onboard power and data-management subsystems.

Older systems for telerobotic control generally include "high-end" data-processing modules at both rovers and control stations. These systems must be operated with customized, highly complex software. They also require wide-band communications between the control stations and rovers. The foregoing attributes have resulted in high cost and complexity, which have inhibited more-widespread application. In particular, the use of "high-end" computer workstations and sophisticated onboard robot data-processing modules results in high costs of acquisition, even for rough prototype systems. Typically, wide-band communications for control and telemetry rely on expensive satellite links and/or special terrestrial communication lines. Moreover, it is necessary to train operators extensively in the use of the associated software to enable competent operation and interpretation of data received from the robots.

The SNSS operates as an integrated unit. It includes operator-interface hardware and software that enable operators to "drive" the rovers while viewing images transmitted in real time from video cameras mounted on the rovers. The operators also have access to easy-to-read displays of data acquired from other sensors aboard the rovers. A combination of simple radio and telephone links provides communications between the rovers and their respective operators.

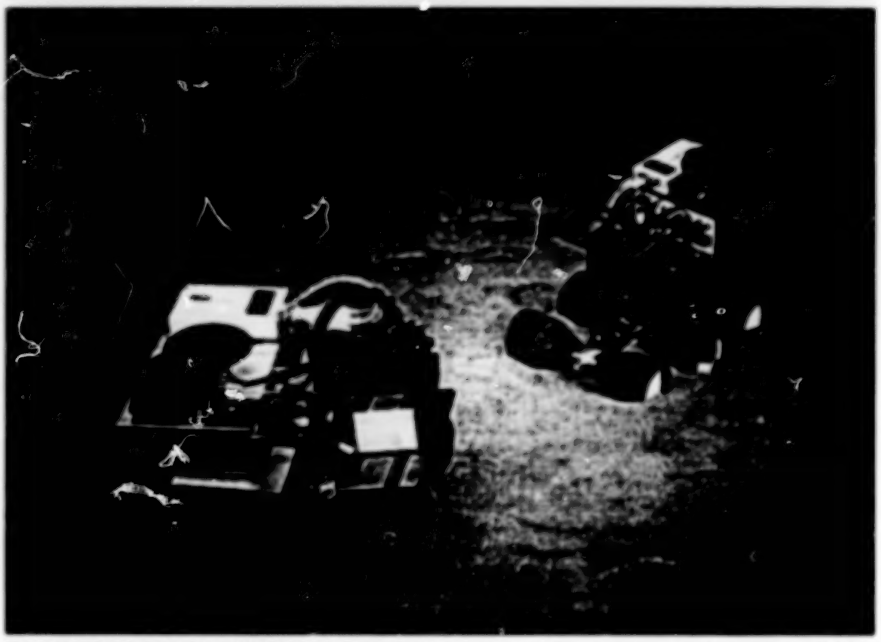

Six-Wheeled Robotic Vehicles carrying video cameras, other sensors, and power and data-management subsystems are operated simultaneously in a demonstration of the SNSS.

The prototype SNSS includes two instrumented six-wheeled rovers (see figure). The capability of the SNSS has been demonstrated in simultaneous operation of both rovers — one in a local operating mode and the other in a remote environment. This demonstration was conducted for intervals as long as two hours without interruption. Images received at the control station from the video cameras were found to be of sufficient quality to support rover navigation. Data received at the control station from other sensor cameras were found to be accurate.

At the time of reporting information for this article, development was continuing and several improvements were expected to be made sequentially during the next two years. One of these improvements would be the incorporation of an "executive" control subsystem that would provide autonomous monitoring and control of robotic devices.

This work was done by David Mazaika, Gregory Nemitz, Michael Simon, John Risque, David Mitchell, and Cris Fitch of International Space Enterprises, Inc., for **NASA's Jet Propulsion Laboratory**. *For further information, contact Greg Nemitz, International Space Enterprises, 4909 Murphy Canyon Road, Suite 220, San Diego, CA 92123, Telephone No.: (619) 637-5773.*

NPO-30020

Digital Video System Images Damaged Gears During Operation

The progression of damage can be documented more quickly, thoroughly, and easily.

Lewis Research Center, Cleveland, Ohio

A high-speed digital video imaging system captures still images of individual teeth on gears meshing at high speed on a gear-test rig. Each gear-tooth image documents the progression of the wear, pitting, spalling, and fractures that lead to overall gear failure. Heretofore, images documenting gear failure were acquired only during post-test analysis and thus did not provide real-time study of the degradation that leads to failure. The high-speed digital imaging system is integrated with another system that measures vibrations and processes the measurements to detect indications of damage. Analysis of the gear-tooth images coupled with vibrational data acquired at the same time should make it possible to better classify

TYPICAL IMAGE SHOWING DAMAGED GEAR TEETH

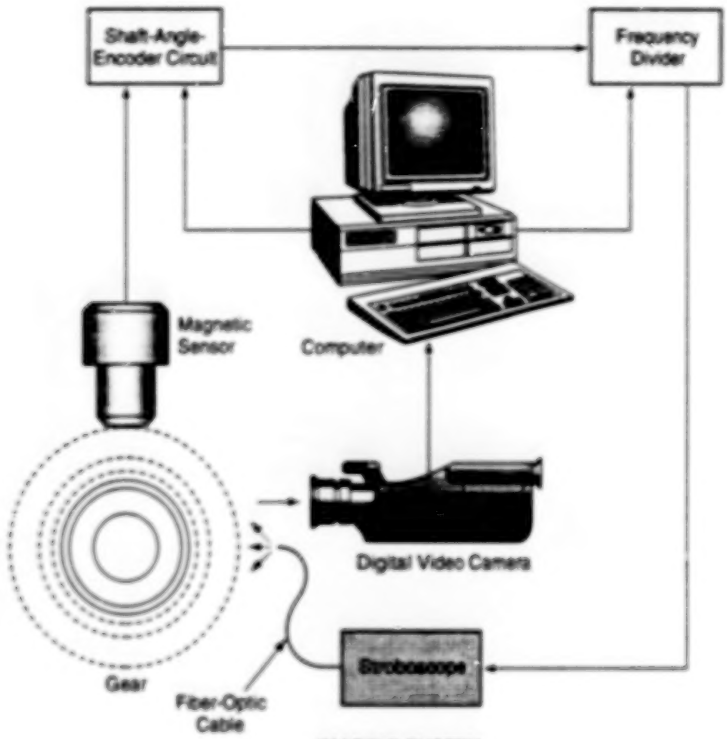

IMAGING SYSTEM

The High-Speed Digital Video Imaging System captures still images of gears meshing at high speed. The system will aid studies of gear damage and the development of techniques for vibration monitoring to detect incipient damage. In comparison with film-based photographic imaging systems, this system provides for easier viewing and storage of data; it gives immediate visual feedback and there is no need for costly and time-consuming film processing.

vibrational signatures according types and degrees of damage and to improve understanding of the events that lead to failure.

The imaging system (see figure) includes a digital video camera aimed at passing gear teeth. The system is located in a darkened room. Illumination is provided by a fiber-optic-coupled stroboscope with a 5-μs pulse duration, which is brief enough to capture images without noticeable blur at typical gear speeds. A magnetic probe senses the rotation of the gear and generates a once-per-revolution pulse. A shaft-angle-encoder circuit divides the once-per-revolution pulses into pulses at smaller intervals corresponding to the passage of individual gear teeth in front of the camera. A frequency divider processes the gear-tooth-passage pulses into stroboscope-trigger pulses at intervals long enough to ensure that only one flash occurs during the camera integration time of 1/30 second.

The imaging system operates automatically, under control by a computer that runs special-purpose software. Each time the computer in the vibration-measuring system determines that vibrations have exceeded a threshold level, it signals the computer in the imaging system to begin a sequence of operations to acquire images of gear teeth. For each tooth, the camera is turned on for its integration time; during that time, at the instant when the designated tooth passes in front of the camera, the stroboscope is flashed to produce a single-exposure still image of the tooth. The images are stored in the frame-grabber memory. This process is repeated until images for *all* the gear teeth have been acquired, then they are transferred to a hard disk in the computer. The computer then resets, and the system awaits the next signal from the vibration-measuring system.

This imaging system is potentially adaptable to numerous other applications in which there are requirements for automatic acquisition of images of moving objects or of events that manifest themselves only during rapid motion. Examples of potential uses include the following:

- Inspection during bottling processes to verify fill levels and capping;
- Detection of improperly mounted or missing electronic components or detection of missing automotive components during manufacturing operations;
- Detection of stamps and preliminary sorting in postal operations;
- In banking, tracking bundles of checks and detecting checks out of order, and/or identifying stacks of money short in their amounts;
- In printing, imaging the product to detect defects without shutting down for false alarms; and
- Inspecting power-generation and manufacturing machinery during operation to identify troubles that cannot be seen when the equipment is shut down.

This work was done by James J. Sims and Howard Broughton of Cortez III Service Corp. for **Lewis Research Center**. *Further information is contained in a TSP [see page 1].*

Inquiries concerning rights for the commercial use of this invention should be addressed to NASA Lewis Research Center, Commercial Technology Office, Attn: Tech Brief Patent Status, Mail Stop 7–3, 21000 Brookpark Road, Cleveland, Ohio 44135. Refer to LEW-16345.

Swept-Frequency Fiber-Optic Readout From Multiple Sensors

Readouts from individual sensors are distinguished by frequency rather than by pulse-travel time.

NASA's Jet Propulsion Laboratory, Pasadena, California

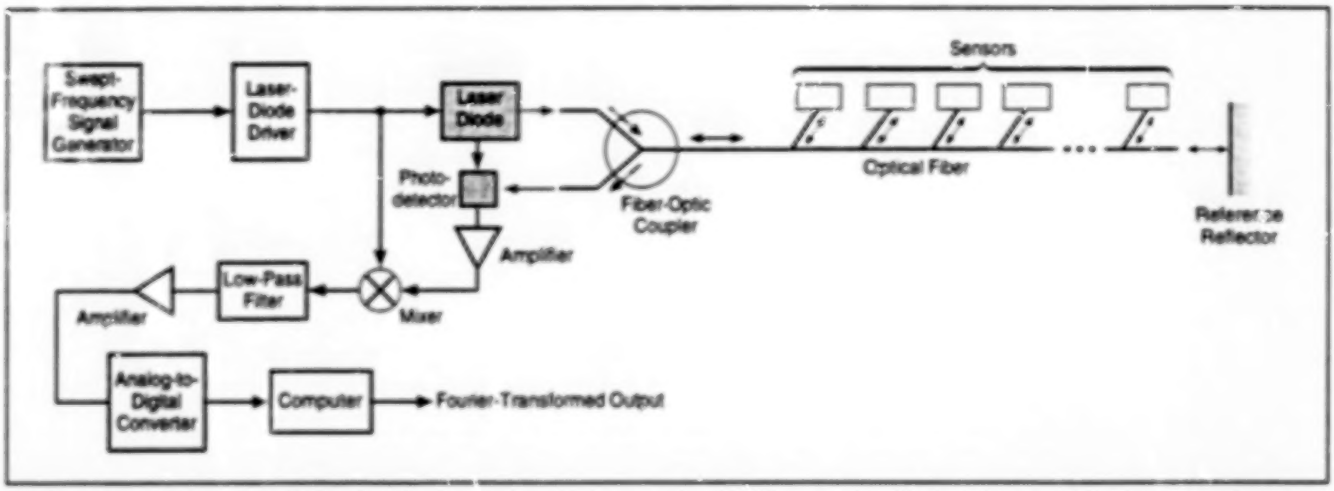

The Propagation Delays of the Reflections from the various sensors along the optical fiber result in differences between the phase of swept-frequency modulating signal and the phases of the modulations in the reflections. These phase differences are accompanied by frequency differences that can be exploited to identify and measure reflections from individual sensors.

A technique of frequency-domain reflectometry has been devised for obtaining readouts from multiple sensor transducers that (a) reflect light to degrees indicative of quantities that one seeks to measure and (b) are connected to, and located at various positions along, an optical fiber. In this technique, a beam of light that interrogates the sensors is amplitude-modulated at a radio frequency that is swept linearly. The beam is launched into the fiber from an input end, travels to the various transducers, and is reflected back to the input end (see figure). As explained in more detail below, the modulation in the light reflected back to the input end can be decomposed into frequency components — a separate frequency component associated with each transducer — and the amplitude of each component can be taken as an indication of the quantity sensed by the corresponding transducer.

This technique offers advantages over time-domain reflectometry as applied to such an array of sensors. In time-domain reflectometry, one would interrogate the transducers by use of a pulsed beam of light in order to distinguish the returns from the individual transducers in terms of their individual round-trip pulse-travel times. The pulses would have to be short enough and the sensors would have to be located far enough apart, consistent with the pulse duration, so that pulses returned from different sensors did not overlap. Thus, time-domain reflectometry would entail restrictions on both the placement of transducers and on pulse durations. Shorter pulses contain less energy than do longer pulses and thus necessitate longer signal-averaging times to obtain adequate measurement sensitivity at low signal levels. Long averaging times are not acceptable in many systems in which real-time or near-real-time responses are required; for example, in process-control applications. In the present swept-frequency technique, the minimum acceptable distance between sensors is much less than in time-domain reflectometry. Moreover, the averaging time needed to achieve a given level of sensitivity is less than in time-domain reflectometry.

Suppose that the interrogating beam of light is amplitude-modulated by a sinusoid of swept angular frequency $\omega(t) = \omega_0 + \alpha t$, where t is time as measured from the beginning of the frequency sweep, ω_0 is the initial angular frequency, and α is the frequency-sweep rate. Suppose that the light reflected back to the input end of the optical fiber is fed to a photodetector, the output of the photodetector is mixed with a replica of the modulating sinusoid, and the output of the mixer is low-pass-filtered so as to retain only the difference-frequency mixer output. It can be shown that the resulting output signal is given by

$$S_{out}(t) = \sum_{n=1}^{N} B_n \cos\left[\tau_n(\omega_0 + \alpha t)\right]$$

where B_n is proportional to the amplitude of the reflection from the nth sensor and τ_n is the round-trip propagation time for the optical signal traveling from the input end to the nth sensor and back to the input end.

Thus, the output-signal component representing the reflection from the nth sensor is a sinusoid of amplitude B_n and frequency $\alpha\tau_n$. By taking the Fourier transform of $S_{out}(t)$, one can obtain its frequency spectrum and thereby extract the amplitude of the reflection from each sensor. Incidentally, the measured frequency of each component can be used to refine the estimate of the round-trip propagation delay for each sensor.

This work was done by George F. Lutes and Xiaotian S. Yao of Caltech for **NASA's Jet Propulsion Laboratory**. *Further information is contained in a TSP [see page 1].*

In accordance with Public Law 96-517, the contractor has elected to retain title to this invention. Inquiries concerning rights for its commercial use should be addressed to

Larry Gilbert, Director
Technology Transfer
California Institute of Technology
Mail Code 315 - 6
Pasadena, CA 91125
(818) 395-3288

Refer to NPO-19725, volume and number of this NASA Tech Briefs *issue, and the page number.*

Image-Analysis System Tracks Objects

A tedious manual image-analysis process has been automated.

Lewis Research Center, Cleveland, Ohio

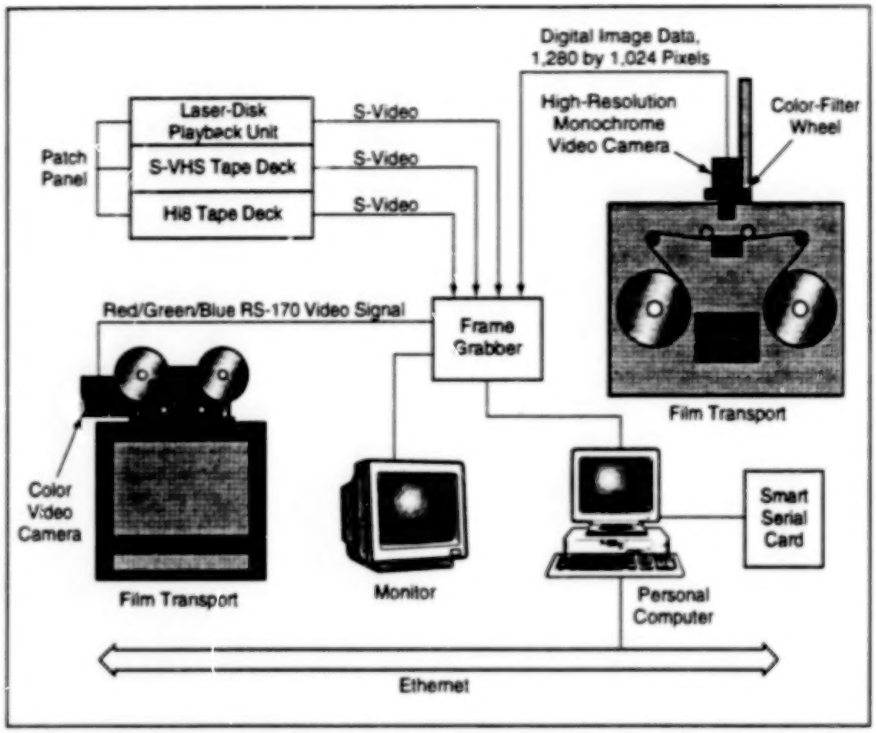

The Computer Analyzes Image Data from any of several playback units, which it controls. Special-purpose software tracks moving objects and/or features in video or photographic image frames.

A personal-computer-based image-processing system digitizes video or film images and then performs various forms of motion analysis by tracking objects and/or features. The system was designed specifically for analysis of the types of images found in microgravity combustion and fluid experiments; the object and/or features to be tracked can include flame fronts, particles, droplets, and fluid interfaces. Since this is not a real-time tracking system but a post-analysis tracking system, the image sequences to be analyzed have been previously recorded on a standard photographic movie film or video tape. Digital image input in the form of image files can be also accepted. The system automates what has previously been a tedious, time-consuming image-analysis process in which a technician or a scientist visually examined and manually took measurements directly from a displayed image, repeating this process until all the image frames were analyzed.

The system (see figure) consists of individual hardware components working under computer control to achieve a high degree of automation. The most important hardware components include 16-mm and 35-mm film transports, a high-resolution digital camera mounted on a *x-y-z* micropositioning stage, an S-VHS tapedeck, a Hi8 tapedeck, a video laserdisk, and a framegrabber. All of the image-input devices are remotely controlled by a computer. Software, called Tracker was developed to integrate the overall operation of the system, including device frame incrementation, grabbing of image frames, image processing of the object's neighborhood, locating the position of the object being tracked, and storing the coordinates to a file. This process is performed repeatedly and automatically until the last frame is reached. Several different tracking methods are supported, including threshold reduction, template matching, and a spline-based active contour model method. The types of data obtained from Tracker are positions, velocities, area measurements, centroids, object outlines and shapes, time sequences of line profiles, 3-d areas, intensity and color characteristics, and size measurements, all as a function of time. The data are presented in a format ready for graphing or further analysis via other packages.

Optionally, the system can be operated in a semiautomatic mode, in which the user manually locates an object by using a mouse to move a crosshair on the display. All other steps are performed as in the automatic mode.

This work was done by Robert B. Klimek and Ted W. Wright of **Lewis Research Center** *and Robert S. Sielken of Trinity University. Further information is contained in a TSP [see page 1].*

Inquiries concerning rights for the commercial use of this invention should be addressed to NASA Lewis Research Center, Commercial Technology Office, Attn: Tech Brief Patent Status, Mail Stop 7–3, 21000 Brookpark Road, Cleveland, Ohio 44135. Refer to LEW-16420.

Telerobot Control for Microsurgery

Hand movements are repeated on a smaller scale, without tremor.

NASA's Jet Propulsion Laboratory, Pasadena, California

A telerobotic system for microsurgery has been designed to reproduce the motions of a surgeon's hand on a more precise scale and with smoother motion than previously possible. This system can be used for surgeries on the eye, brain, ear, and face and in the repair of fine blood vessels and nerves. The surgeon holds a handle attached to a master robot arm and moves it to specify the motions of a surgical instrument on the slave robot arm. The surgeon's hand motions are scaled down and filtered to enable precise surgical-instrument positioning without tremor (see figure).

The master arm measures the position of the model-tool position in 6 degrees of freedom (DOF) and reflects forces with 3 DOF. It measures input position in increments of 0.001 in. (25.4 μm) in translation and 0.07° in rotation.

The slave arm has 6 DOF and responds with movements in increments of 20 μm. The system provides several modes of control, and can be switched easily between modes.

The system includes the following subsystems:

- The mechanical subsystem, including motors, encoders, gear and cable drive mechanisms, and robot links and joints;
- The electrical subsystem, including controller terminal blocks, cables, safety electronic circuits, and amplifiers;
- The servocontrol subsystem, including a servocontrol circuit board, software, communication electronics, and shared memory software; and
- A software subsystem that resides partly in a UNIX host computer and partly in the servocontrol subsystem and that implements algorithms for the forward and inverse kinematics of the slave robot, algorithms for demonstration modes of control, and a graphical user interface.

This work was done by Timothy Ohm, Hari Das, Guillermo Rodriguez, Curtis Boswell, Paul Schenker, and Ed Barlow of Caltech; Eric Paljug of McKinsey & Co., Inc.; and Steve Charles of MDS, Inc., for **NASA's Jet Propulsion Laboratory**. *Further information is contained in a TSP [see page 1].*

In accordance with Public Law 96-517, the contractor has elected to retain title to this invention. Inquiries concerning rights for its commercial use should be addressed to

Technology Reporting Office
JPL
Mail Stop 122-116
4800 Oak Grove Drive
Pasadena, CA 91109
(818) 354-2240

Refer to NPO-19823, volume and number of this NASA Tech Briefs *issue, and the page number.*

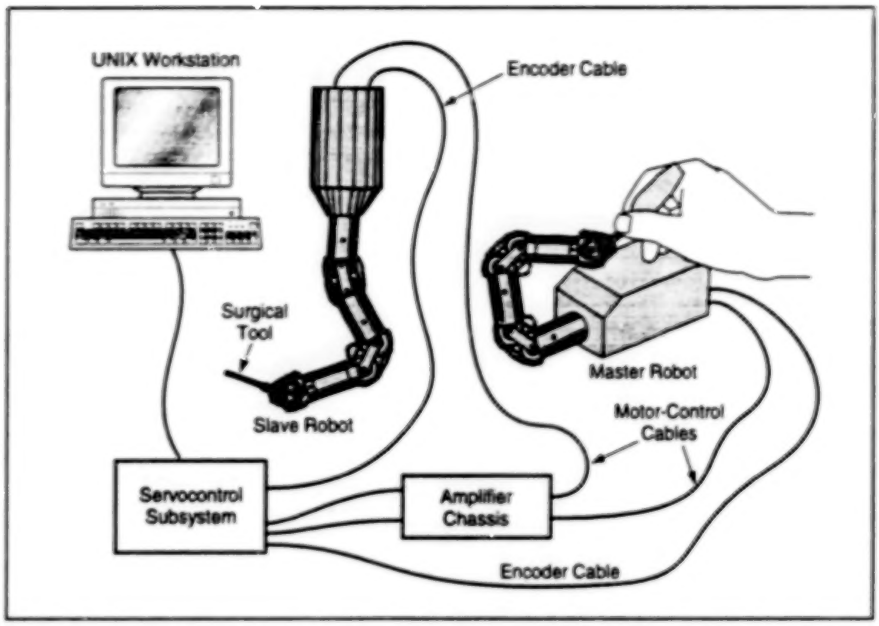

Small Movements of a Surgeon's Hand are scaled down to even smaller movements of a surgical tool at the tip of the slave robot arm. The system removes hand tremor from the control signal, so that only the desired movement is reproduced in miniature by the slave robot arm.

Neural-Network Modules for High-Speed Image Processing

These modules would offer unprecedented computational power in small, low-power packages.

NASA's Jet Propulsion Laboratory, Pasadena, California

JPL has recently designed, fabricated, and demonstrated custom ICs for high-speed image processing. Derived from highly parallel computing architectures based on neural network models, these circuits are implemented with JPL-pioneered extremely low-power neuron and synapse circuit elements. Furthermore, their ultra-low power and high-speed characteristics are making it possible for the first time to integrate multiple chips in 3-dimensional (3-D) modules (sugarcube-sized chipstacks).

Denoted "neuroprocessing modules" (NPMs), these 3-D packaged devices would be capable of processing images at rates of the order of 10^{12} operations per second. The original NPMs are intended for military use for recognition of targets by comparison of features in infrared images with previously recorded images of known targets. Potential civilian applications for NPMs include artifi-

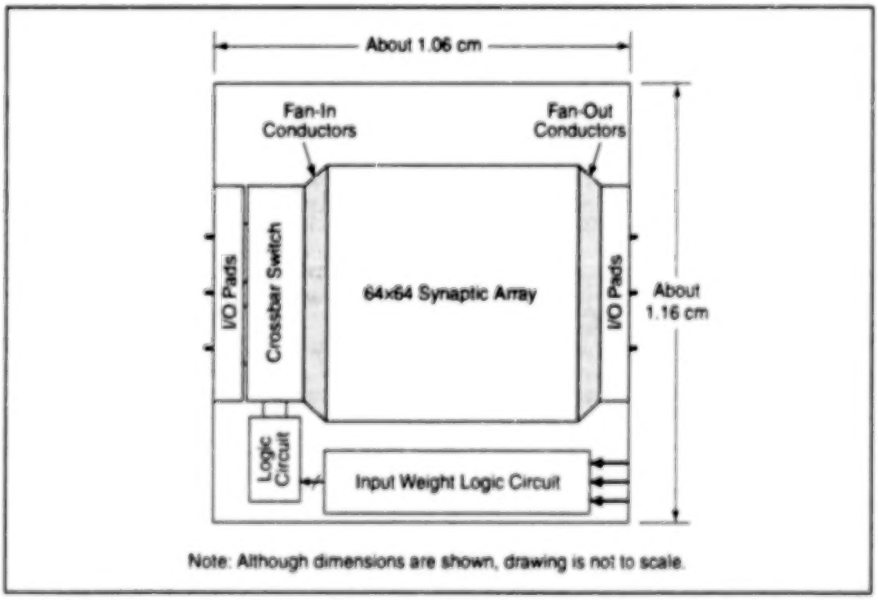

A Typical NPM would be no larger than a sugar cube, yet it would contain integrated circuitry capable of processing the output of a 64 × 64 array of infrared photodetectors at a rate of 1,000 frames per second.

cial vision, speech recognition, and autonomous control for robots.

The NPMs offer unprecedented computing ability in small packages. They include novel high-speed analog circuits that can operate at temperatures from 77 to 350 K and consume little power. This combination of high computing speed, low power, and small size facilitates integration with other compact, low-power, high-speed circuitry with which NPMs would be required to interact.

A typical NPM would consist of 64 identical neuroprocessing chips and would process the analog outputs (each containing 8 to 12 bits of information) from a 64 × 64 array of infrared photodetectors. Thus, for example, an NPM chip would include a 64 × 64 synaptic array plus a multistage crossbar switch, digital logic circuits, and input/output (I/O) pads (see figure). During each frame cycle, the image information embodied in the photodetector outputs would be compared with stored information on at least 64 known targets. The time needed for signals from the photodetectors to be processed by a 3-D neural network in an NPM would be about 200 ns: this would be short enough to enable processing of 1,000 image frames per second.

This work was done by Tuan Duong, Taher Daud, and Anilkumar Thakoor of Caltech, and Chris Sauders of Irvine Sensors Corp. for **NASA's Jet Propulsion Laboratory**. *Further information is contained in a TSP [see page 1].*
NPO-19881

Hydrogen-Fire-Detector Calibration Unit

A tabletop unit contains an ultraviolet source and calibration circuits.

John F. Kennedy Space Center, Florida

A microprocessor-controlled, tabletop apparatus has been developed for use in testing ultraviolet-sensitive alarm circuits that detect hydrogen fires at various distances. The apparatus includes a krypton discharge lamp that emits ultraviolet light of about the same intensity and in the same wavelength range (180 to 240 nm) as observed in hydrogen fires that were previously used to test the hydrogen-fire detectors. By eliminating the need to test with hydrogen fires, the apparatus obviously contributes to overall safety.

The apparatus includes a bracket that holds the hydrogen-fire detector to be tested in the required geometric relationship with respect to the krypton discharge lamp. The main functional characteristic of the apparatus is that it provides ultraviolet light in the required spectral range at a stable, repeatable, and uniform intensity across the face of an ultraviolet-sensitive detector tube in the fire detector. The necessary uniformity of intensity is provided by reflective and diffusive optical elements associated with the lamp.

Repeatability and stability of intensity are provided via microprocessor control of the positions of adjustable optical elements and by electronic feedback control of the power supplied to the lamp. The intensity feedback is obtained from an ultraviolet-sensitive photodetector near the lamp. A spinning chopper wheel modulates the light seen by the detector to enhance the performance of the feedback system. In response to the feedback signal, the microprocessor adjusts the power supplied to the lamp to maintain the intensity at a value selected by the technician.

Electronic control of the power supplied to the lamp can vary the intensity by a factor no larger than about 2, but a factor of about 100 is required for the complete range of tests to simulate the signals from a standard hydrogen fire at distances from 10 to 64 feet (3 to 19 m). To provide the necessary increments of intensity over this large dynamic range, the apparatus is also equipped with a microprocessor-controlled iris and a microprocessor-controlled filter wheel that contains neutral-density filters of different densities.

After startup, a liquid-crystal display unit on the apparatus presents three options to the technician: (1) functionality check, (2) specification check, or (3) alarm-time-versus-distance measurement. The functionality check involves determining whether a power relay within the unit is operational, turning on the lamp, and determining whether the ultraviolet light supplied by an internal lamp can trigger the alarm function in the hydrogen-fire detector under test.

The specification check includes a calibration needed to determine whether a hydrogen-fire detector satisfies its performance requirements. During a specification check, the apparatus projects ultraviolet light at known intensities into the fire detector to determine whether the minimum- and maximum-sensitivity requirements are satisfied.

The alarm-time-versus-distance measurement is carried out by projecting ultraviolet light into the fire detector at an intensity representative of that of a standard hydrogen fire located well within the alarm distance of the detector. The time taken to alarm is then measured, and the detector is allowed to come out of an alarm state. The intensity of ultraviolet light is then dropped to correspond to a slightly larger distance, and the alarm time measured again. This process is repeated until the alarm time is greater than 30 seconds. This measurement provides a characterization of the performance of the fire detector versus the distance to a standard hydrogen fire.

This work was done by Gregory A. Hall and William E. Larson of **Kennedy Space Center** *and Robert C. Youngquist, John S. Moerk, William D. Haskell, Robert B. Cox, Jimmy D. Polk, Stephen J. Stout, and James P. Strobel of I-NET, Inc. Further information is contained in a TSP [see page 1].*

This invention has been patented by NASA (U.S. Patent No. 5,561,290). Inquiries concerning nonexclusive or exclusive license for its commercial development should be addressed to the Patent Counsel, Kennedy Space Center [see page 1]. Refer to KSC-11722.

Reconfigurable Pointing Control for Spaceborne High-Resolution Spectroscopic Instruments

A collection of documents summarizes preliminary efforts to develop improved pointing control for spaceborne scientific instruments. A significant effort was expended to develop a theory to provide a pointing-control-performance criterion, the satisfaction of which would ensure the acquisition of high-quality data by high-resolution spectroscopic instruments. The theory is presented and it is found that the criterion is very stringent and difficult to satisfy by use of standard three-axis spacecraft control equipment now in use. This finding leads to the second major effort, regarding a novel reconfigurable-control concept proposed to satisfy the pointing criterion while using currently available gyroscopic spacecraft hardware. This concept involves switching the control error (which one seeks to null) among detuned Kalman filters. The feasibility of the concept is verified by use of a covariance analysis, and effectiveness is demonstrated by example calculations for the Infrared Spectrograph (IRS) payload aboard the Space Infrared Telescope Facility (SIRTF). Numerical results indicate that by proper choice of filter detuning and handoff timing, the optical flux offset could be held (with 0.95 probability) to within 6 percent of the ideal flux. In contrast, the corresponding flux offset would be 12 percent with conventional three-axis control.

This work was done by David S. Bayard, Tooraj Kia, and Jeff Van Cleve of Caltech for **NASA's Jet Propulsion Laboratory**. *To obtain a copy of the collection, "Reconfigurable Pointing Control for High Resolution Space Spectroscopy," see TSP's [page 1].*
NPO-20182

BLANK PAGE

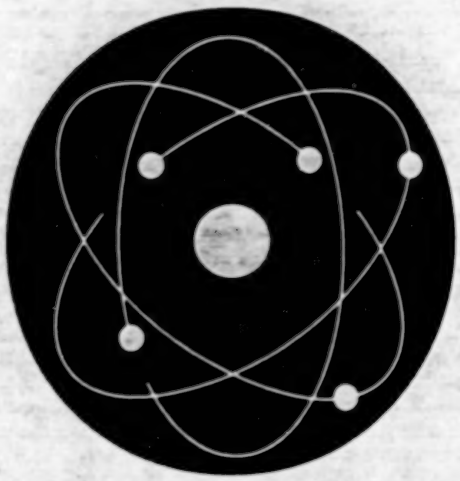

Physical Sciences

Hardware, Techniques, and Processes

Books and Reports

BLANK PAGE

Optical Correlator Has Adjustable Sensitivity to Translation

This instrument can recognize partly obscured, modified, and imperfectly aligned objects.

NASA's Jet Propulsion Laboratory, Pasadena, California

A compact optoelectronic image correlator of the Vander Lugt type is designed for adjustable sensitivity to, and some tolerance of, translation of an image or object to be recognized. Denoted a "translation sensitivity adjustable compact optical correlator" (TSACOC), this instrument can recognize partly obscured, modified, and imperfectly aligned images and objects. In contrast, Vander Lugt correlators of older design are characterized by fixed sensitivities to translation and are unable to recognize such images and objects. The TSACOC offers advantages of speed and storage capacity over older optical correlators. The basic TSACOC design can be adapted to a variety of commercial applications, including recognition of fingerprints, verification of paper money and credit cards, photographic identification, and literature searches.

The TSACOC includes a laser with optics to generate a collimated beam of light, a spatial light modulator, a multichannel replication holographic element, Fourier-transform lenses, a holographic matched spatial filter (MSF) with an electronically controlled array of shutters, and an array of photodetectors in a classification output plane. Adjustability of sensitivity to translation is achieved by use of a converging reference laser beam (see Figure 1).

In operation in the object-recognition mode, the collimated laser beam passes through the spatial light modulator, which enhances the beam and enters the input image to be identified. The beam as spatially modulated by the image then passes through the multichannel replication holographic element, which contains images of all the known objects to be searched. Continuing on its way, the beam then passes through a Fourier-transform lens to the MSF with its electronically controlled shutters, where a matching function is performed. Finally, the beam as thus processed impinges on the classification output plane, forming whichever one of the stored images correlates with the input image.

Figure 2 schematically illustrates a simplified experimental TSACOC for recognizing fingerprints. An MSF containing the information on a known fingerprint is made by use of both the object and reference beams, with the known finger pressed against the prism.

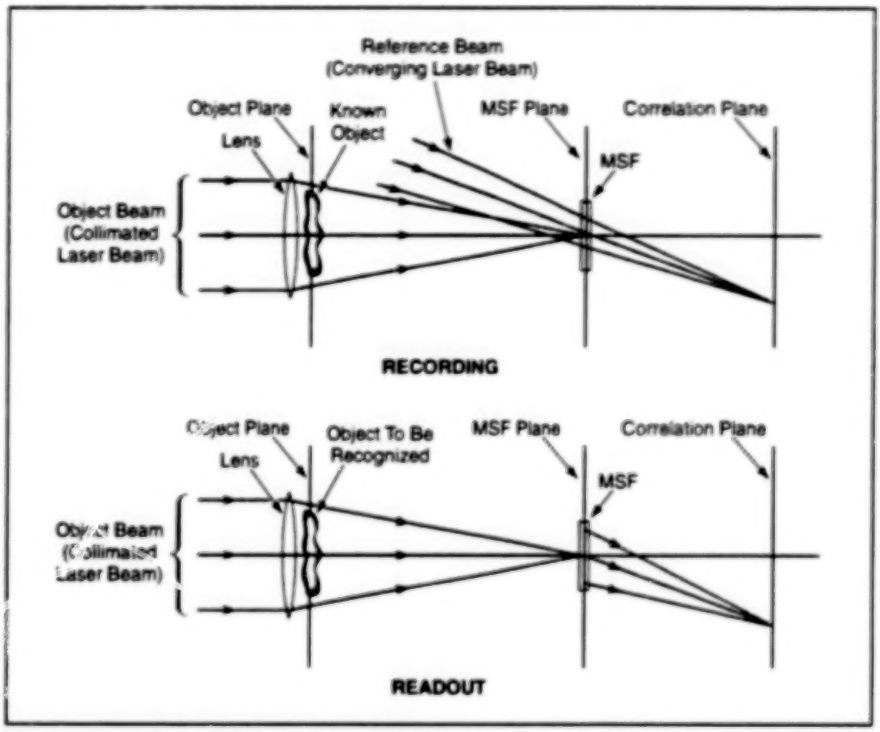

Figure 1. Recording and Readout in the TSACOC are performed with similar (nominally identical) configurations. Unlike in other optical correlators, a converging reference beam is used in recording.

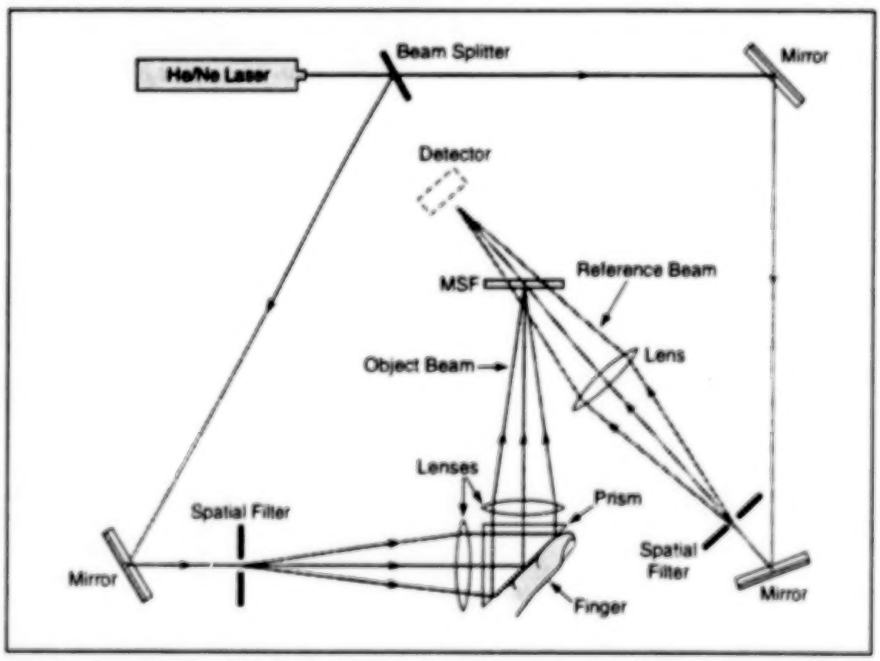

Figure 2. This Simplified TSACOC is an experimental prototype of an instrument for recognizing fingerprints.

Thereafter, to verify that an unidentified finger is the same finger as that represented in the MSF, the reference beam is blocked off, and the unidentified finger is pressed against the prism. Experiments have shown that it is desirable to provide a fixture to hold the finger as nearly as possible in the same position in which it was held while making the MSF. A preliminary prototype, which is the size of a suitcase, has been built for commercialization.

This work was done by Hua-Kuang Liu and Neville Marzwell of Caltech for **NASA's Jet Propulsion Laboratory**. *Further information is contained in a TSP [see page 1].*

In accordance with Public Law 96-517, the contractor has elected to retain title to this invention. Inquiries concerning rights for its commercial use should be addressed to

Larry Gilbert, Director
Technology Transfer
California Institute of Technology
Mail Code 315-6
Pasadena, CA 91125
(818) 395-3288

Refer to NPO-19808, volume and number of this NASA Tech Briefs *issue, and the page number.*

Advanced X-Ray Imaging Spectrometer

Increases in sensitivity and resolution are made possible by development of improved detectors used in conjunction with a coded aperture.

NASA's Jet Propulsion Laboratory, Pasadena, California

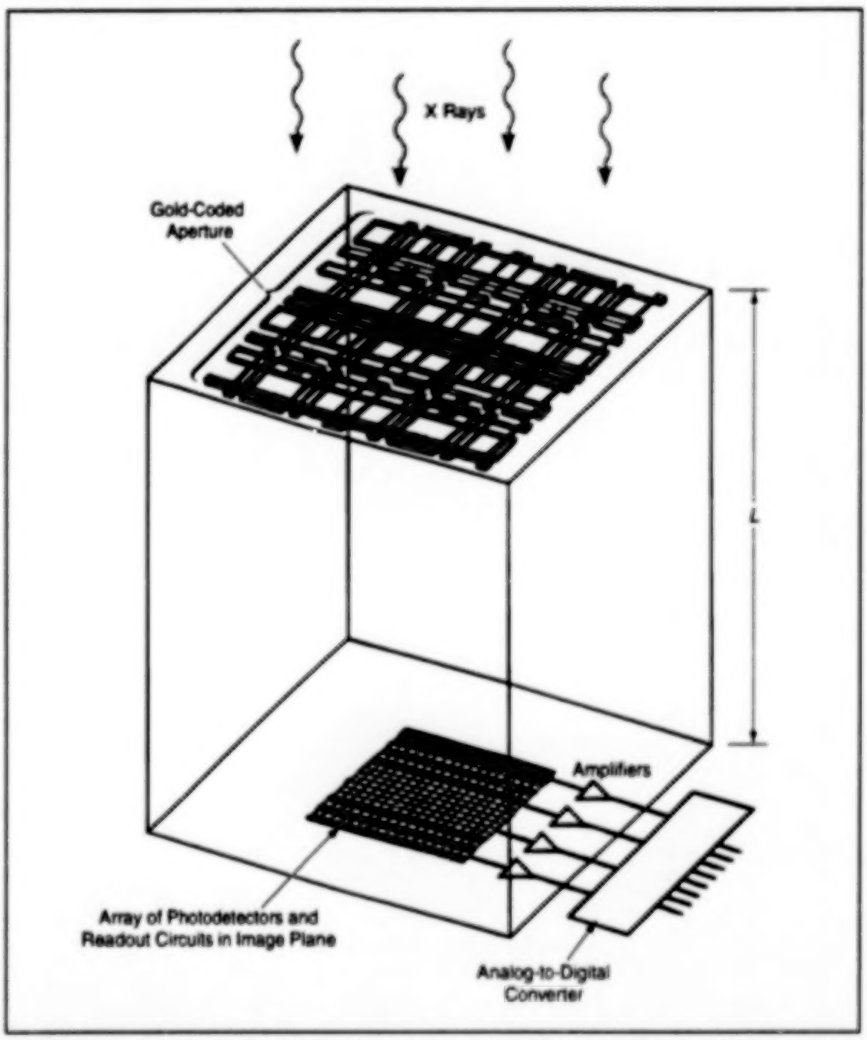

Coded Aperture spatially modulates the incident x rays. The aperture pattern is designed so that the resulting pattern of x-ray intensity on the image plane can be deconvolved to extract an image of the x-ray source.

An advanced x-ray imaging spectrometer (AXIS) with electronic readout features high sensitivity with high spatial and spectral resolution. Prior to this innovation, to perform x-ray imaging and x-ray spectroscopy, it has been necessary to use separate instruments, so that it has been difficult or impossible to associate x-ray spectra with x-ray image features. Furthermore, prior photographic-film and electronic x-ray-imaging instruments have yielded poor spatial resolution and required long exposure times (because of low sensitivity). Offering a capability for sensitive, high-resolution imaging with fine spectroscopy within each pixel, the AXIS opens new possibilities for x-ray observations in astrophysics, laboratory microscopy, industrial inspection, and medicine.

The image plane in the AXIS consists of electronic circuitry in a 1,024-by-1,024 array of pixels containing x-ray photodetectors and on-pixel readout circuits. The detector array is made from high-purity, deeply depleted silicon. The deeply-depleted characteristic results in high sensitivity to x rays at photon energies up through 40 keV. The use of high-purity silicon with on-pixel circuitry results in low leakage current and low noise, enabling fine spectroscopy at or near room temperature. In circuitry outside the image plane, the outputs of the on-pixel preamplifiers are further amplified, then digitized.

To achieve high spatial resolution for imaging, it is necessary to modulate the incoming x rays. For this purpose, the x rays pass through coded aperture (see figure). The coded aperture is fabricated from gold using semiconductor-processing techniques. [Such use of coded apertures to produce spatial modulation for imaging was described previously in "Gamma-Ray Imager With High Spatial and Spectral Resolution" (NPO-19140), *NASA Tech Briefs*, Vol. 20, No. 2 (February 1996), page 49 and "Gamma-Ray Imaging With Two-Dimensionally-Coded Apertures" (NPO-19331), *NASA Tech Briefs*, Vol. 20, No. 11 (November 1996), page 4a.] The digitized pixel outputs are sent to a computer. Using a deconvolution algorithm based on the known geometric relationships among the x-ray source, the coded aperture, and pixels, the computer reconstructs an image of the x-ray source from the digitized detector pixel outputs with a spectrum associated with each image pixel. The spatial resolution of the image can be increased (trading field of view) by increasing the distance, *L*, between the aperture plate and the image plane.

This work was done by John L. Callas and George A. Soli of Caltech for **NASA's Jet Propulsion Laboratory**. *Further information is contained in a TSP [see page 1].*

In accordance with Public Law 96-517, the contractor has elected to retain title to this invention. Inquiries concerning rights for its commercial use should be addressed to

Technology Reporting Office
JPL
Mail Stop 122-116
4800 Oak Grove Drive
Pasadena, CA 91109

(818) 354-2240
Refer to NPO-19663, volume and number of this NASA Tech Briefs issue, and the page number.

Tailored Scattering of Light for Better Illumination

Sources of light would appear to be spread nearly evenly over larger areas.

Lyndon B. Johnson Space Center, Houston, Texas

Two types of light-scattering devices have been proposed to make artificial illumination more nearly even and diffuse, as many people seem to prefer. The general concept of using light-scattering devices to make artificial illumination more comfortable is not new; what is new are the specific proposed design concepts for light-scattering devices, which may prove to be more effective for the purpose than prior light-scattering devices have been.

In designing light-scattering devices for artificial illumination, the effect that one seeks to achieve is to make each source of light (incandescent or fluorescent bulb) appear to occupy an area much larger than its actual size and to emit diffuse light evenly over the much larger area. In the case of multiple sources of light (e.g., a ceiling array of incandescent or fluorescent bulbs), one seeks to make all the sources appear to blend into one source that occupies a substantial area of (or the entire) ceiling and to emit diffuse light evenly from the entire area.

According to one of the two proposals (see Figure 1), the sources in a ceiling array would be connected by a flat translucent sheet made of transparent plastic or glass filled with light-scattering particles. The light would be coupled from each source into the sheet via a coupling taper that would be integral with the sheet. The coupling taper would provide a transition in light-transmission cross section from the source to the surrounding area of the sheet. The outer surface of the taper would be covered with a thin, partially reflective layer of metal so that light traveling directly from the source through the taper to the space below would be no brighter than the light scattered from elsewhere in the sheet.

The density of the particles would be made to vary with position in the sheet, such that the brightness of light scattered from every point on the sheet would be approximately the same. The needed spatial variation of density could be determined experimentally and/or theoretically.

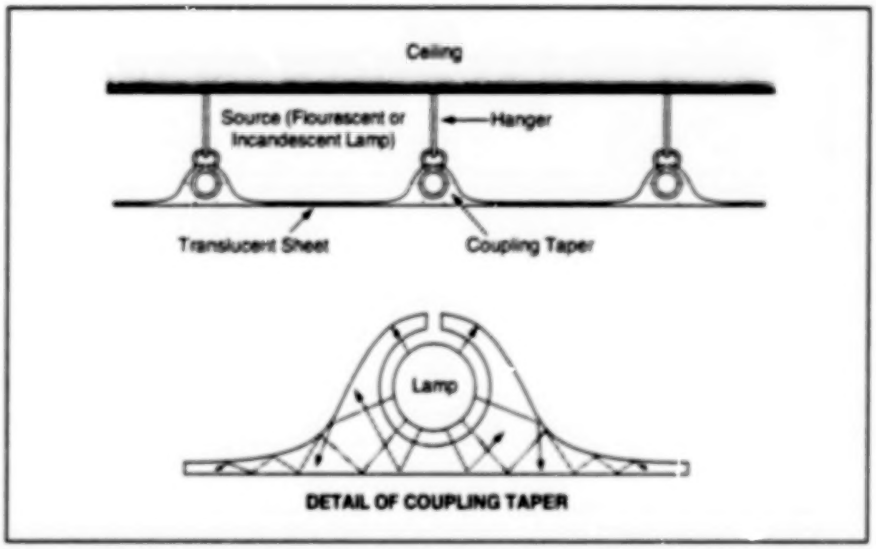

Figure 1. Light Propagating in the Sheet by internal reflection would be scattered out, providing diffuse illumination.

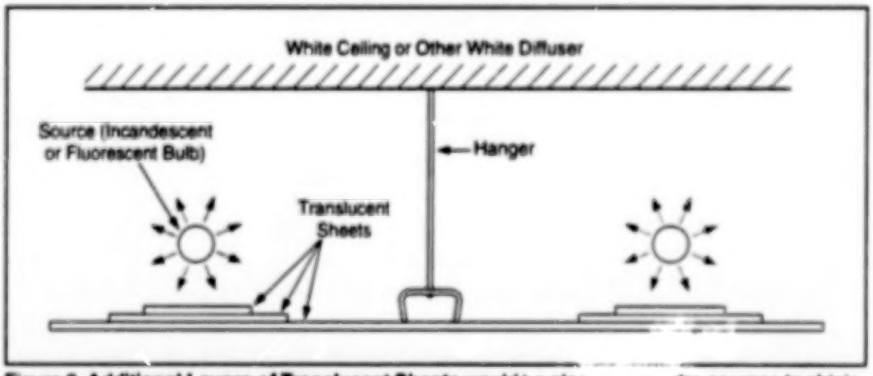

Figure 2. Additional Layers of Translucent Sheets would be placed under the sources to obtain additional back-scattering under the sources.

According to the other proposal (see Figure 2), light would be scattered from both an upper white diffuse reflecting surface (which could be the ceiling) and by a translucent sheet below the sources. Additional layers of translucent material would be stacked under each source in a judiciously chosen pattern to obtain increased diffuse reflection of light up to the ceiling in the vicinity of the source. As before, the net effect would be more nearly even illumination of the space below.

Devices of the second type were successfully developed, and they created a very even illumination with equal or slightly less light loss than that produced by standard, discrete, commercial diffusers. A prototype of the first type was also made and evaluated.

This work was done by Hendrik Gemtsen of Advanced Environmental Research Group for **Johnson Space Center**. *Further information is contained in a TSP [see page 1].*
MSC-22374

Laser Probe for Characterizing Droplets in Clouds

Incipient icing of aircraft surfaces could be detected and quantified.

Lewis Research Center, Cleveland, Ohio

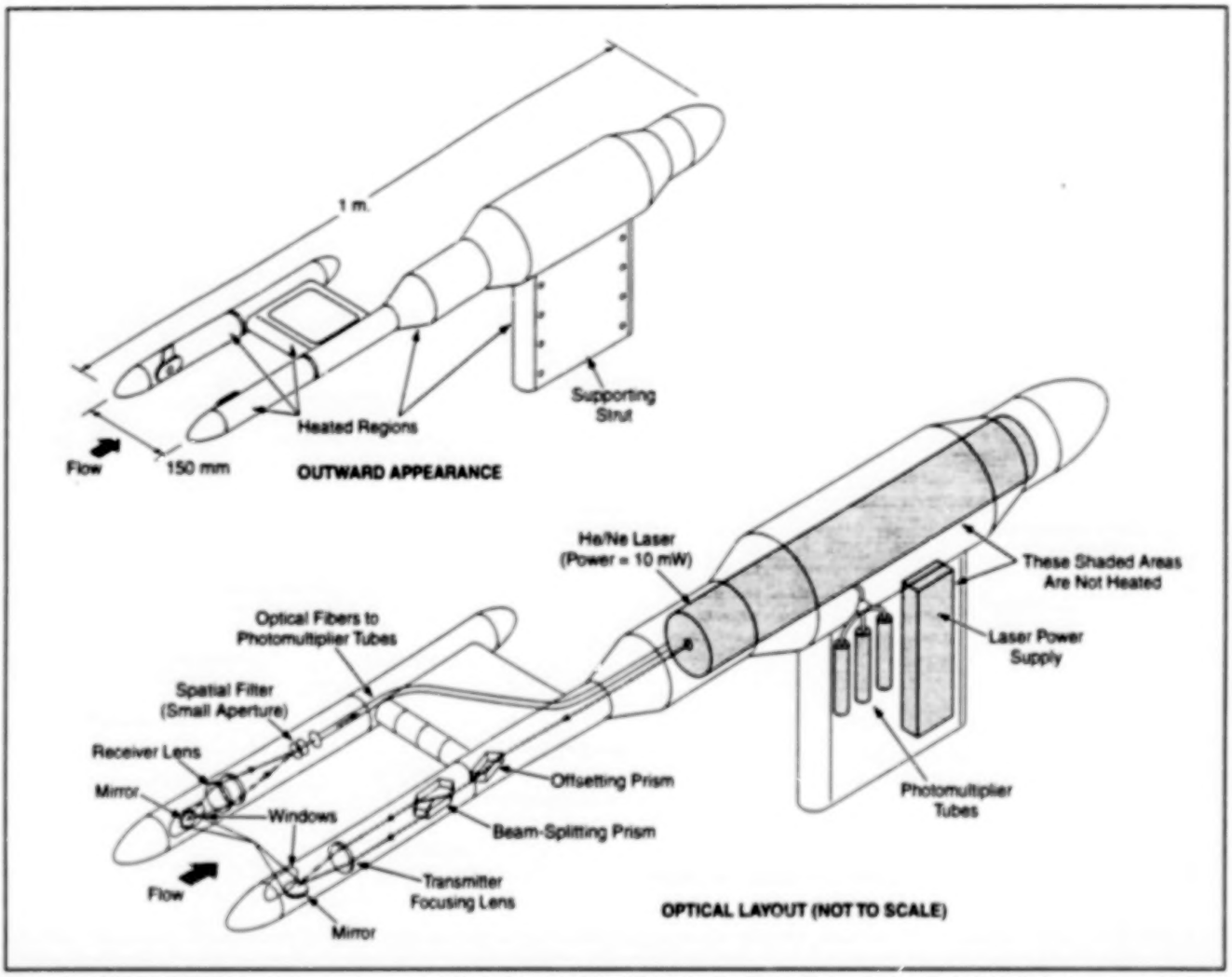

This **Laser-Based ADA Probe** measures the sizes of cloud water droplets under icing conditions. The regions indicated by shading are heated to prevent icing of the probe.

The figure shows the outward appearance and optical layout of a laser probe for measuring water droplets in clouds. This probe is a prototype of instruments that would be mounted on aircraft or used in icing wind tunnels for real-time measurement of droplet sizes (typically of the order of microns) and determination of the liquid water contents of clouds to quantify the potential for accretion of ice on aircraft surfaces. Similar laser probes are used to measure the sizes of solid particles and liquid droplets suspended in flowing gases and liquids in a variety of natural, industrial, medical, and agricultural processes.

This probe is called an "Airborne Droplet Analyzer" (ADA-100), which is based on the phase Doppler technique, which is an extension of the laser Doppler velocimeter technique. As in a laser Doppler velocimeter, a laser beam is split into two coherent beams, which are then made to intersect in a small probe volume, where they form interference fringes. A droplet moving through the probe volume scatters light in a burst of oscillations (called a "Doppler burst") as it passes through the interference fringes. The scattered light includes far-field interference fringes with a spatial interval inversely proportional to the size of the droplet.

Some of the scattered light is focused onto a small aperture. Mounted in precise positions behind the aperture are the input ends of three optical fibers, each of which feeds light to a photomultiplier tube. The outputs of the photomultiplier tubes are fed to a Doppler signal analyzer (DSA), which is capable of processing signal components at frequencies up to 160 MHz. The DSA digitally samples the photomultiplier outputs and performs discrete Fourier transforms to determine frequencies and phases.

By the laser Doppler velocimeter principle, the outputs of the three photomultiplier tubes for the Doppler burst of a given droplet oscillate at the same frequency, which is proportional to the velocity of the droplet through the interference fringes. By the phase Doppler principle, the difference between the phases of the oscillations in the outputs of any two of the photodetectors is proportional to the size of the droplet. Thus, one can calculate the size of the droplet from the phase difference for two photomultipliers. The use of three photomultipliers instead of two extends the range of phase measurements and thus droplet sizes that can be deter-

mined, affords some redundancy for verifying calculated droplet sizes, and provides a basis for rejecting spurious signals from scattering by ice crystals.

To characterize a cloud, it is necessary to accumulate data from many Doppler bursts to obtain, among other things, a droplet-size distribution. In interpreting and using the droplet-size distribution, it is necessary to correct for the variation of the probe volume (and thus the sensitivity of the probe) with droplet size. One also needs velocity and frequency-of-droplet-arrival data, along with the droplet-size distribution, to calculate the liquid water content of the cloud.

In tests in the NASA Lewis icing research wind tunnel, the probe has been shown to measure liquid water contents repeatably and accurately within 20 percent of nominal expected values over a wide range of operating conditions. At the time of reporting the information for this article, tests aboard the NASA Lewis Twin Otter research aircraft were planned.

This work was done by R. C. Rudoff, E. J. Bachalo, and W. D. Bachalo of Aerometrics, Inc., for **Lewis Research Center**. *Further information is contained in a TSP [see page 1].*

Inquiries concerning rights for the commercial use of this invention should be addressed to the Patent Counsel, Lewis Research Center [see page 1]. Refer to LEW-16158.

Better Cells for Multiple-Pass Absorption of Light in Gases

These cells overcome some of the limitation of older multiple-pass absorption cells.

Ames Research Center, Moffett Field, California

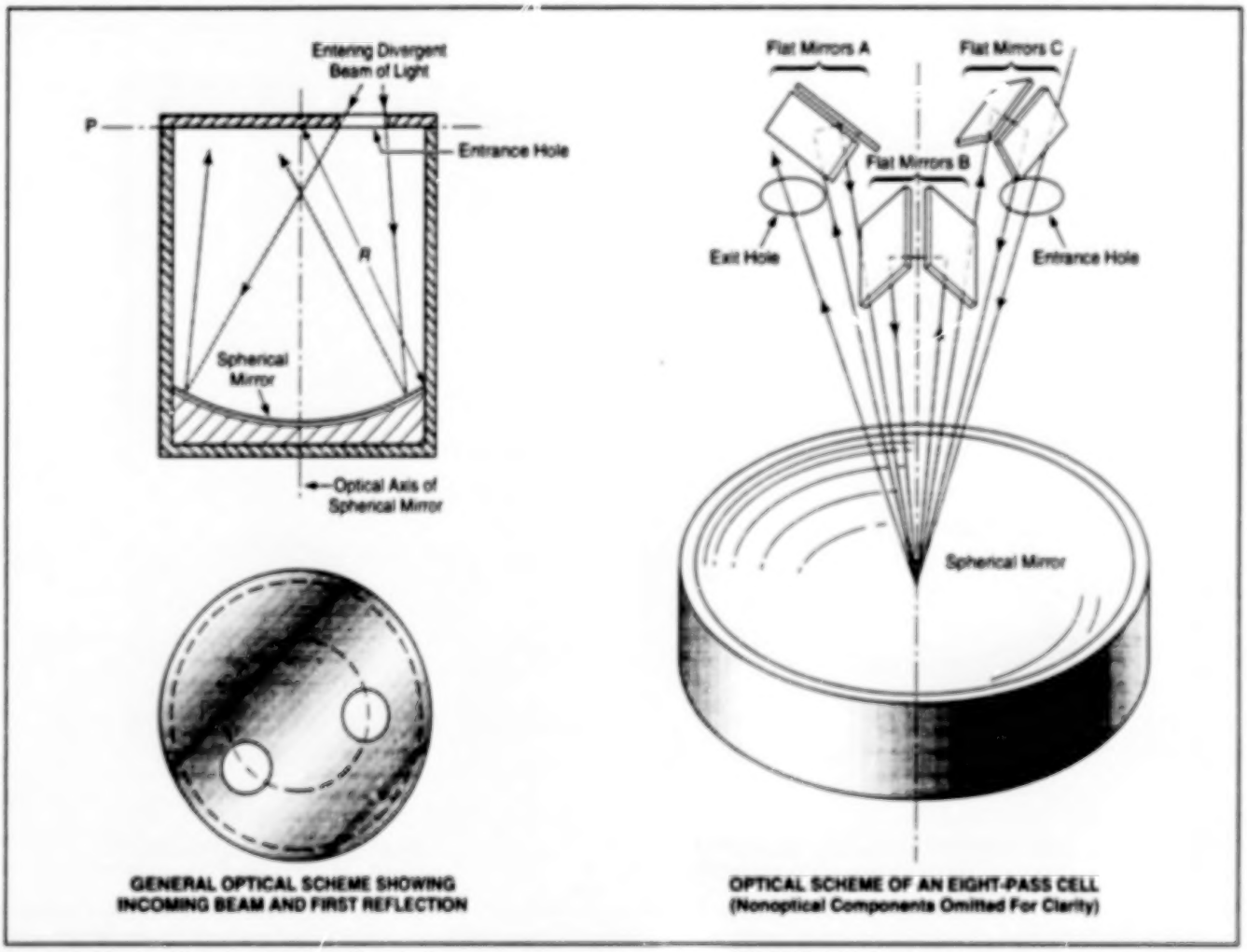

GENERAL OPTICAL SCHEME SHOWING INCOMING BEAM AND FIRST REFLECTION

OPTICAL SCHEME OF AN EIGHT-PASS CELL (Nonoptical Components Omitted For Clarity)

Multiple Passes of a Beam of Light through a cell are achieved by reflection between a spherical mirror and multiple pairs of suitably positioned and oriented flat mirrors. In comparison with older multiple-pass configurations, this one is less sensitive to misalignment and better able to accommodate a wide and/or divergent beam of light.

A new multiple-pass optical gas measurement cell has been developed that provides improved analytical accuracy and reduced size and cost, compared to older designs.

Optical sampling cells allow the measurement of light absorption in samples of gas, using the Beer-Lambert relation. Single pass cells are not difficult to manufacture, but the light path is too short for practical use with weak gas concentrations or with gases that have low absorption properties. In these situations, multiple-pass cells are used, providing for a longer path for the light to travel. However, accu-

racy of the light path is more difficult to control in multiple-path cells. Traditional multiple-pass optical cells with analytical levels of accuracy are relatively large, and need a bright, well-collimated light source for best performance.

The new design developed at the NASA Ames Research Center overcomes several of the limitations inherent in older gas cells, by combining a single spherical lens and two or more flat mirrors to extend the length of the light path.

The left part of the figure illustrates the principles of operation of the new design. A beam, or bundle, of light, which can be divergent, enters the entrance hole, and is reflected by a spherical mirror of radius R and focusing on a top cover on plane P and approximately height R above the spherical mirror. Without additional mirrors, the light beam would thus be focused on the top cover of the device. However, the light is not allowed to strike plane P. Instead, pairs of flat mirrors (one to three pairs would be typical embodiments) are placed near the entrance, and are positioned and oriented to redirect the beam to the spherical mirror. The positions and orientations of the flat mirrors are chosen to make the beam come to a focus between them, so that the central ray of the light beam is reflected back toward the center of the spherical mirror. The last flat mirror is arranged such that, after the final reflection from the spherical mirror, the light beam passes through an exit hole on the top cover. The exit hole is on the same plane as the entrance hole, but at a different azimuthal position on the top cover.

The right part of the figure illustrates the path followed by the central ray of the beam in an eight-pass cell based on this concept. The ray enters the cell (pass 1), and is reflected by the spherical mirror back toward the first of six flat mirrors (pass 2). Passes 3 through 7 are back and forth between the spherical mirror and the remaining five flat mirrors. After the last reflection from the spherical mirror, the ray leaves through the exit hole in the top cover (pass 8).

Unlike some older multiple-pass absorption cells, it is not necessary to use narrow, well-collimated beams of light with this design when only a few passes are necessary. This is due to the property of the combined spherical and flat mirrors' tendency to reduce stray light paths within the cell, thus reducing errors when calculating gas absorption values.

Another advantage of the new design arises from the need for accurate knowledge of the length of the optical path within the cell in order to compute the light absorption using the Beer-Lambert relation. The configuration of the mirrors in the new design makes it easier to manufacture cells with precisely known light-path lengths.

This work was done by Richard Pearson, Dana H. Lynch, and William D. Gunter of **Ames Research Center**. *Further information is contained in a TSP [see page 1].*

This invention has been patented by NASA (U.S. Patent No. 5,459,566). Inquiries concerning nonexclusive or exclusive license for its commercial development should be addressed to the Patent Counsel, Ames Research Center (see page 1). Refer to ARC-13384.

Electrochemical Process for Treatment of Wastewater

The treated water is potable.

Lyndon B. Johnson Space Center, Houston, Texas

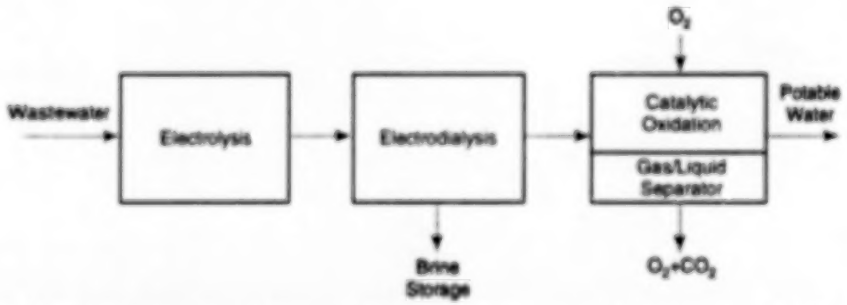

This Electrochemical Water-Treatment Process comprises three subprocesses, each of which plays an essential role in relation with the others.

A prototype apparatus implements an electrochemical process for treatment of wastewater streams that contain various proportions of urine, laundry water, and bath water. The process comprises three sequential subprocesses: a batch electrolysis process followed by a batch electrodialysis process followed by a continuous-flow catalytic oxidation process (see figure). Each of the first two subprocesses removes a different group of contaminants and/or passes on partially reacted contaminants to the next subprocess. The electrochemical energy produced in the electrolysis subprocess results in oxidation of organic contaminants except organic acids. The electrodialysis subprocess removes organic acids and ions. The catalytic oxidation subprocess removes most of the remaining contaminants.

At the beginning of the process, a batch of wastewater (2.3 L in the case of the prototype apparatus) is transferred to a reservoir in the electrolysis section. The electrolysis subprocess takes 260 to 280 min and includes a foam-suppression preprocess: The wastewater is recirculated through the electrolysis section along one of two alternative paths depending on the time. Before electrolysis starts and during the first 30 min of electrolysis, water flows through a regenerable foam-suppression unit, then the electrolysis cell, and back to the reservoir. This path reduces the concentration of foam-forming contaminants to tolerable levels. After 30 min of electrolysis, the path changes to bypass the foam-suppression unit.

The polarity of the voltage applied to the electrolytic cell is reversed once per minute to counteract the buildup of polarized ions near the electrodes and increase the concentration of reactants at the surfaces of the electrodes. The liquid being processed is recirculated through the electrolytic cell at a constant rate of 1 L/min. An oxidation/reduction-potential sensor indicates the end point of the electrolysis, which is defined as the point at which energy-utilization efficiency decreases during electrolysis. A gas-conditioning unit absorbs water vapor and chlorine produced by the electrolysis process. The total concentration of carbon in organic compounds ["total organic carbon" (TOC) for short] and the pH of the processed liquid are more than halved by the electrolysis process. Remaining organic materials are converted to low-molecular-weight organic acids

that can be separated efficiently by electrodialysis.

After electrolysis, the water is transferred to a reservoir in the electrodialysis section. In the electrodialysis subprocess, an electric field causes ions to migrate through membranes, thereby concentrating the contaminants into a brine while forming a deionized product water that is relatively free of contaminants. The statuses of the brine and the product water are monitored (to determine the end point for electrodialysis) by use of electrical-conductivity meters. The brine is stored, while the deionized product water is moved on to catalytic oxidation.

In the catalytic oxidation subprocess, the TOC of the remaining contaminants is reduced to below 500 micrograms per liter — a level that satisfies NASA's specification for potable water. Oxidation byproducts (oxygen and carbon dioxide), are removed by a gas/liquid separator at the outlet of the catalytic oxidizer.

This work was done by James R. Akse of Umpqua Research Co. for **Johnson Space Center**. *Further information is contained in a TSP [see page 1].*
MSC-22427

Books and Reports

More About a Laser-Speckle Surface-Strain Gauge

The report, "Compact Simultaneous-Beam Optical Strain Measurement System — Phase V," is one in a series of documents about an optoelectronic instrument that uses laser speckle for noncontact measurement of strains on the surfaces of specimens, which can be hot even though the instrument remains at room temperature. Several prior articles in *NASA Tech Briefs* have described this instrument at various stages of development; the most recent description appeared in "Improvements in a Laser-Speckle Surface-Strain Gauge" (LEW-15914), Vol. 20, No. 4 (April 1996), page 54. The report reiterates information from the prior articles and supporting documents and describes some more-recent advances. One notable advance addresses a disadvantageous reduction in the separation of speckle patterns that are generated by two lasers and imaged in a video camera. Such a reduction occurs during observation of a depolarizing specimen. The report proposes the use of two different laser wavelengths, combined with the use of a refracting prism in front of the camera, to increase the separation of the corresponding speckle patterns.

This work was done by Christian T. Lant of Sverdrup Technology, Inc., for **Lewis Research Center**. *To obtain a copy of the report, see TSP's [page 1].*

Inquiries concerning rights for the commercial use of this invention should be addressed to NASA Lewis Research Center, Commercial Technology Office, Attn: Tech Brief Patent Status, Mail Stop 7–3, 21000 Brookpark Road, Cleveland, Ohio 44135. Refer to LEW-16441.

Macrosegregation and Nucleation in Undercooled Pb/Sn Alloys

A report describes an experimental study of macrosegregation and nucleation in three alloys of Pb and Sn. The alloys had tin contents of 12.5, 61.9 (eutectic), and 77 weight percent. Ingots of the alloys, each with a volume of 2.7 cm^3, were melted, then frozen with undercoolings ranging from 4 to 34 K and cooling rates from 0.04 to 4 K/s. The nucleation behavior of the Pb/Sn system was found to be nonreciprocal; the solid Sn phase effectively nucleated the Pb phase of the eutectic, but large undercoolings developed in Sn-rich eutectic liquid in the presence of the solid Pb phase. This phenomenon is believed to be mainly a result of differences between interfacial energies of (1) solid Sn/eutectic liquid and (2) solid Pb/eutectic liquid. Amounts of macrosegregation in eutectic ingots were found to increase with undercooling. The macrosegregation was attributed primarily to a sink/float mechanism and the nucleation behavior of the alloy: The primary phase in the undercooled eutectic comprises lead-rich dendrites, which grow rapidly into the undercooled liquid, then soon break apart on account of recalescence and Sn enrichment of the liquid. The settling of fragmented Pb dendrites to the bottom causes the macrosegregation. As an example of macrosegregation, a eutectic ingot undercooled by 20 K at a rate of 4 K/s exhibited a final Sn content of 72 weight percent at the top and 55 weight percent at the bottom.

This work was done by Henry C. de Groh III of **Lewis Research Center**. *To obtain a copy of the report, "Macrosegregation and Nucleation in Undercooled Pb-Sn Alloys," see TSP's [page 1].*

Inquiries concerning rights for the commercial use of this invention should be addressed to NASA Lewis Research Center, Commercial Technology Office, Attn: Tech Brief Patent Status, Mail Stop 7–3, 21000 Brookpark Road, Cleveland, Ohio 44135. Refer to LEW-16414.

High-Temperature Fatigue Testing of PMCs

A report describes an experimental study of the tensile and cyclic fatigue behavior of a polyimide-matrix/carbon-fiber composite material under elevated-temperature conditions. The study was undertaken primarily to develop and refine techniques of high-temperature, uniaxial (tension/compression) fatigue testing of polymer-matrix composite (PMC) materials in general. The major accomplishments of the study were the following:

- Development of a untabbed, dog-bone specimen geometry that yielded consistent gauge-section failures under all test conditions;
- A thermocouple-mounting and -calibration technique for accurate measurement of the temperature in a specimen heated radiantly by quartz lamps;
- The use of high-temperature extensometry for monitoring strain during cyclic fatigue testing at high temperatures; and
- The use of stress-vs.-strain data, real-time measurements of static tensile and compressive moduli, and changes in maximum and minimum strain to monitor fatigue damage.

This work was done by John R. Ellis of **Lewis Research Center**, *Andrew L. Gyekenyesi of Cleveland State University, and Michael G. Castelli and Christopher S. Burke of NYMA, Inc. To obtain a copy of the report, "A Study of Elevated Temperature Testing Techniques for the Fatigue Behavior of*

PMCS: Application to T650-35/AMB21," see TSP's [page 1].

Inquiries concerning rights for the commercial use of this invention should be addressed to NASA Lewis Research Center, Commercial Technology Office, Attn: Tech Brief Patent Status, Mail Stop 7–3, 21000 Brookpark Road, Cleveland, Ohio 44135. Refer to LEW-16496.

Factors That Affect Readings of Ultrasonic Bolt-Load Gauges

Three reports discuss the principles of operation and factors that affect the readings of ultrasonic extensometers used to measure preloads in bolts, studs, and similar fasteners. These instruments measure "ultrasonic lengths" proportional to round-trip times of travel of ultrasonic pulses along fasteners. To a first approximation, the amount by which the ultrasonic length of a fastener under tensile load differs from the unloaded length is proportional to the load, and can thus be used to indicate the load. However, the reading of the ultrasonic instrument is complicated by such other effects as thermal expansion of the fastener, dependence of the speed of sound on temperature and stress, and variations in tension along the gripped portion(s) of the length of fastener. The first report describes these effects; discusses measurement tolerances; presents equations for the propagation of errors in preload measurements; discusses uncertainties pertaining to statistical variations in distributions of stresses, transducer coupling, and temporal and spatial variations of temperature; and discusses the many factors that affect the accuracies of instruments. The second and third reports address ultrasonic measurements of preload in a sleeve bolt, which expands upon installation to provide an interference fit in a hole. In this case, the measurements are affected by pressure from the interference fit and by friction, which gives rise to hysteresis and to differences between the loads at the two ends of the fastener.

This work was done by Ajay M. Koshti of Rockwell International Corp. for **Johnson Space Center**. *To obtain copies of the reports, "Estimation of Accuracy in Ultrasonic Preload Measurements," "Preload Measurement in Sleeve Bolts Using An Ultrasonic Bolt Gage," and "Preload measurement in sleeve bolts using an ultrasonic technique," see TSP's [page 1].*
MSC-22674

Materials

Hardware, Techniques, and Processes

Books and Reports

BLANK PAGE

Modified CVI Process for Making SiC/SiC Composites

Removable surface layers eliminate the need for time-consuming grinding-off of integral surface layers.

Lewis Research Center, Cleveland, Ohio

A modified chemical-vapor infiltration (CVI) process makes high-quality composites of silicon carbide fibers in silicon carbide matrices. In this process, one adds a sacrificial surface layer of SiC fiber preform that can later be removed easily, by scraping or tapping, when it becomes clogged with infiltrate ("canned off," in CVI terminology).

In comparison with other CVI processes, this process is faster and costs less because unlike the other processes, this one does not involve time-consuming grinding-off of surface layers that have become clogged with infiltrate. This process can be used for making parts that have variable thicknesses and complex, irregular shapes, as well as parts that have constant thicknesses and simple shapes. This process also ensures that the infiltrate consists only of silicon carbide, without the silicon that is sometimes found in SiC/SiC composites made by other processes.

The advantages of this process can be understood better by comparison with one of the other processes; namely, conventional forced-flow isothermal CVI, in which a porous (SiC-fiber) preform is held at constant temperature while reactant gases are forced through it. The infiltrating gases react to deposit silicon carbide in the pores. However, pores near the surface tend to become filled before those inside the preform. The canned-off surface pores greatly reduce the rate of infiltration to, and deposition in, the pores deeper in the preform. To promote further infiltration and deposition deep within the preform, the canned-off surface layer must be removed by diamond grinding (this subprocess is called "skinning" in the industry). The ground preform must be then returned to the CVI reactor for further infiltration.

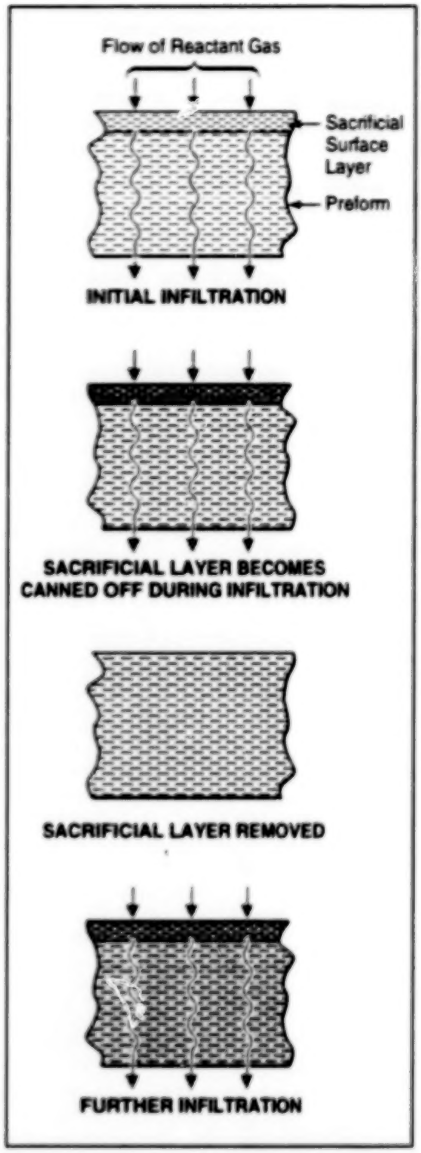

The Modified CVI Process resembles conventional forced-flow isothermal CVI in some respects, but costs less because it does not include a time-consuming grinding step.

One version of the modified CVI process (see figure) is similar to conventional forced-flow isothermal CVI in some respects. However, unlike in the conventional process, the upstream surface of the preform is first covered with the sacrificial surface layer, which is typically made of either (a) the same material as that of the preform but without a protective fiber coating like that used in the preform or (b) any other high-temperature material that allows diffusion of the reactants and does not become bonded to the preform. The preform is then subjected to CVI. As CVI progresses, the differential pressure of reactant gases across the preform is monitored continuously; when the pressure has risen sufficiently to indicate that the sacrificial layer has become canned off, the preform is removed from the CVI reactor, the sacrificial layer is peeled or tapped off (this takes about two minutes at most), a new sacrificial layer is applied to the surface, and the preform is returned to the reactor for further infiltration.

The sacrificial layer also acts as a diffuser, helping to distribute the reactant gases more evenly. It also acts as a filter, screening out contaminants so that the material deposited in the pores is pure silicon carbide only.

This work was done by M. A. Kmetz, Paul Allard, Dave Wagner, and Chris Kogstrom of United Technologies Pratt & Whitney for **Lewis Research Center**. *Further information is contained in a TSP [see page 1].*

Inquiries concerning rights for the commercial use of this invention should be addressed to NASA Lewis Research Center, Commercial Technology Office, Attn: Tech Brief Patent Status, Mail Stop 7–3, 21000 Brookpark Road, Cleveland, Ohio 44135. Refer to LEW-15691.

Unsymmetrical Squaraine Dyes for Nonlinear Optics

Molecular structures are engineered to enhance second-order polarizabilities.

NASA's Jet Propulsion Laboratory, Pasadena, California

Dyes based on unsymmetrical squaraine molecules (see Figure 1) have been invented for use in a variety of optical devices that exploit nonlinear optical properties to change the frequency and/or polarization of light in useful ways. Examples of such devices include second-harmonic generators, spatial light modulators, parametric oscillators, and some interferometers.

The unsymmetrical squaraine molecular structures are engineered to obtain large values of first electronic hyperpolarizability (β); that is, the second-order polarizability that gives rise to the

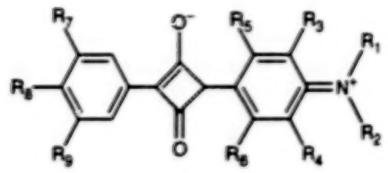

Notes:

1. R_1 is alkyl, $(CH_2)_nOH$ where n = 1 to 8, $(CH_2)_nSH$ where n = 1 to 8, phenylmethyl, or 4-halophenylmethyl. Alternatively, $R_1 + R_3 = (CH_2)_3$.
2. R_2 is alkyl, $(CH_2)_nOH$ where n = 1 to 8, $(CH_2)_nSH$ where n = 1 to 8, phenylmethyl, or 4-halophenylmethyl. Alternatively, $R_2 + R_4 = (CH_2)_3$.
3. $R_1 + R_2$ is derived from a cyclic amine of the form $N(CH_2)_n$ where n = 3 to 10.
4. R_5 is H, F, OH, SH, CH_3, C_2H_5, OCH_3, or SCH_3.
5. R_6 is H, F, OH, SH, CH_3, C_2H_5, OCH_3, or SCH_3.
6. R_7 is H, alkyloxy or aryloxy.
7. R_8 is H, alkyloxy, or aryloxy.
8. R_9 is alkyloxy, or aryloxy.

Figure 1. This **General Structural Formula** is only one of nine such formulas that describe the numerous unsymmetrical squaraine dyes of the invention. Note the wide variety of compounds represented by variations in the groups R_1 through R_9.

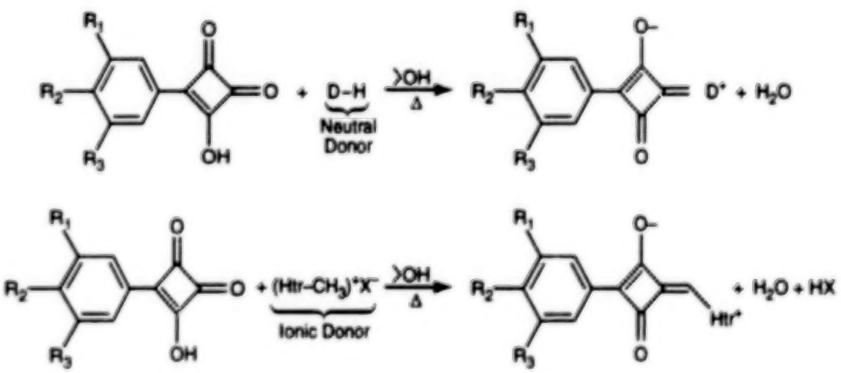

Figure 2. These **Dyes Are Synthesized** by condensing monosubstituted squaric acid precursors with neutral or ionic donors.

desired nonlinear optical response.

The molecular-engineering strategy is derived from some observations concerning two limiting charge-transfer resonance forms that occur in the molecules of interest. Each molecule can be characterized, in part, by a linear combination of these two forms. If one form completely dominates, the molecule is designated as being polyenelike; if the two forms contribute equally, the molecule is designated as being cyaninelike. It has been discovered that (a) it is necessary to obtain an optimal linear combination of the two forms in order to maximize β, and that (b) the value of β can be correlated with the bond-length alternation (BLA), which is the difference between the lengths of adjacent carbon-carbon bonds. As one proceeds from a polyenelike limit (BLA > 0.12 Å) to a cyaninelike limit (BLA = 0 Å), β reaches a peak at BLA ≈ 0.04 Å.

Past efforts to reach this peak from the polyene limit by adding electron donors or acceptors to decrease the magnitude of BLA have usually resulted in BLA > 0.10 Å — far from the value needed to maximize β. The development of the present unsymmetrical squaraine dyes followed a different approach — starting from the cyanine limit of BLA = 0. Squaraine dyes are analogous to cyanine dyes in that like cyanine dyes, they are characterized by two degenerate resonance forms and sharp and intense visible or near-infrared absorption spectral bands. However, unlike ionic cyanines, squaraines are neutral molecules that are suitable for measurement of electric-field-induced second-harmonic generation.

The unsymmetrical squaraine dyes of this invention are synthesized by condensing monosubstituted squaric acids with neutral or ionic donors. For example, in the synthesis illustrated in the upper part of Figure 2, the monosubstituted squaric acid precursors could be 1-(4-isopentyloxyphenyl)-2-hydroxycyclobutene-2,4-dione, and the neutral donor (D-H) could be 4-N,N-dibutylamino-3′,5′-dihydroxystilbene. For another example, in the synthesis illustrated in the lower part of Figure 2, the monosubstituted squaric acid precursor could be 1-(4-methoxyphenyl)-2-hydroxycyclobutene-2,4-dione and the ionic donor $(Htr\text{-}CH_3)^+X^-$ could be N-butyllepidinum iodide.

Depending on specific applications, these dyes can be used alone (e.g., in crystalline and/or thin-film form) or can be incorporated into thin films, crystals, liquids, and/or gases in mixtures with other materials that are conventionally used in nonlinear optical devices. A particularly convenient and effective way of using a dye of this invention is to disperse the polar dye molecules in a polymeric binder. The polymer/dye mixture can be heated to a temperature at which the polymer becomes sufficiently soft so that upon application of an electric field, the polar molecules line up along the direction of the field. When the mixture cools, the polar molecules are locked into their field-aligned orientation, and so the electric field can be removed without loss of orientation.

This work was done by Seth R. Marder, Chin-Ti Chen, and Lap-Tak Cheng of Caltech for **NASA's Jet Propulsion Laboratory**. *Further information is contained in a TSP [see page 1].*

In accordance with Public Law 96-517, the contractor has elected to retain title to this invention. Inquiries concerning rights for its commercial use should be addressed to

Larry Gilbert, Director
Technology Transfer
California Institute of Technology
Mail Code 315 - 6
Pasadena, CA 91125
(818) 395-3288

Refer to NPO-19398, volume and number of this NASA Tech Briefs *issue, and the page number.*

Adhesively Bonded Strain Gauges for Temperatures up to 400 °C

Bonding conditions are consistent with chemical properties and temperature limitations of substrates.

Lewis Research Center, Cleveland, Ohio

Strain gauges with improved adhesive bonding have been developed for use in measuring creep and stress-relaxation effects associated with aging in PMR-15 polyimide resin at test temperatures up to and even somewhat above the maximum use temperature of 371 °C. Even near the upper limit of test temperatures, the improved adhesive bonding provides secure attachment to substrates of both PMR-15 composites and titanium alloy 6242.

The development of these strain gauges and the improved adhesive bonding were necessitated by the limitations of previously available strain gauges. The best previously available adhesively bonded strain gauges could not withstand prolonged exposure to temperatures above 232 °C and were recommended for no more than 150 hours of operation at 280 °C. The adhesive in those gauges had to be cured at temperatures up to 42 °C above the intended test temperatures; some substrate materials, including PMR-15 composites, cannot withstand this much heating above test temperatures.

The improved bonding of the present strain gauges is achieved by use of a procedure and materials compatible with the cure chemistry and with the processing requirements for the substrate material. The maximum bonding temperature does not exceed the intended test temperature or the maximum substrate-fabrication temperature. Also, unlike standard previously available adhesively bonded strain gauges, the present strain gauges are not backed with permanent organic supporting films that must be bonded to the substrates; the present gauges are manufactured with temporary supporting films, and the gauges themselves, rather than the supporting films, are adhesively bonded directly to the substrates.

In the case of a PMR-15 substrate, the improved bonding procedure is initiated after the cure and before the postcure stage of the substrate-fabrication process. The adhesive is a slurry that is made by preparing a solution of poly(amic acid) in N-methyl-2-pyrrolidinone, then adding a partially reacted (imidized but not cross-linked) PMR-15 powder. The poly(amic acid) solution is used to obtain adequate flow and wetting of the substrate.

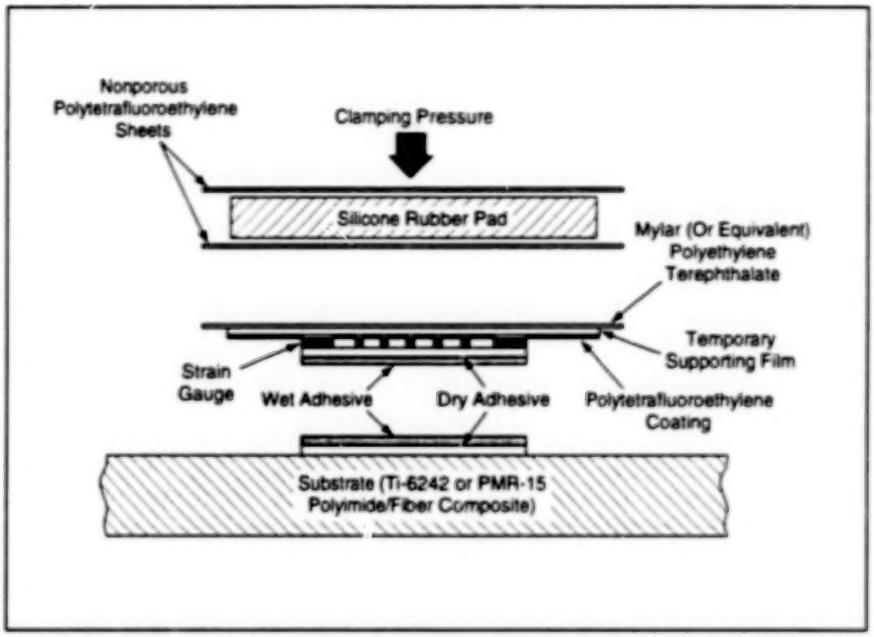

A Strain Gauge Is Bonded to a substrate by pressing together adhesive-covered gauge and substrate surfaces, then heating the entire assembly to cure the adhesive and postcure the substrate. The adhesive is formulated to be compatible with the cure chemistry, processing requirements, and temperature limitation of the substrate.

The gauge is cleaned by exposure to ultraviolet light and ozone. A first coat of adhesive is applied to the substrate and to the gauge face opposite the temporary supporting film, then this first coat is dried by heating to temperatures up to 205 °C. A second coat of adhesive is applied, then the gauge and substrate are clamped together (see figure) and heated according to the normal postcure schedule of 205 °C for 10 minutes followed by 316 °C for two hours.

In a test of the gauges and improved bonding, a gauge remained bonded to a PMR-15 composite substrate and exhibited adequate resistance to creep after aging for a month at 316 °C. The present gauge/adhesive system has also been shown to withstand thermal cycling up to 364 °C and to withstand maximum temperatures up to 400 °C for short times.

Though the adhesive bonding system has been demonstrated on PMR-15 resin and titanium-alloy substrates, bonding to PMR-15 composites and to other polymeric and metal substrate materials should be possible. For bonding to other polymeric substrates, the adhesive system would be modified by replacing the poly(amic acid) and the PMR-15 powder with materials more similar to, and/or more compatible with, the substrate material.

This work was done by Gary D. Roberts, Kathy C. Chuang, and J. Michael Pereira of **Lewis Research Center**; *Christopher Rabzak of NYMA, Inc.; and Douglas T. Jayne of Ohio Aerospace Institute. Further information is contained in a TSP [see page 1].*

Inquiries concerning rights for the commercial use of this invention should be addressed to NASA Lewis Research Center, Commercial Technology Office, Attn: Tech Brief Patent Status, Mail Stop 7–3, 21000 Brookpark Road, Cleveland, Ohio 44135. Refer to LEW-16347.

Books and Reports

Experiments on Growth of GaN on $MgAl_2O_4$

A report describes an experimental study of the growth of gallium nitride on magnesium aluminate substrates. GaN exists in wurtzite and zinc-blende phases; the zinc-blende phase is more desirable for use as a semiconductor in optoelectronic devices. $MgAl_2O_4$ would be an excellent candidate substrate material for epitaxial growth of GaN, except that there is a mismatch of 10 percent between the GaN and $MgAl_2O_4$ crystalline lattices. In the experiments, low pressure metal/organic chemical vapor deposition from triethylgallium and ammonia source gases was used to grow GaN on (111)- and (100)-oriented $MgAl_2O_4$ substrates, with the expectation that the threefold symmetric (111) $MgAl_2O_4$ substrate would promote the growth of wurtzite GaN, while the fourfold-symmetric (100) MgAl2O4 would favor the zinc-blende phase. As expected, the GaN film that formed on the (111) substrate was of single-crystal wurtzite, albeit with a high density of stacking faults near the GaN/$MgAl_2O_4$ interface. However, the GaN film that formed on the (100) $MgAl_2O_4$ substrate was not single crystal zinc blende as expected; instead, the GaN film was found to be divided into five different regions, four of which contained the wurtzite phase in various lattice orientations and one containing the zinc-blende phase. Interfacial bonding, rather than lattice mismatch, appears to play a key role in determining the epitaxial characteristics of GaN films on $MgAl_2O_4$.

This work was done by Thomas George and William T. Pike of Caltech for **NASA's Jet Propulsion Laboratory**. *To obtain a copy of the report, "Novel Symmetry in the Growth of Gallium Nitride on Magnesium Aluminate Substrates," see TSP's [page 1].*
NPO-19871

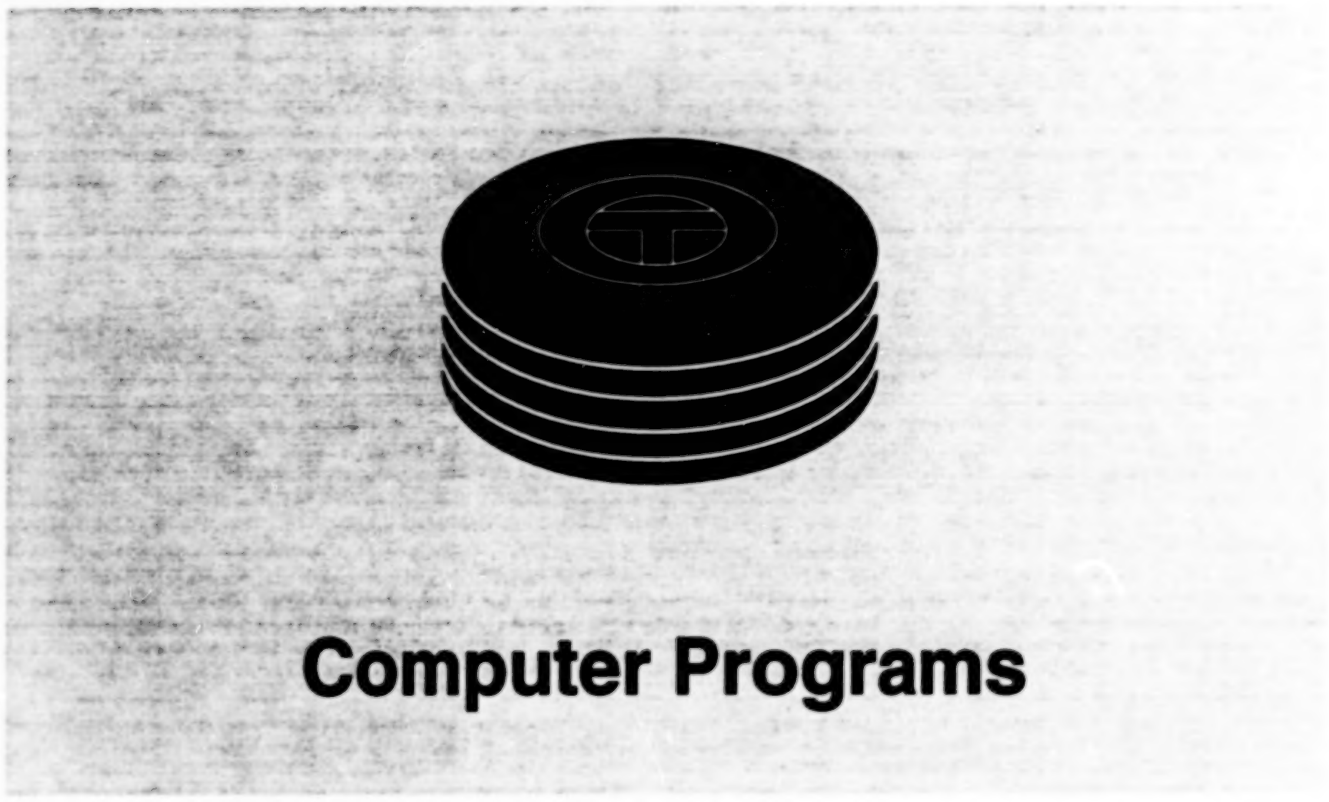

Computer Programs

Machinery

Mathematics and Information Sciences

BLANK PAGE

Computer Programs

These programs may be obtained from COSMIC. Please contact

COSMIC®
Computer Services Annex
University of Georgia
Athens, GA 30602
Telephone No. (404) 542-3265.

Machinery

Program for Analyzing Flutter of Propfan Blades

Two subprograms perform different parts of aeroelastic-stability analysis.

Stimulated by the interest in improvement of aircraft fuel efficiency, Lewis Research Center initiated an effort to develop refined analytical methods and associated computer codes for predicting flutter of propfans. The ASTROP2 computer program performs aeroelastic-stability analysis of rotating propfan blades. It uses strip theory to integrate aerodynamic forces calculated by use of a two-dimensional model of aerodynamics with a three-dimensional model of the structure.

The flutter analysis is performed by two separate subprograms. The first subprogram calculates the structural dynamics at the strips required for the analysis of aeroelasticity. The second subprogram uses the structural data from the first subprogram and calculates the aeroelastic stability. Each subprogram can be used and modified independently.

ASTROP2 is written in FORTRAN 77 and has been successfully compiled and run on a SUN 4 SLC workstation running SunOS 4.1.3_U1, an SGI IRIS INDIGO workstation running IRIX 6.2, and a SUN 4 IPC workstation running SunOS 5.4/Solaris 2.4. The program also functioned properly on a CRAY/Y-MP computer running UNICOS 8.0.4.1 with the CFT77 6.0.5.0 compiler. The standard distribution medium for ASTROP2 is a 4-mm digital audio tape in UNIX tar format. Alternate distribution media and formats are available on request. ASTROP2 was released in 1996.

This program was written by J. M. Lucero of **Lewis Research Center**, *T. S. Reddy of the University of Toledo, and G. V. Narayanan of Sverdrup, Inc. For further information, see TSP's [page 1].*
LEW-16407

Mathematics and Information Sciences

The SPICE System

The Navigation and Ancillary Information Facility (NAIF) at JPL has built a multimission, multidiscipline information system named SPICE, which is of use to scientists and engineers involved with mission evaluation, mission operations, observation planning, and science data analysis. SPICE has two principal components — a set of data file specifications and a collection of software used to write SPICE files and to read and utilize the data within SPICE files. The SPICE files, called "kernels," contain a variety of space science geometry, including ephemerides and size, shape, and orientation for planets, satellites, comets, and asteroids; spacecraft trajectory; spacecraft orientation; and instrument viewing geometry. Also included in SPICE files is nongeometric information, such as sequence of events and electronic notebook. The software component of SPICE is the NAIF Toolkit. The principal component of this Toolkit is a large library of FORTRAN subroutines known as SPICELIB. Included in SPICELIB are subroutines used in both writing and reading SPICE kernel files, and higher-level routines used to process SPICE kernel data to compute a wide assortment of observation geometry, such as observer-target direction and range, sub latitude and longitude, lighting angles, and the like. Users integrate selected NAIF Toolkit routines into their own application programs to help accomplish whatever objectives are at hand. The kernel file structures and Toolkit software are designed with portability as a key attribute: the SPICE system will work on any computer that supports ANSI FORTRAN 77, and C language interfaces to the most used subroutines are being added. Flexibility is also a key attribute: the system architecture is easily extended to handle new requirements. A customer may choose to use a subset of the SPICE capabilities. SPICE defines the data standards for ancillary data to be archived within NASA's Planetary Data System. SPICE is used on most NASA planetary missions and was used by the Russian Mars 96 mission. It has been used to support a number of astrophysics and space physics applications, and has been successfully demonstrated with Earth-observing spacecraft. SPICE is also used by terrestrial observatories.

This program was written by Charles Acton, Nathaniel Bachman, Kevin Gehringer, William Taber, and Boris Semenov of Caltech for **NASA's Jet Propulsion Laboratory**. *For further information, see TSP's [page 1].*
NPO-19984

Computer Program for Emulating MIL-STD-1750a Computer

CPU_1750a is a software program that implements the MIL-STD-1750a Military Standard Sixteen-bit Computer Instruction Set Architecture. It emulates a MIL-STD-1750a compliant computer hardware system.

CPU_1750a provides a unified mechanism for integration with software that emulates peripherial hardware. It is used to implement a software emulation of a complete digital avionics system such that MIL-STD-1750a software may be developed and tested prior to the availability of hardware. The extensive visibility provided by CPU_1750a allows development and debugging to proceed more rapidly than is possible on many hardware-based development systems.

Powerful user interfaces can be quickly created. CPU_1750a provides read/write access to internal state (registers, memory, and page registers, and emulator control variables and functions) that is designed to be comparable with Tool Command Language (Tcl). Breakpoints and instruction trace are controlled via Tcl, and may in turn activate Tcl procedures upon activation.

CPU_1750a fully implements the MIL-STD-1750a instruction set. It passes all SEAFAC VSW V2.1 verification tests. CPU_1750a can be configured with multiple personalities, which can be selected during runtime. Three personalities are currently available: MIL-STD-1750a, IBM GVSC, and IBM GVSC with breakpoints and instruction trace capability. Personalities are implemented so that performance of one personality is not dependent upon features implemented in another personality so that performance is always as high as possible.

CPU_1750a implements all mandatory and optional MIL-STD-1750a features, including: interval timers, expanded mem-

ory, memory block protect, startup ROM, and access lock/key.

CPU_1750a is written in C++. It executes over 400,000 instructions per second on a Sun SPARC 10/51.

This program was written by William K. Reinholtz and Mohammad Shahabuddin of Caltech for **NASA's Jet Propulsion Laboratory**. *For further information, see TSP's [page 1].*

In accordance with Public Law 96-517, the contractor has elected to retain title to this invention. Inquiries concerning rights for its commercial use should be addressed to

Technology Reporting Office
JPL
Mail Stop 122-116
4800 Oak Grove Drive
Pasadena, CA 91109
(818) 354-2240

Refer to NPO-19734, volume and number of this NASA Tech Briefs issue, and the page number.

Mechanics

Hardware, Techniques, and Processes

Books and Reports

BLANK PAGE

Rolled-Up Ramp Deploys Itself on Command

The ramp unfurls itself when pyrotechnic cutters are activated to release bindings.

NASA's Jet Propulsion Laboratory, Pasadena, California

The figure illustrates various aspects of a springy ramp that can be rolled tightly into a cylinder, which is then wrapped circumferentially with tie-down cables. On subsequent command, pyrotechnic devices can be activated to cut the tie-down cables, causing the ramp to deploy itself by unrolling under its own spring force. The ramp was designed to facilitate the egress of a small rover vehicle from the Mars *Pathfinder* spacecraft; modified versions of the ramp might be useful on Earth as compactly stowed, lightweight, deployable emergency-exit ramps in buildings, land vehicles, and aircraft.

Lying lengthwise along the track are two stainless-steel tubular spring (STEM™, or equivalent) elements that can be pushed flat, against their springiness, for stowage. These elements provide the required strength, stiffness, and deployment force. Five crosswise aluminum alloy battens are attached to the STEM™ (or equivalent) elements. Thin stainless-steel tracks are located on the outboard side of each spring element; in the original spacecraft application, these are the surfaces along which the vehicle wheels are intended to roll. The tracks are attached to the STEM™ (or equivalent) and battens by screws and rivets, respectively. The tracks play a large role in reacting all inplane shear loads.

A lightweight aromatic polyamid/epoxy open-weave mesh covers the midspan of the ramp over most of its length. The mesh is attached to, and sandwiched between, the STEM™ (or equivalent) elements and tracks, and is pocketed for restraint at each batten. A cylindrical spool is attached to the outboard tip of each track and centered on the axis of the corresponding STEM™ (or equivalent) element. The spools assist during initiation of roll-up for stowage.

The inboard end of each STEM™ (or equivalent) element is fastened to a shim, which in turn, is attached to a mounting surface. Continuous strips of stainless-steel/nylon hybrid hook-and-pile material are attached to the outer sides of the top and bottom surfaces of the tracks. These strips resist peeling with just enough force to reduce the speed of unrolling and to damp spurious unrolling movements, ensuring coordinated deployment movement like that of a carpet unrolling from a fixed end.

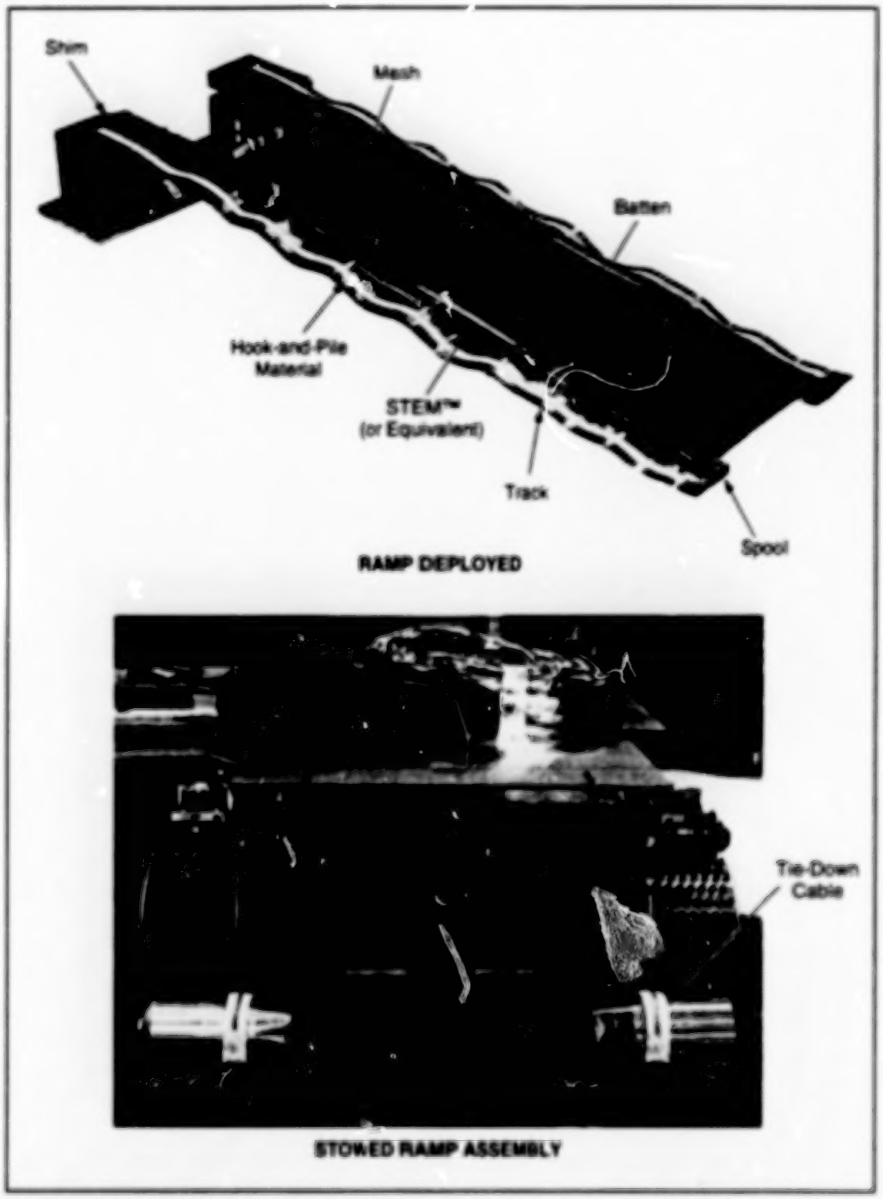

The Ramp Can Be Rolled into a cylinder for compact stowage until needed. On command, it unrolls itself under its own spring force.

When stowed, the ramp is rolled up into a cylinder 7.62 cm in diameter and 42 cm long. Once the pyrotechnic devices are actuated, it takes the ramp about 1 second to unroll to its full length of 136 cm.

This work was done by Lee Sword, Howard Eisen, and Curtis Tucker of Caltech and Brian Spence, Keith Edwards, Jack Sanders, and Geoff Marks of Astro Aerospace for **NASA's Jet Propulsion Laboratory**. *Further information is contained in a TSP [see page 1].*

Inquiries concerning rights for the commercial use of this invention should be addressed to the Patent Counsel, NASA Resident Office-JPL [see page 1]. Refer to NPO-19906.

Portable Computer Workstations for Engineering Teams

Units could be assembled in modular fashion to perform specific team engineering tasks.

NASA's Jet Propulsion Laboratory, Pasadena, California

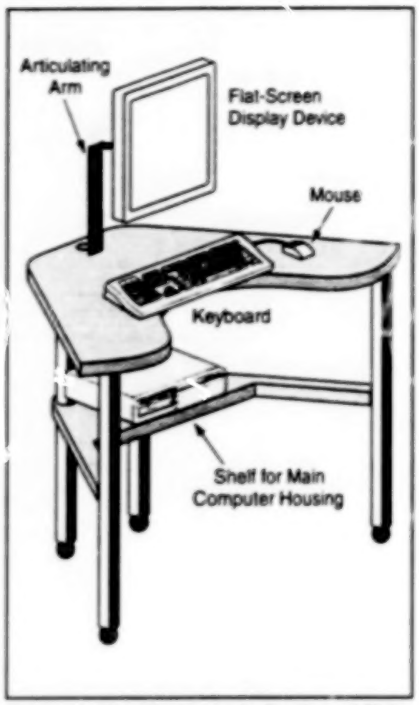

Figure 1. The **Ergonomic Design of This Unit** would provide for efficient utilization of space and adjustability for the user's comfort.

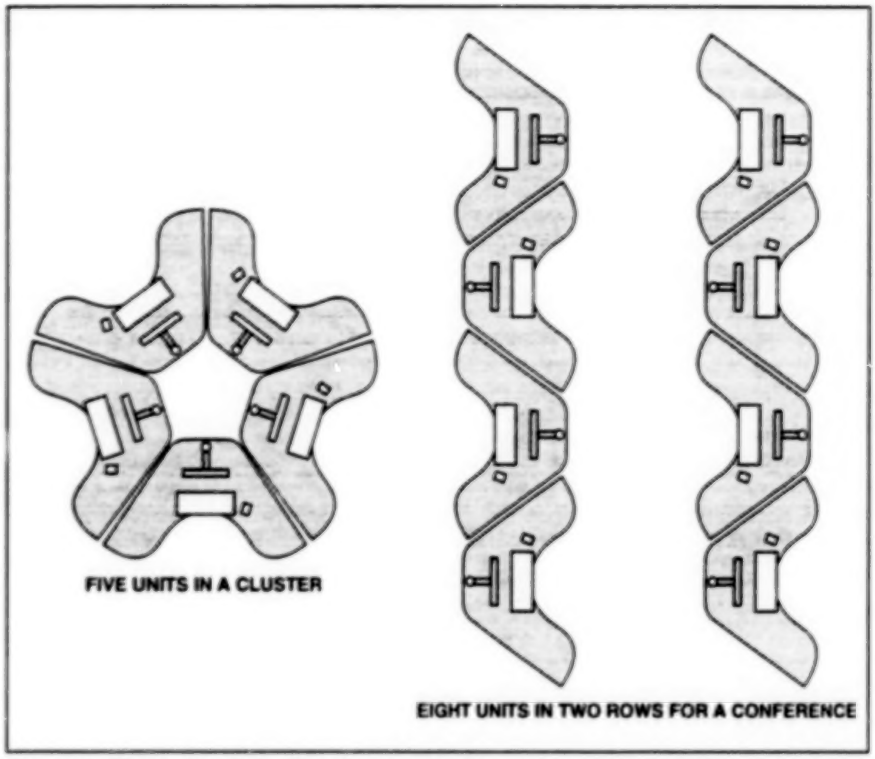

Figure 2. **These Are Only Two** of many possible ways in which multiple units could be arranged to promote collaboration among multiple users.

Figure 1 illustrates a proposed ergonomically designed unit of furniture that would house a personal computer workstation. The unit could be used alone but is meant to be assembled with other such units in modular fashion for use by an engineering design team. The unique configuration of the unit is chosen to facilitate face-to-face verbal and visual communication and thereby promote collaboration among engineers on the team who specialize in different disciplines.

The main computer housing would be placed on the shelf below the table to maximize the work space available to the user on the table. The shelf would be set back to provide room for the seated user. The height of the table could be adjusted to suit the user, or to enable storage of the unit under a conference table or other piece of furniture.

The computer video output would be presented on a large, high-resolution, flat-screen display device, which would be mounted on an articulating arm that the user could adjust to position and orient the screen for comfort in viewing. The articulating arm could also be used to fold the screen out of the way for storage.

The peculiar nonrectangular shape of the table is chosen to please the eye and to promote creativity. Because of its bilateral symmetry, the table would be suitable for either a right- or a left-handed user. The unit would be light in weight and mounted on wheels for portability. Multiple units could readily be wheeled together in any of a large variety of cluster or line arrangements (see Figure 2) according to the number of collaborators and the preferred mode of interaction.

This work was done by Danette G. Klein and James Duke of Caltech for **NASA's Jet Propulsion Laboratory**. *Further information is contained in a TSP [see page 1].*

NPO-20010

Planetary Speed Reducer With Balls Instead of Gears

The basic design can be adapted to numerous applications.

NASA's Jet Propulsion Laboratory, Pasadena, California

A novel friction-drive speed-reducing mechanism weighs less and occupies less space than does conventional gearing. This speed reducer can be manufactured readily with loose dimensional tolerances, does not have to be lubricated, and can function even when contaminated with dust. The basic design gives a reduction ratio of about 150 to 1 and can be readily modified to obtain other reduction ratios. The basic design can also be miniaturized and adapted to a variety of applications that could include miniature robots, small instruments, and toys.

This speed reducer (see figure) has a differential planetary configuration, but with balls instead of planet gears and cones instead of ring gears. A spring presses the balls between two cones, one of which is stationary, the other of which can rotate and is connected to an

output shaft. The conical tapers are chosen to make the radius of contact between the stationary cone and the balls slightly greater than the corresponding radius for the rotating cone. Rotation of an input shaft causes the balls to rotate in planetary fashion. The small difference between the radii of contact produces a differential rotation that is coupled to the output shaft.

This work was done by Donald B. Bickler of Caltech for **NASA's Jet Propulsion Laboratory**. *No further documentation is available.*

In accordance with Public Law 96-517, the contractor has elected to retain title to this invention. Inquiries concerning rights for its commercial use should be addressed to

Technology Reporting Office
JPL
Mail Stop 122-116
4800 Oak Grove Drive
Pasadena, CA 91109
(818) 354-2240

Refer to NPO-19951, volume and number of this NASA Tech Briefs *issue, and the page number.*

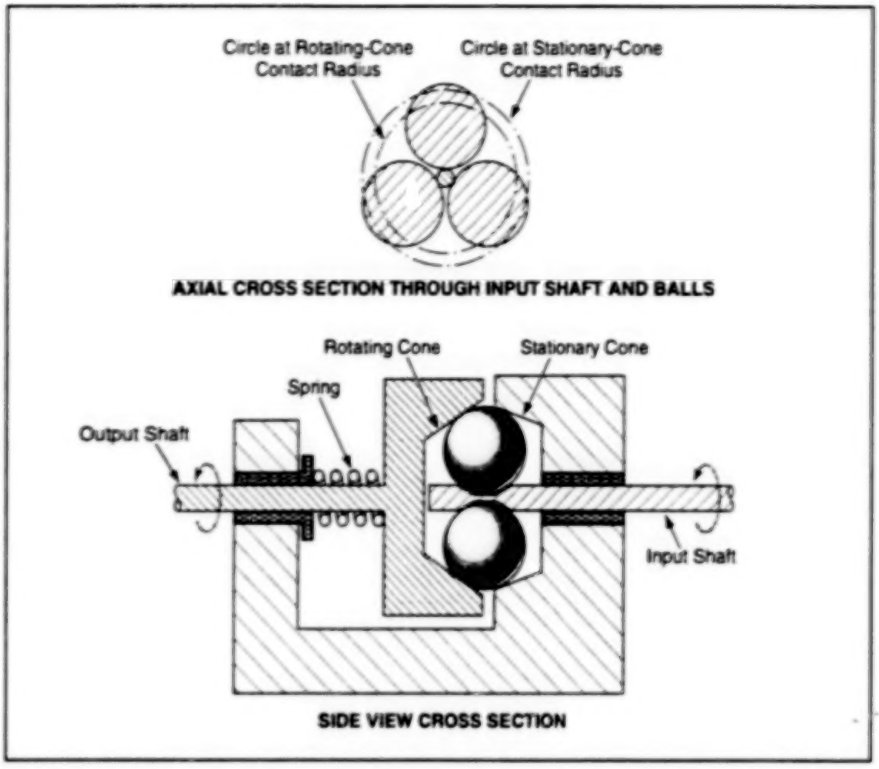

The **Balls and Cones** function analogously to planet gears and ring gears. The speed-reduction ratio depends on the ratio between the radii of contact of the two cones with the balls.

Identifying Loose Joints in an Adaptive Truss Structure

Gaps are measured in a sequence of static force-vs.-displacement measurements.

NASA's Jet Propulsion Laboratory, Pasadena, California

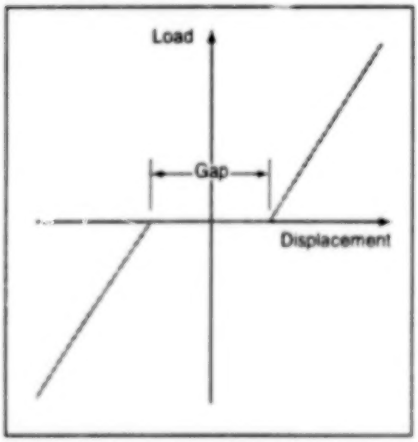

Figure 1. The **Load-vs.-Displacement Curve** for a member with a loose joint is nonlinear in that it exhibits zero stiffness within the looseness gap and nonzero stiffness on both sides of the gap.

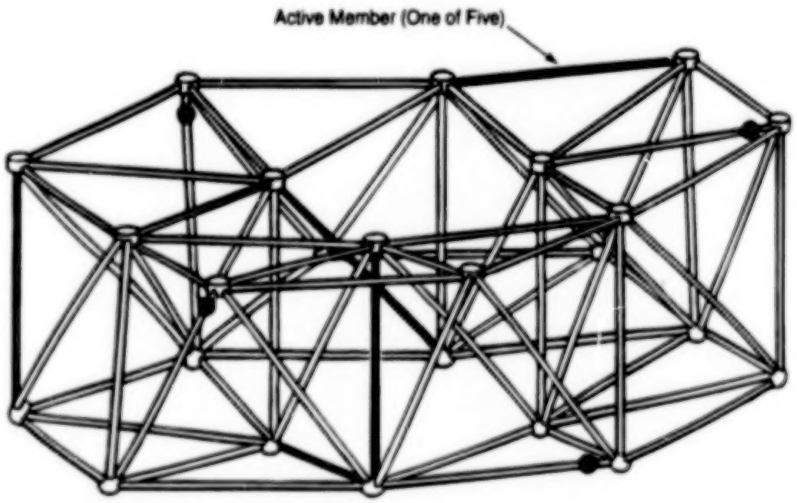

Figure 2. This **Adaptive Truss Structure** contains five active members. The black balls shown near the ends of four of the passive members indicate that the joints at those ends of those members are loose.

A method of identification of loose joints in an adaptive truss structure is based on identification of nonlinear force-vs.-displacement behaviors in the structural members connected via the loose joints (see Figure 1). "Adaptive truss structure" as used here denotes a truss structure, at least some of the members of which are active (see Figure 2). An active member is one that contains an actuator that can apply a controllable force to the ends of the member and/or cause a controllable change in the length of the member.

Truss structures are made adaptive to provide active control for suppression of vibrations and/or to maintain precise geometric relationships among optical components mounted on the structures. Accurate knowledge of the stiffness characteristics of a structure is necessary for precise control. It is important to identify loose joints because looseness gives rise to large changes in stiffness. When either or both joint(s) at the end of a member is (are) loose

and the state of the structure is such that the ends of the member lie within the looseness gap, then the member does not interact with the rest of the structure and thus does not contribute to the stiffness of the structure. The effect on the structure is equivalent to that of removing the member.

The method of identification of loose joints involves instrumenting the structure with displacement sensors and using some or all of the actuators that are already in the structure. First, some combination of actuators is used to stress the structure enough to close all gaps. With all gaps closed, the structure can be expected to exhibit linear load-vs.-displacement characteristics.

Next, the applied loads are decreased by small amounts while the corresponding decrements in the displacements are measured. If there is a loose joint, then at some point in the unloading process, the gap in it will open. A nonlinearity in the plot of load-vs.-displacement data obtained in this unloading process indicates that a gap has opened somewhere in the structure. When the unloading process is complete, the accumulated number of such nonlinearities indicates the total number of gaps that have opened and thus the number of loose joints.

Once the number of loose joints has been established, their locations and the sizes of the gaps in them are determined, one by one, in a recursive sequence of measurements and calculations. In this sequence, known displacements are applied via the active members and the displacements of the ends of the other members are measured and compared with displacements computed according to linear (no-gap) force-vs.-displacement relations to identify specific gap-opening nonlinearities in joints in which they occur.

This work was done by Robin J. Bruno of Caltech for **NASA's Jet Propulsion Laboratory**. *Further information is contained in a TSP [see page 1].*
NPO-19415

Model-Based Placement of Gearbox-Monitoring Accelerometers

Locations are ranked with respect to utility for measuring vibrations to diagnose faults.

Lewis Research Center, Cleveland, Ohio

A model-based methodology has been devised as a systematic means for selecting locations of accelerometers on a helicopter gearbox to measure vibrations indicative of cracked or pitted gear teeth, damaged bearings, and other gearbox faults. In the envisioned application, the outputs of the accelerometers would be fed to an onboard computer and processed to diagnose faults during flight. However, it is not practical to install and process the readings of a large number of accelerometers, each positioned on or near a gearbox component vulnerable to failure. The problem then becomes one of selecting locations for a limited number of accelerometers in such a way as to obtain the required diagnostic capability to some quantifiable degree. The methodology offers a solution that involves quantification of the significance of each accelerometer and its location in diagnosis.

Ideally, the significance of each accelerometer and its location could be determined empirically by comparing the results of diagnoses performed with and without the accelerometer. However, to be able to do this, one would need a comprehensive set of measurement data associated with all possible faults; in general, such a set of data is not available. The methodology provides a partial substitute for such an empirical assessment, on the basis of (a) relationships between component faults and accelerometer readings as expressed by an influence mathematical model obtained from (b) a lumped-masses-and-springs simplified mathematical model of the vibrational properties of the gearbox.

The influence model is used to compute the following three indices that represent the effectiveness of accelerometers for monitoring various gearbox components:

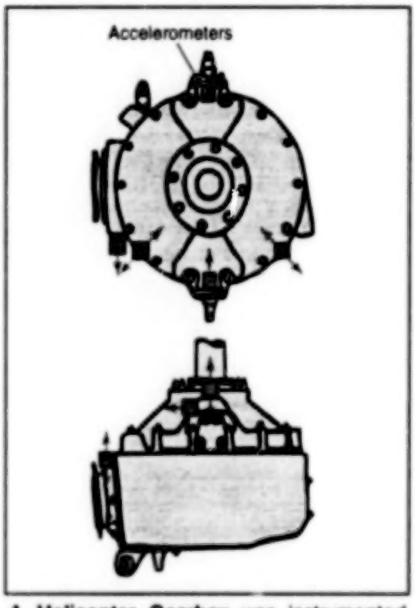

A Helicopter Gearbox was instrumented with accelerometers at eight locations for experiments on monitoring vibrations to diagnose faults.

- The diagnosability index for each component is defined as a sum of coefficients of influence of that component on all the accelerometers, and is taken to be an indication of the ability to diagnose a fault in that component.
- The coverage index of an accelerometer is defined as a sum of coefficients of influence of all gearbox components on that accelerometer, and is taken as a measure of the "reach" or "coverage" of the accelerometer; that is, of the number of gearbox components that the accelerometer can monitor.
- The redundancy index of an accelerometer is a measure of the overlap of the sensory domain of that accelerometer with the sensory domains of other accelerometers; an accelerometer is deemed to be redundant if the components it covers are already covered, with greater coefficients of influence, by other accelerometers.

Accelerometers alone or in groups can be ranked according to the effects of the deletion of the specified accelerometers upon these indices. Those accelerometers, the deletion of which would result in the greatest losses in the values of these indices, are ranked highest to indicate their significance in diagnosis.

This model-based methodology was tested in experiments on an OH-58A main rotor gearbox. In the experiments, piezoelectric accelerometers were installed at eight locations on the gearbox (see figure) and used to measure vibrations in five tests that lasted for various numbers of days. During the tests, nine pitting failures and two cracking failures occurred. The outputs of the accelerometers were digitized and processed by diagnostic algorithms. The model-based methodology was applied and used to rank the individual accelerometers. These rankings were found to agree well with rankings obtained empirically.

This work was done by Vinay B. Jammu, Kerning Wang, and Kourosh Danai of The University of Massachusetts and David G. Lewicki of the Propulsion Directorate of the U.S. Army Research Laboratory for **Lewis Research Center**. *Further information is contained in a TSP [see page 1].*

Inquiries concerning rights for the commercial use of this invention should be addressed to NASA Lewis Research Center, Commercial Technology Office, Attn: Tech Brief Patent Status, Mail Stop 7-3, 21000 Brookpark Road, Cleveland, Ohio 44135. Refer to LEW-16452.

Improved Spherical Gas Bearing

The improved bearing makes a ball-and-socket joint nearly frictionless.

Lyndon B. Johnson Space Center, Houston, Texas

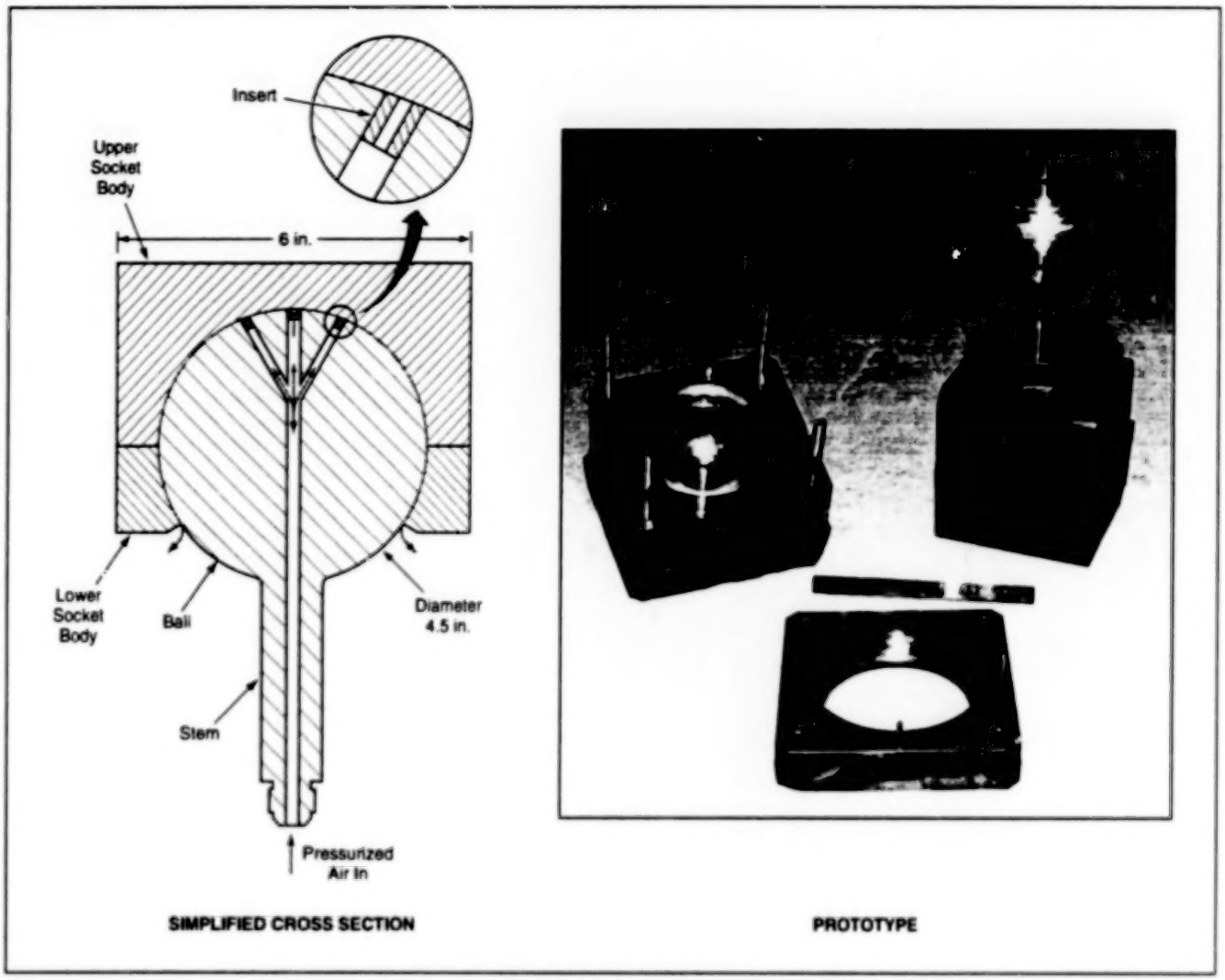

This Improved Spherical Gas Bearing is basically a ball-and-socket joint lubricated by pressurized air that is injected via holes in the ball. The prototype was made from stainless steel and aluminum bronze.

A spherical gas bearing that serves as a low-friction ball-and-socket joint incorporates improvements over older spherical gas bearings. The improvements are such as to create a safer joint that is even closer to being frictionless. Also in comparison with a typical older spherical gas bearing, the improved bearing can be manufactured at lower cost, can be made smaller for the same load capacity, and offers more freedom of rotation. Researchers at the Johnson Space Center use this spherical gas bearing with various satellite mockups to simulate the frictionless conditions of microgravity for crew training. Bearings like this one can also be used in other applications to provide rotational freedom with low friction for large loads.

This spherical gas bearing offers advantages over other means of supporting large loads; such means include magnetic levitation and alternative joints. Both conventional (non-gas-bearing) ball-and-socket and rod-end joints can support large loads, but they exhibit high levels of internal friction. Magnetic levitation relies on sophisticated control systems that consume much power and that induce undesirable eddy currents and magnetic fields. In comparison with the present spherical gas bearing, older types of spherical gas bearings are more expensive to manufacture because they include jeweled orifices in gas passageways that are machined into their sockets. Moreover, unlike the present spherical gas bearing, older spherical gas bearings generally have no provisions to contain their balls in their sockets, so that the older bearings are less safe.

This spherical gas bearing has a basic ball-and-socket configuration and includes three major components: (1) a ball with an integral stem, (2) an upper socket body that contains a hemispherical socket, and (3) a lower socket body that contains a partial continuation of the spherical socket surface and that includes a hole through which the stem passes (see figure). These components can be made from any number of metal alloys or a combination of metal alloys.

The upper and lower socket bodies start out as square (viewed along vertical lines) blocks, and the spherical depressions that constitute the bearing surfaces are machined into them, with the center lines

of the spheres coincident with the vertical center lines of the blocks. The diameter of the socket is slightly larger than that of the ball. The lower socket body serves mainly to prevent inadvertent separation of the bearing — an important safety consideration in applications that involve interactions with humans. In addition, changes in the mounting of the lower socket body cause changes in airflow patterns and in the level of clearance between the ball and the upper socket body.

The stem is used to rigidly attach the bearing to a mount and to deliver pressurized air to the narrow radial gap between the ball and socket surfaces. A passageway for the pressurized air is machined through the center of the ball and along the axis of the stem. The pressurized air enters through a single orifice at the base of the stem. Near the top of the ball, branch passageways deliver the pressurized air to exit holes, the number and arrangement of which can be chosen to maximize the load capacity of the bearings. The exit holes contain bronze inserts (in place of the jeweled inserts of older designs).

Once the socket is assembled around the ball and pressurized air is supplied, the gap between the ball and socket becomes filled with pressurized air, which exerts an upward force on the socket. When the net upward force of the air equals the weight of the socket plus any attached load, the socket levitates, allowing more air to enter the cavity. The film of pressurized air continues to increase until equilibrium is reached between the pressure and volume of the incoming air and the load on the socket. Traveling fully along the surfaces of the ball/socket interface and then dissipating into the atmosphere, the air serves as a lubricant, centering the socket on the ball and preventing contact between the ball and socket surfaces.

This work was done by Thomas Smith of **Johnson Space Center**. *No further documentation is available.*
MSC-22718

Focus-Ring Mechanism Translates Lenses Without Rotation

The parts of the mechanism need not be highly precise.

NASA's Jet Propulsion Laboratory, Pasadena, California

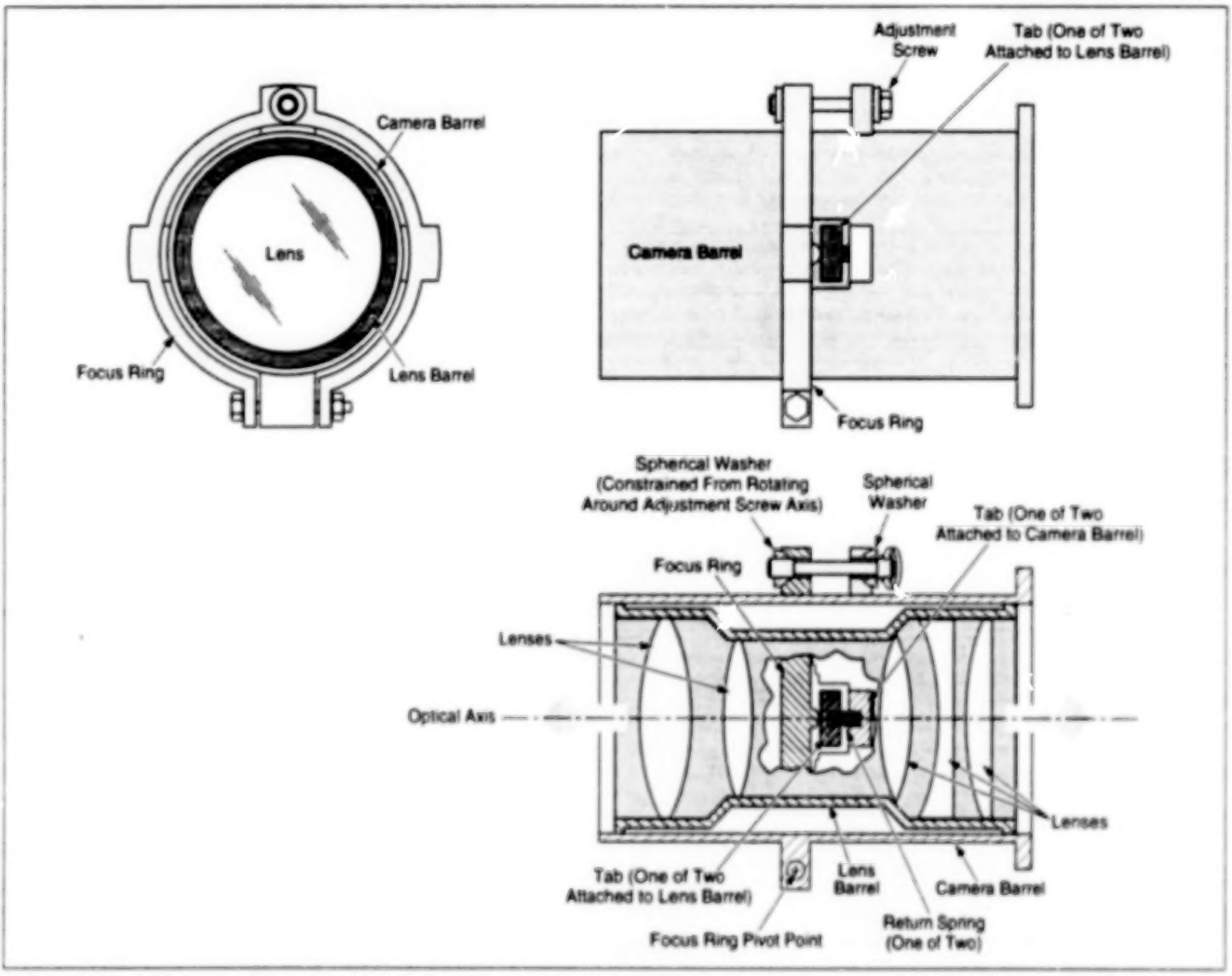

Rotation of the Adjustment Screw pivots the ring slightly, causing the ring to push on the tabs and thereby translate the lens barrel along the optical axis.

The figure illustrates a camera lens barrel and a mechanism for translating the lens barrel along its optical axis. Unlike some other focusing mechanisms, this one does not rotate the lens barrel about the optical axis — an essential feature if the lenses and/or other optics in the barrel are asymmetric and are required to be kept in a specified alignment with respect to a line in the focal plane.

The lens barrel slides axially within a stationary camera barrel. The mechanism

includes a focus ring that is approximately concentric with the barrels. The focus ring pivots about a fixed point under the camera barrel, and the tilt of the ring can be varied by use of an adjustment screw atop the camera barrel. As the tilt of the ring changes, it pushes axially on (or allows itself to be pushed axially by) tabs on the lens barrel. These tabs are spring-loaded against similar but fixed tabs on the camera barrel. As the tabs on the lens barrel push against (or are pushed by) the spring load, the lens barrel translates along the axis.

The adjustment screw could be any of a variety of suitable screws with standard fine pitches, e.g., 32 threads per inch [pitch of 0.3125 in. (about 0.79 mm)]. Because the point of contact between the ring and the lens barrel is halfway along the lever arm, the axial translation of the lens is half that of the adjustment screw. Thus, continuing the above example, one full turn of the screw translates the lens assembly about 0.016 in. (0.4 mm), while a partial turn of 10° translates the ring only about 0.00043 in. (0.011 mm).

The only motion-producing surfaces that need be machined to high precision are the outer-diameter surface of the lens barrel and the inner-diameter surface of the camera barrel; these surfaces are required to mate with each other in a smooth sliding fit with minimal radial play. The parts of the focusing mechanism can be fabricated without high precision. The adjustment screw and the spherical bearings on which the ends of the adjustment screw turns can be fabricated easily and inexpensively.

The mechanism can be upgraded in several ways. The adjustment screw could be modified to accept a motor drive so that the lens system could be focused under remote control. The adjustment screw could be made as a differential screw by machining it with dual threads, each having a slightly different pitch; this would greatly increase the resolution of the focus adjustment. Radial play could be eliminated by mounting the lens barrel on flexures configured to allow movement along the optical axis; in that case, it would no longer be necessary to enclose the lens barrel in a camera barrel.

This work was done by Richard E. Fleischner of Caltech for **NASA's Jet Propulsion Laboratory**. *Further information is contained in a TSP [see page 1].*
NPO-19711

Books and Reports

Using Genetic Algorithms To Plan a Spacecraft Landing

A report summarizes a study in robust flightpath planning for a low-lift spacecraft to land on Mars. The basic problem was one of optimization: to plan a sequence of control actions — specifically, shifts in the position of an internal proof mass to change the center of mass of the spacecraft and thereby shift its angle of attack — to make the final landing position as insensitive as possible to such perturbations as errors and uncertainties in approach-trajectory parameters and in mathematical modeling of the Martian atmosphere. In the study, landing trajectories were computed by a nonlinear mathematical model of the descent dynamics, and optimization was performed by use of genetic algorithms to minimize a quadratic cost function of the landing miss distance over several realistically perturbed trajectories. It was found that by suitable scheduling of proof-mass shifts, the perturbed trajectories could be made to coalesce to a "bounce and drop" form, with root-mean-square landing errors reduced from 111 to 43 km. The results of this study also indicate that while genetic algorithms require long processing times (200 hours in this case), they are fairly easy to program and can provide useful solutions to complex optimization problems.

This work was done by David S. Bayard and Hamid Kohen of Caltech for **NASA's Jet Propulsion Laboratory**. *To obtain a copy of the report, "Robust Flight Path Determination for Mars Precision Landing Using Genetic Algorithms," see TSP's [page 1].*
NPO-20185

BLANK PAGE

Machinery

Hardware, Techniques, and Processes

Books and Reports

BLANK PAGE

Designing Electrically Powered Actuators for Aircraft

Flight controls will be operated by relatively lightweight power-by-wire systems.

Dryden Flight Research Center, Edwards, California

Under the Electrically Powered Actuation Design (EPAD) validation program and as part of a joint Air Force/Navy/NASA effort, Dryden Flight Research Center has begun testing an electrohydrostatic actuator (EHA) in its F/A-18 Systems Research Aircraft (SRA). The EHA is a prototype of similar electrically powered flight-control actuators that promise to significantly reduce the weights, costs, amounts of needed logistical support, and amounts of needed maintenance of future aircraft.

The EHA operates the left aileron in the F/A-18 aircraft, without use of a conventional hydraulic system that would ordinarily power multiple hydraulic mechanisms in the aircraft. The EHA includes a hydraulic subsystem that contains a small (in comparison with a conventional hydraulic system) amount of hydraulic fluid. Taking its signals directly from a flight-control computer in the aircraft, the EHA uses electrical power generated by the aircraft engines to drive the pump in its hydraulic subsystem.

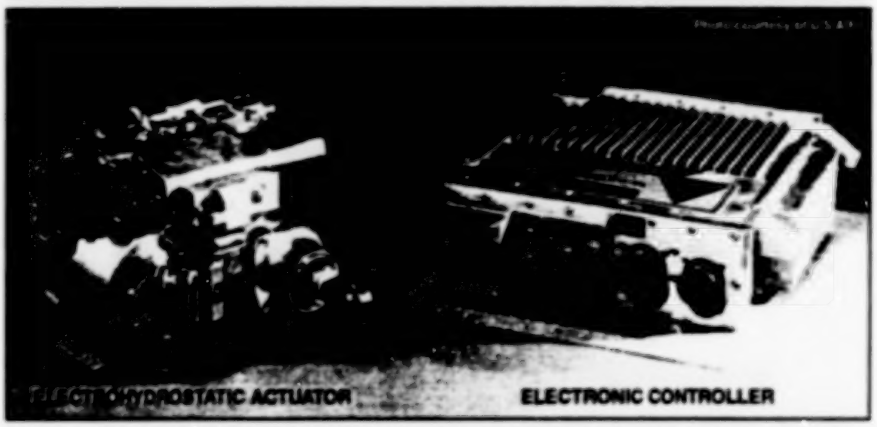

Figure 1. This Flight-Control Actuator comprising an electrohydrostatic actuator and electronic controller are used to operate the left aileron in the F/A-18 Systems Research Aircraft, without need for the usual central aircraft hydraulic system.

Figure 2. Flight Tests of the flight-control actuator in the F/A-18 Systems Research Aircraft were begun in January 1996.

For many years, NASA, the U. S. Air Force, and the U. S. Navy have sought to eliminate sophisticated but heavy hydraulic systems in aircraft in favor of electrical "power-by-wire" systems for operating flight controls. Besides reductions in weight, cost, and the amount of needed support, the incorporation of such electrical systems eliminates the need for hydraulic lines in fuselages and wing boxes, thereby diminishing vulnerability in combat. The power-by-wire arrangement will also reduce complexity and increase reliability.

A major milestone on the road to an all-electric airplane, the EHA offers the potential to eliminate or minimize dependence on pneumatic, hydraulic, and related mechan-

ical systems during flights of future aircraft. The EHA and systems related to the EHA could lead to fuel saving between 5 and 9 percent on an all-electric passenger airplane, a reduction of 30 to 50 percent in the amount of needed ground equipment, a reduction of takeoff weight by 600 to 1,000 lb (270 to 450 kg), and a 14-percent reduction in the portion of the area of a military aircraft that is vulnerable to such threats as small-arms fire.

The U. S. Air Force Wright Laboratories (in Ohio) managed the overall EPAD EHA program. Contractors included Lockheed Martin (Binghamton, New York), which was responsible for the EHA electronic circuits and other components; Vickers Electro-Mech (Wichita, Kansas and Jackson, Mississippi), for the pump and motor; Dynamic Controls Incorporated (Dayton, Ohio) for the power-control unit and interface control electronics; and Dowty Aerospace (Los Angeles, California) for the assembled actuator. Dryden Flight Research Center performed ground testing, installed and integrated the EHA in the SRA, provided the necessary data-acquisition systems, and was responsible for flight safety.

The EHA is the second of three actuators to be tested under the EPAD program. In May 1993, Dryden Flight Research Center first flew the SRA with a "smart" actuator sponsored by the U. S. Navy and built by H. R. Textron. The third actuator is an electromechanical one that Dryden will fly on the SRA at the end of 1997.

This work was done by Gordon Fullerton, Harry Miller, Robert Navarro, Mauricio Rivas, Joel Sitz, Bob Varanai, and Eddie Zavala of **Dryden Flight Research Center**; *Gavin Jenney of Dynamic Controls, Inc.; Dave Dawson of Wright Laboratories; Dennis Trosen of the U. S. Air Force; Sean Donley of the U. S. Navy; and Joe Dutko of Lockheed-Martin. No further documentation is available.*

In accordance with Public Law 96-517, the contractor has elected to retain title to this invention. Inquiries concerning rights for its commercial use should be addressed to

Bob Webb
Lockheed Martin
600 Main St.
Johnson City, NY 13790-1888
(607) 770-2937

Refer to DRC-96-09, volume and number of this NASA Tech Briefs *issue, and the page number.*

Quantifying Gear Damage by Optimal Tracking of Vibrations

A one-dimensional mathematical model of gear-mesh dynamics yields useful results.

Lewis Research Center, Cleveland, Ohio

A technique for quantifying damage in gear teeth in a transmission is based on the observation that damage (which can include wear, pits, and fractures) alters the gear-mesh stiffness and thereby alters the vibrations of the transmission during operation. The essence of this technique is to process vibration measurements (instantaneous amplitude as a function of time or gear angle) to estimate the time-varying gear-mesh stiffness and quantify deviations from the periodic mesh-stiffness variations of gears in good condition. The technique involves mathematical modeling of gear-mesh dynamics coupled with nonlinear numerical optimization.

The gear-mesh dynamics are represented by a one-dimensional mathematical model equivalent to the model of a mass m (roughly, the mass of a pinion in mesh with a larger gear) suspended on a spring with time-varying stiffness $k(t)$ and moving in a frictional medium with damping coefficient c. The time-varying spring stiffness is set equal to the time-varying gear-mesh stiffness and represented as

$$k(t) = k_{ave} - k_{periodic}(t) - k_{perturb}(t),$$

where k_{ave} is a constant or time-averaged component, $k_{periodic}$ is the periodic variation in stiffness of the tooth-pass cycles of gears in good condition, and $k_{perturb}(t)$ is a

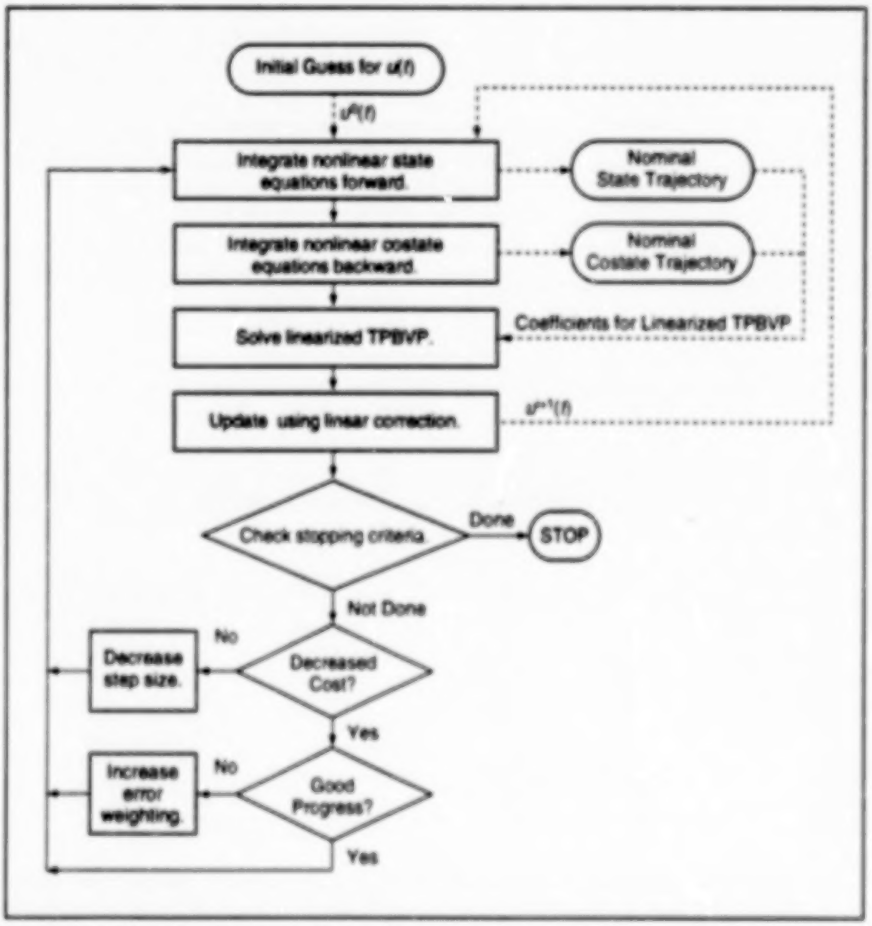

The Optimal-Tracking Problem Is Solved Numerically in an iterative procedure. The objective is to find an approximation for $u(t)$ that minimizes a cost functional.

stiffness perturbation associated with damage. The equation of motion is therefore

$$\ddot{x} + (c/m)\dot{x} + \Omega^2 x = u(t)x,$$

where x is a displacement, t is time, $\Omega^2 = k_{shaft}/m$, and $u(t) = [k_{periodic}(t) + k_{perturb}(t)]/m$. Note that $u(t)$ is proportional to the total of time-varying components of stiffness. By defining state variables $x_1 = \dot{x}$ and $x_2 = x$, one can divide the equation of motion into two equations in state-variable form:

$$\dot{x}_1 = -(c/m)x_1 - \Omega^2 x_2 + u(t)x^2 \text{ and}$$

$$\dot{x}_2 = x_1.$$

Suppose that vibration measurements $\tilde{x}_2(t)$ corresponding to the modeled state variable $x_2(t)$ are acquired during the interval $[t_0, t_f]$. The problem is to find the function $u(t)$ that makes the model output $x_2(t)$ approximate the measurement data $\tilde{x}_2(t)$. The problem is solved by following an optimal-tracking approach: The objective in this approach is to minimize a quadratic cost functional that (1) penalizes the deviation of $x_2(t)$ from throughout the interval $[t_0, t_f]$, (2) imposes an additional penalty on the deviation of $x_2(t_f)$ from $\tilde{x}_2(t_f)$, and (3) penalizes too large an estimate of $u(t)$ throughout the interval $[t_0, t_f]$. In the optimal-tracking formulation, the state-variable equations of motion are treated as equality constraints imposed on the minimization of cost and as such they are appended to the cost function by use of time-varying Lagrange multipliers, which are governed by differential equations called the "costate equations." The state-variable equations of motion and the costate equations, taken together with a stationarity condition and end-point conditions, constitute the system of equations of a two-point boundary-value problem (TPBVP). The equations are solved numerically in an iterative procedure illustrated schematically in the figure.

The technique was tested on a set of fictitious data generated by a computer simulation of a one-degree-of-freedom mechanical system with time-varying stiffness. The solution of the optimal-tracking problem was found to closely approximate the stiffness profile used in the simulation. In another test, the technique was applied to experimental data from a gear-test rig. Despite the simplicity of the one-dimensional dynamical model, the technique was found to be useful in that changes in the estimated stiffness profile could be correlated with damage.

This technique has further enhanced vibration analysis of the gear transmission done by a previously developed time-frequency Wigner-Ville distribution technique, which gives indications of the type and location, but not the extent of the damage. The two techniques are used together to monitor for the onset of damage during operation of gear trains, or to diagnose gear trains during maintenance.

This work was done by R. C. Hendricks of **Lewis Research Center** *and F. K. Choy, R. J. Vallette, V. Polyshchuk, and M. J. Braun of the University of Akron. Further information is contained in a TSP [see page 1].*

Inquiries concerning rights for the commercial use of this invention should be addressed to NASA Lewis Research Center, Commercial Technology Office, Attn: Tech Brief Patent Status, Mail Stop 7-3, 21000 Brookpark Road, Cleveland, Ohio 44135. Refer to LEW-16454.

Force-Feedback Device for Microsurgery

This device provides an unprecedented combination of accuracy, control, and workspace volume.

NASA's Jet Propulsion Laboratory, Pasadena, California

A force-feedback device for robot-assisted microsurgery measures the position of a user's hand with great sensitivity — within 30 μm in translation and 0.07° in rotation. The device acts as the master manipulator in a master/slave system for extremely precise surgical procedures. It currently provides force feedback to the user in 3 axes with minimal inertia and friction but can be configured for 6-axis force feedback. It is compactly packaged and is symmetric for either right- or left-hand operation.

The device is set up to provide a maximum feedback force of 6 oz (1.7 N), although it can produce a force up to 47 oz (13 N) and a torque up to 42 oz-in. (0.3 N-m). It is preferable to minimize the force feedback in order to minimize friction and reflected inertia. It operates in a work envelope of 50-mm diameter.

The device includes a tendon-driven arm that comprises a base, shoulder joint, midarm link, elbow joint, forearm link, and wrist joint. A stylus for user manipulation is attached to the wrist (see figure). Motions along and around the various axes are decoupled from each other by double-jointed, tendon-driven revolute joints described in "Double-Jointed, Cable Driven Robot Arms" (NPO-19361), *NASA Tech Briefs*, Vol. 20, No. 10 (October 1996), page 1b.

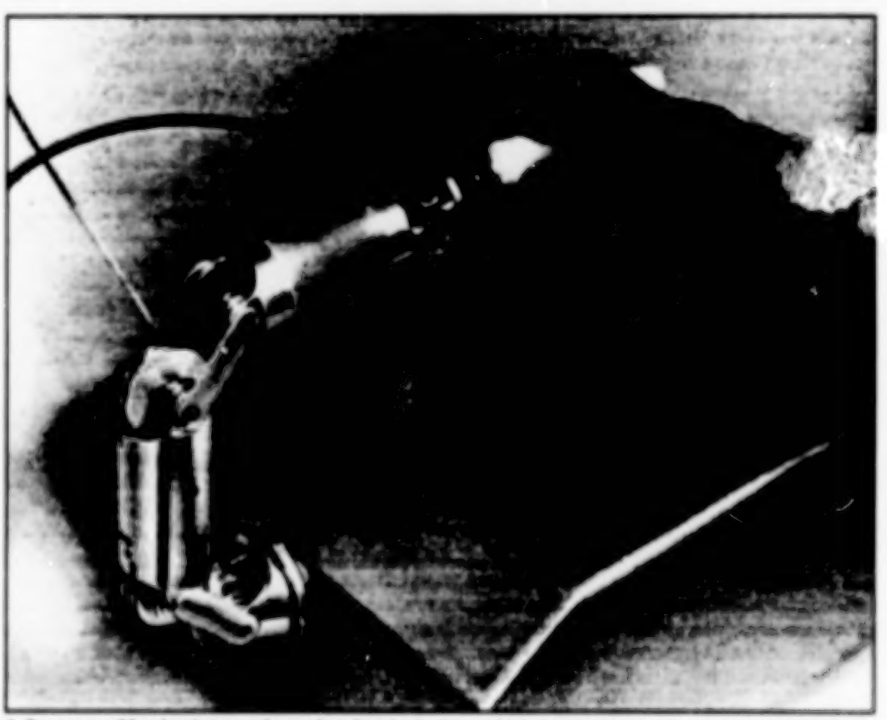

A Surgeon Manipulates a force-feedback device, which is a master robot arm used to control a slave robot arm that performs microsurgical manipulations. The master arm reflects forces and torques from the slave back to the surgeon's hand.

The base houses dc brushless motors that drive the joints between the links to create the force feedback on the torso,

shoulder, and elbow axes. Also in the base are six high-resolution optical encoders (40,000 counts per revolution) that measure the positions and orientations of the arm links. The use of high-resolution optical encoders — one for each axis — reduces the amount of gearing needed to achieve the requisite positional resolution without excessive friction.

This work was done by Timothy Ohm of Caltech for **NASA's Jet Propulsion Laboratory**. *Further information is contained in a TSP [see page 1].*

In accordance with Public Law 96-517, the contractor has elected to retain title to this invention. Inquiries concerning rights for its commercial use should be addressed to

Technology Reporting Office
JPL
Mail Stop 122-116
4800 Oak Grove Drive
Pasadena, CA 91109
(818) 354-2240

Refer to NPO-19822, volume and number of this NASA Tech Briefs issue, and the page number.

Traveling-Wave Rotary Actuators

Piezoelectrically generated traveling waves drive harmonic gears.

NASA's Jet Propulsion Laboratory, Pasadena, California

Two experimental rotary actuators combine the light weight, small volume, and cleanliness of a piezoelectric traveling-wave motor with the positive action and high torque of a harmonic gear motor. The actuators contain piezoelectric inserts that drive flexible spline gears in sinusoidal patterns; the spline gears, in turn, drive internal spur gears.

A conventional piezoelectric traveling-wave motor relies on friction between a driving flexing stator and a driven member. Friction gives rise to elements of uncertainty and slippage. A conventional harmonic gear includes a flexible gear driven by an electromagnetic motor; it produces a large, dependable torque, but the motor and gear are large, complex, and often dirty.

The figure illustrates two experimental rotary actuators. In each actuator, piezoelectric elements attached to a stationary shaft alternately bend a spline gear to larger and smaller radii at several points around the circumference. The piezoelectric elements are activated in sequence so that the teeth on the spline rise and fall in a sinusoidal wave that travels circumferentially. The teeth at the crest of the wave engage an internal spur gear (the output gear) and thus turn the gear as the crest travels around the circumference.

This work was done by Virginia G. Ford and John Kievit of Caltech for **NASA's Jet Propulsion Laboratory**. *Further information is contained in a TSP [see page 1].*
NPO-19261

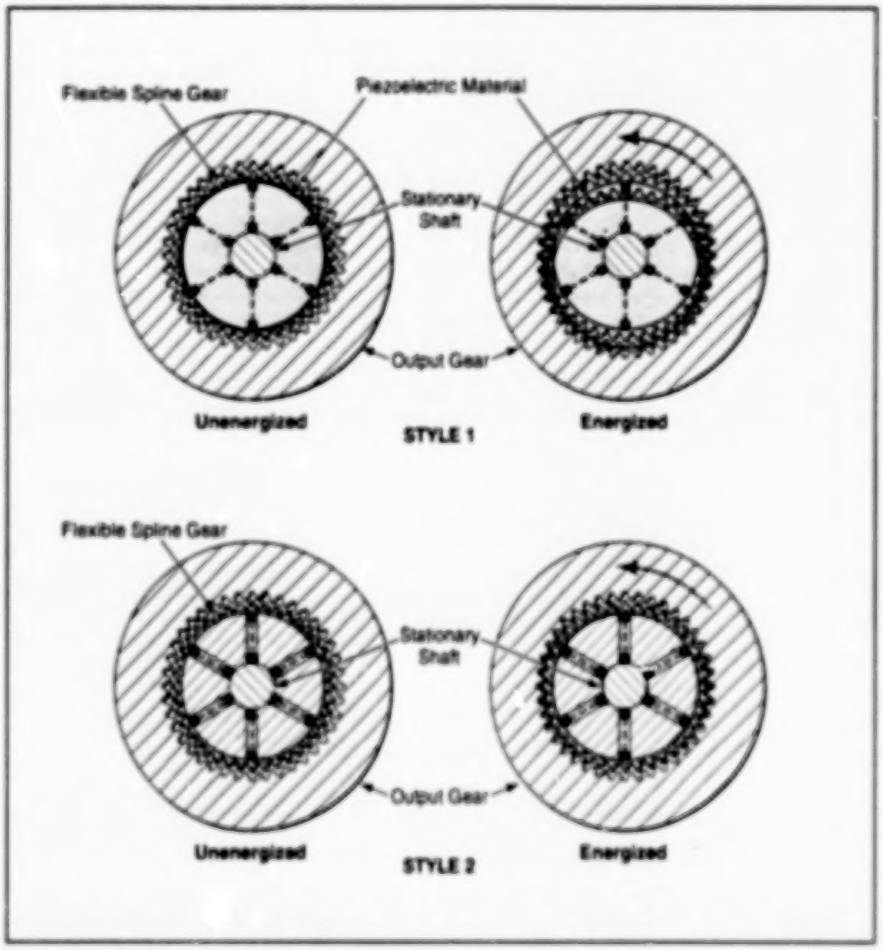

Piezoelectric Elements on a Stationary Shaft create a wave on a flexible spline gear. The spline teeth on the wave engage and drive the teeth of the internal spur gear.

Heat Pump for Quick Warming of Automobile Passenger Space

The air-conditioner would be operated in reverse, drawing on exhaust heat.

NASA's Jet Propulsion Laboratory, Pasadena, California

A proposed system for quick heating of the passenger compartment in a cold automobile would exploit the vapor-compression cycle of an automotive air-conditioner. The system would likely cost and weigh less than do quick-heating systems based on storage and release of heat in phase-change materials. Unlike an electric heater, this system would not impose an excessive additional drain on the automobile battery.

The proposed system would consist mostly of an ordinary automotive air-conditioning system, with some additional switches, valves, and plumbing to enable operation in either the quick-heating mode or the traditional cooling mode. In the quick-heating mode, the vapor-compres-

sion cycle would be run in reverse: whereas the passenger-space heat exchanger serves as an evaporator that takes heat from the passenger space in the cooling mode, it would serve as a condenser that would deliver heat to the passenger space in the quick-heating mode (see figure).

The evaporator for the quick-heating mode would be an additional heat exchanger in direct or indirect contact with the exhaust pipe; this would make it possible to provide much more heat than could readily be extracted from cold ambient air. Even in the coldest weather, a typical cold idling engine produces ample low-grade exhaust condensation heat in the approximate temperature range of 70 to 110 °F (21 to 43 °C). The refrigerant fluid passing through the evaporator would absorb some of this heat, and compression would raise the temperature of the fluid passing through the condenser to about 150 °F (66 °C). This fluid temperature is typical for an automotive heater.

One potential disadvantage of this system is that the chlorofluorocarbon refrigerant fluid of a typical automotive air-conditioner could decompose when exposed to very high exhaust temperatures. It is possible, however, to overcome this disadvantage by use of a thermal switch, such as a manifold, to divert the flow of exhaust from the evaporator once the engine has warmed up. Alternatively, a more stable refrigerant could be used, such as CO_2, which has recently been demonstrated in automobile air-conditioning systems.

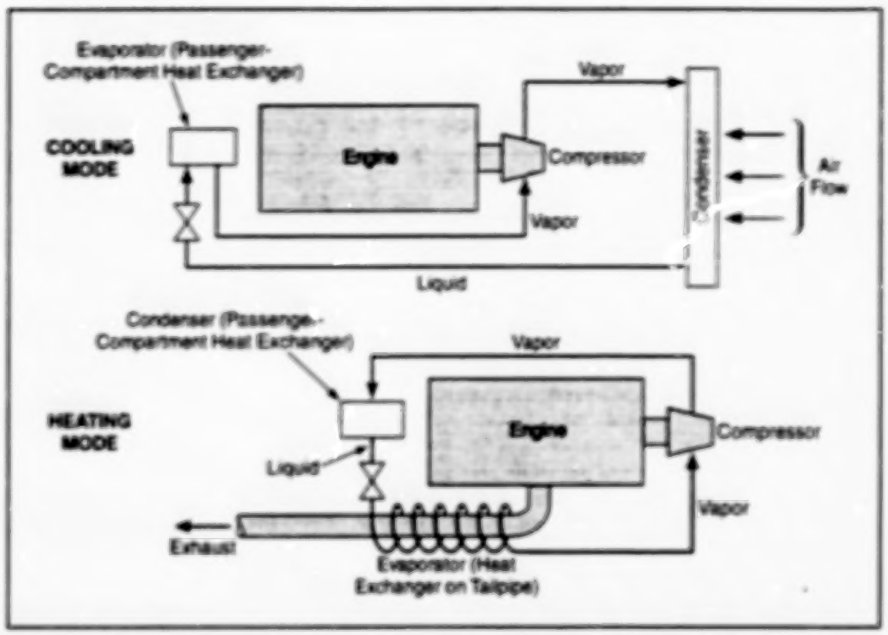

The Vapor-Compression Cycle of the air-conditioner would be exploited for traditional cooling or for quick heating, depending on valve and switch settings that would delineate flow paths.

This work was done by Jack A. Jones of Caltech for **NASA's Jet Propulsion Laboratory**. *Further information is contained in a TSP [see page 1].*
NPO-19868

Rotordynamic Seal and Bearing Tester

This tool advances seal bearing technology through demonstration in a realistic environment.

Marshall Space Flight Center, Alabama

A rotordynamic seal and bearing tester (RSBT) has been developed to provide seal bearing data for space vehicles, such as the Space Shuttle and the Reusable Launch Vehicle. This RSBT is an improved version of an apparatus previously reported in "Dynamic Tester for Rotor Seals and Bearings" (MFS-28493), in *NASA Tech Briefs*, Vol. 15, No. 12 (December 1991), page 80.

The RSBT tool was designed to advance seal bearing technology through demonstration in a realistic environment where data are reliably produced to specify the rotordynamics and load-carrying capacity of seal bearings. Previous experience has shown that conventional testers in which test rotors are supported by ball bearings are ill-designed for testing seal bearings.

The rotor of the RSBT is fully suspended on seal bearings that are the very test article from which the rotordynamic data are to be extracted with the instrumentation of the tester. The tester design is based on the same bulk-flow analysis used for the decision to retrofit the high-pressure turbopumps in the Space Shuttle main engines. The instrumentation is a set of reliable proximity probes, readily accessible from outside the tester housing for calibration and inspection. The test rotor is tubular to supply the test seal bearing and the whirl bushing with lubrication without causing axial thrust. The added benefit is a light rotor that has a high resonance frequency outside the speed range of the rotor.

The squeeze film of the seal bearing generates a strong damping effect that makes the tester dynamically inert. The tester and its rotor are coaxially arranged with a stationary center bolt tying the two housing parts together. The bolt, which runs through the bore of the rotor end to the other end of the rotor, has multiple holes in the head to feed the flow from the outside to the rotor bore.

The whirl bushing, which rides on the rotor, is suspended on its own duplex seal bearing. It is lubricated as orifices ooze liquid from the rotor to the duplex seal bearing gaps. The liquid discharges into axial thrust bearings that axially guide on the whirl bushing ends.

The rotor has two separate rings of orifices to feed the two seal bearings of the whirl bushing independently. Two seal bearings form the duplex seal bearing of the whirl bushing. Thus stabilized against tilt disturbances, the whirl bushing freely spins and generates a strong whirl force that eventually squeezes the seal bearings of the rotor.

The whirl bushing, together with turbines, makes the tester leak-proof. This feature is essential for operating with cryogenics and hazardous liquids. The housing completely encloses the rotor and whirl bushing.

The tubular rotor is driven by its turbine at a constant speed. The speed is recorded with pressure and temperature as the test condition for a certain test. Test runs at different speeds are made when investigat-

ing the effect of the speed on the rotordynamic parameters of a test seal bearing.

Power for the RSBT is provided through pressurized water or any other working fluid of the seal bearings being tested. Therefore, the facility requires pumps for continuous testing or a blow-down tank for short-duration test runs. The RSBT testing facility consists of a laboratory room, the DSAS, a fluid supply, fluid sump tank, pump speed control, vent valves, electric power, a rack, and a tester pedestal.

The design of the RSBT is unique in its simplicity, low cost, and reliability. This tool should eliminate the long-standing misconceptions about fluid bearings and encourage the design of less costly, yet highly reliable, turbopumps, motors, hazardous-material pumps, jet engines, air-conditioners, and nuclear equipment.

This work was done by George L. von Pragenau of Provident Technology for the **Marshall Space Flight Center**. *Further information is contained in a TSP [see page 1].*

Inquiries concerning rights for the commercial use of this invention should be addressed to the Patent Counsel, Marshall Space Flight Center [see page 1]. Refer to MFS-26472.

Books and Reports

Adaptive Footpads With Pyrotechnically Anchored Tethers

A report describes a proposed system for landing a spacecraft on a comet, asteroid, small planet, or other extraterrestrial body with low gravitation. The system would include three terrain-conforming footpads rigid enough to withstand impact on a hard surface and broad enough to land on a soft surface without sinking excessively. Each footpad would be equipped with sensors, a pyrotechnically actuated harpoon, and a winch connected to the harpoon via a tether. The harpoon would include a hard tip for penetrating and anchoring in hard material, plus deployable fins and fabric for anchoring in soft material. In response to sensor outputs, a computer would command the pyrotechnic devices to fire, driving the harpoons into the body. The winch would then be activated to pull the footpads into contact with the body. In computational simulations, the system has been found to be capable of arresting rebound and rollover during landings on terrains with a variety of slopes and obstacles.

This work was done by Randel Lindemann, Donald Sevilla, Kevin Burke, and Greg Gillis-Smith of Caltech for **NASA's Jet Propulsion Laboratory**. *To obtain a copy of the report, "Adaptive Footpad With a Pyrotechnically Anchored Tether for Landing Gear on Low Gravity Planetary Bodies," see TSP's [page 1].*
NPO-20117

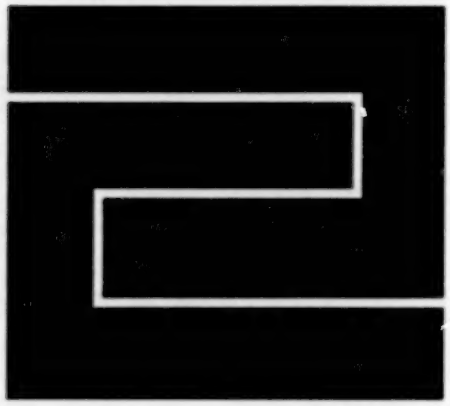

Fabrication Technology

Hardware, Techniques, and Processes

BLANK PAGE

Fabricating and Testing an Ultrathin Mirror

A network of pockets and manifolds minimizes handling and damage risks to mirrors during fabrication and testing.

Marshall Space Flight Center, Alabama

A new method to fabricate and test ultrathin optics has been developed to improve on the traditional process. This method uses a block not only to support the optic during processing but also to support the optic in a nearly strain-free deterministic manner during testing.

The rear surface of the optic (which is larger than the specified dimensions of the finished optic) is ground against the front surface of the block to form matching surfaces. Vacuum, which is applied through a manifold to a network of pockets machined into the block, secures the optic to the block for optical fabrication. For testing, the air is forced through the manifold, floating the mirror on a uniform film of air between the block and the optic.

The network of carefully designed pockets and manifolds is machined into the front surface of the block before it is ground against the rear surface of the optic. Each pocket consists of a central vent, a land, and an annular exhaust vent. Two manifolds are used to connect the pockets — one connects all the central vents, the second connects the annular exhaust vents.

The mirror blank is firmly attached to the block for machining to near final thickness, fine grinding, polishing, and figuring by applying and maintaining a partial vacuum on both the central and exhaust vents. The annular exhaust vents and the separate manifold are required for subsequent operations when the pockets are used to support the mirror during testing. The partial vacuum, as well as the number, spacing, and pocket design are chosen to minimize the deflection of the optic into the pockets during machining, grinding, and polishing.

This network of pockets and manifolds is also used to supply abrasive slurry to the interface between the optic and the block during match grinding operations. During grinding, a change to a finer abrasive can be made without removing the optic from the block by simply feeding a finer abrasive slurry through the manifolds, flushing away the coarser abrasive. When grinding is complete, the interface between the optic and the block is cleaned without separating the two components. Water or other cleaning fluid is pumped through the manifolds, flushing away any remaining abrasive slurry. If necessary, dry air can be blown through the manifolds to evaporate any remaining cleaning fluids. This *in situ* cleaning reduces the risk to the optic by eliminating the need to lift and handle the optic.

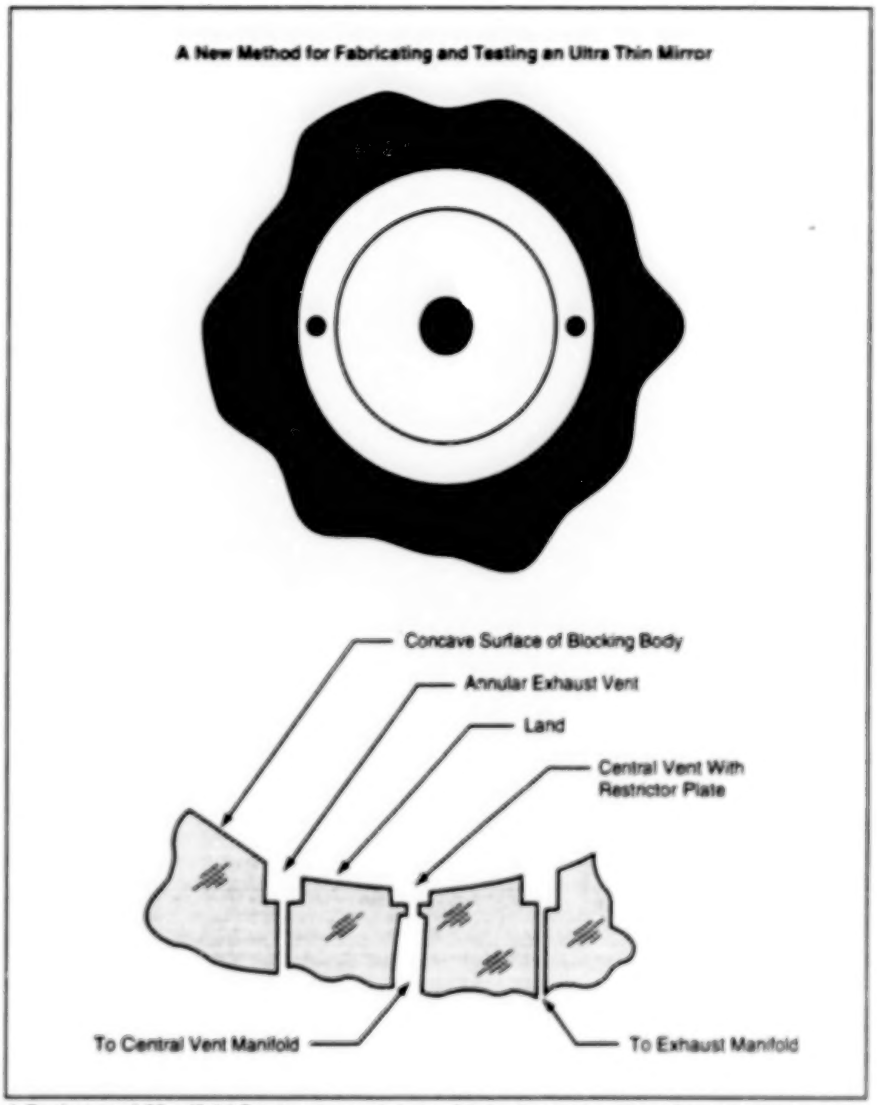

A **Pocket-and-Manifold System** is used during fabrication and testing of an ultrathin mirror.

Upon completion of the match grinding and cleaning, the front surface of the optic, attached to the body by vacuum, is machined to near-final thickness, fine ground, polished, and figured.

Support for in-process and final testing of the optic is accomplished by supplying air or a similar gas through the central vent of each pocket. This gas is vented through the annular exhaust ring surrounding each central vent. The airflow through each central vent is controlled by a precision restrictor plate. If the total cross-sectional area of the restrictor plates is small compared to the capacity of the supply manifold and the annular exhaust vents, the air pressure at the inlet of each restrictor plate will be identical. This will result in an equal, normal pressure being exerted on the mirror at each pocket since an equal amount of gas is flowing through each of the orifices. Using this known force, the thickness of the optic, and the configuration of the pockets, the gravity-induced deformation of the optic can be determined and subtracted from the measured figure of the optic to obtain the actual figure. *In situ* testing eliminates handling of the thin, fragile optic and the associated risks.

This work was done by Howard D. Hall of **Marshall Space Flight Center**. *Further information is contained in a TSP [see page 1].*

MFS-31174

Holographic Lithography With Phase Feedback

Better gratings can be made at lower cost.

Marshall Space Flight Center, Alabama

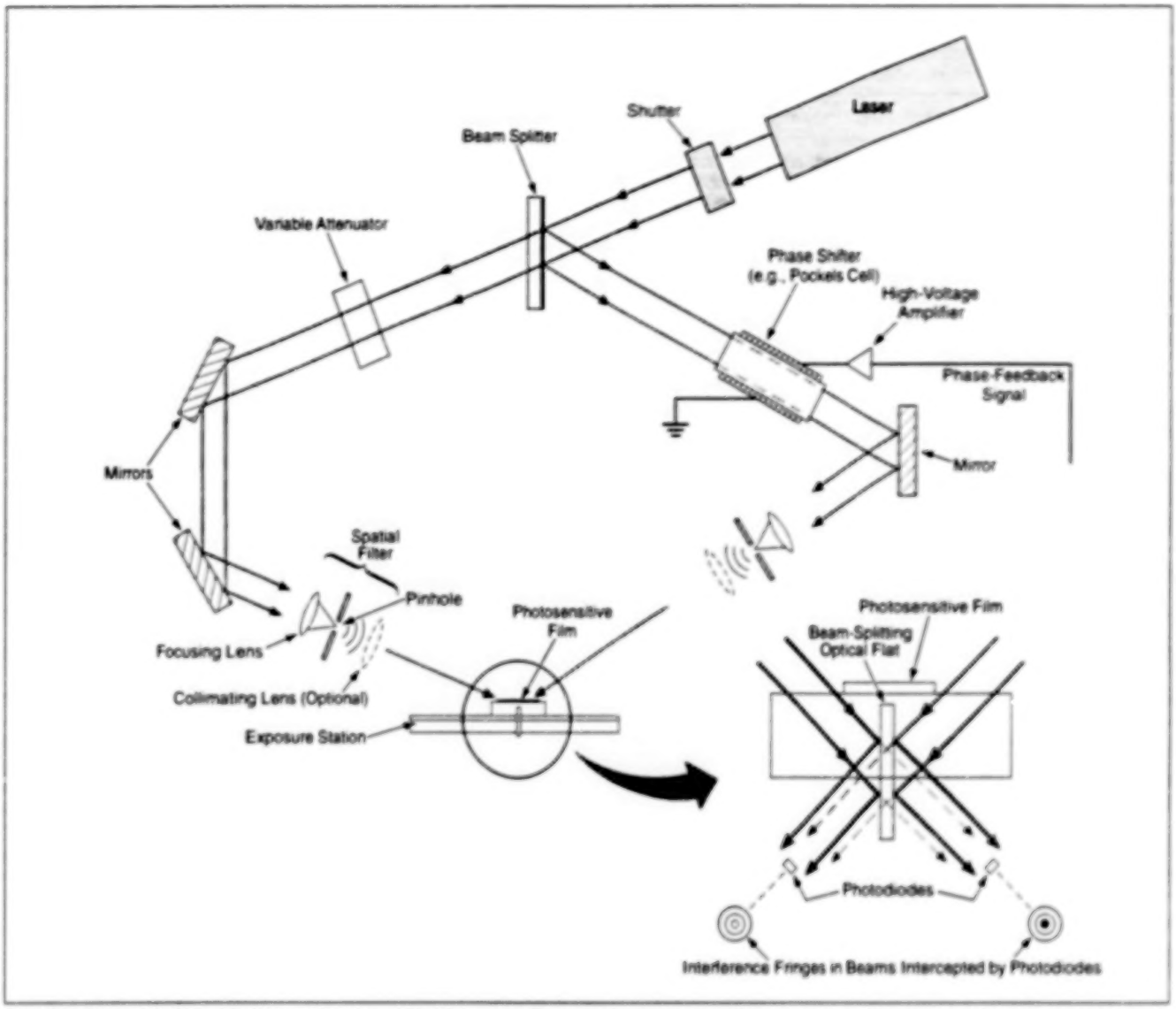

This **Interferometric Apparatus** is used in holographic lithography. For phase feedback, the difference between the phases of the right and left beams is measured by use of the two photodiodes positioned at the centers of the bull's-eye interference patterns. A feedback signal derived from the outputs of the photodiodes is applied to the phase shifter to cancel the phase difference.

Phase feedback can be used to stabilize interference fringes in holographic lithography. For decades, holographic lithography has been used to make precise gratings for scientific and industrial applications. The figure schematically illustrates a typical interferometer used in holographic lithography, with or without phase feedback. A laser beam is split into two beams, which are reflected and spatially filtered to produce two beams with spherical or planar wavefronts that impinge on an exposure station. A variable attenuator is used to adjust the irradiance of one of the beams to make the irradiances of both beams equal (this adjustment maximizes the achievable fringe contrast). A photosensitive film (e.g., a photographic emulsion or a photoresist on a suitable substrate) is mounted on the exposure station, where it is exposed to the interfering laser beams.

In the absence of deliberate stabilization measures, mechanical vibrations of an interferometer used in holographic lithography give rise to fluctuations in the relative phases of two interfering laser beams, causing the interference fringes to oscillate. This oscillation degrades the quality (in particular, when averaged over the exposure time, it degrades the contrast) of any grating that one attempts to make by use of the interference fringes. Heretofore, it has been standard practice to attempt to stabilize the fringes by mounting the interferometer on a high-quality vibration-isolation table. The present technique using phase feedback is potentially more effective for stabilizing the fringe pattern in space and time, making it possible to produce larger, higher-contrast gratings while using a vibration-isolation table of lower quality and thus lower cost.

The present phase-feedback technique involves a beam-splitting optical flat mounted on the exposure station just above (out of the plane of the figure) the photosensitive film. Each of the two beams coming from the left and right is partially reflected from, and partially transmitted through, this optical flat, and the overlapping reflected and transmitted beams on each side is sampled

by a photodiode. The overlapping beams are characterized by "bull's-eye" (in the case of spherical wavefronts) or parallel-line (in the case of planar wavefronts) fringe patterns that arise because of interference between the transmitted and reflected beams. In the bull's-eye case, the central spot and the successive rings on one side tend to darken, while the central spot and the corresponding rings on the other side tend to brighten.

The difference between the two bull's-eye patterns depends on, and fluctuates with, the fluctuating phase difference between the right and left laser beams. The photodiodes sense the irradiances in the central spots, and thus the outputs of the photodiodes indicate the instantaneous difference between the phases of the two beams. The outputs of the photodiodes are amplified and otherwise processed into a high-voltage signal that is applied to a Pockels cell or other phase shifter in the path of one beam to cancel the phase difference.

This work was done by Eric Hyde Anderson, Henry I. Smith, and Mark L. Schattenburg of Massachusetts Institute of Technology for **Marshall Space Flight Center**. *Further information is contained in a TSP [see page 1].*

In accordance with Public Law 96-517, the contractor has elected to retain title to this invention. Inquiries concerning rights for its commercial use should be addressed to

Massachusetts Institute of Technology
77 Massachusetts Avenue
Cambridge, MA 02139

Refer to MFS-26299, volume and number of this NASA Tech Briefs issue, and the page number.

Soldering Parts Together at Precise Faying Surfaces

By capillary action, the faying surfaces are pulled into intimate contact.

NASA's Jet Propulsion Laboratory, Pasadena, California

A special method of low-temperature metal bonding (in essence, a special method of soldering) has been devised for joining two parts at faying surfaces that are required to conform to submicron tolerances. In principle, the method is not limited to joining parts made of a particular material or geometry; however, in practice, the method is likely to be particularly useful for bonding micromachined silicon wafers to form miniature sensors and actuators.

The method is best explained by use of an example in which two silicon wafers are joined at flat surfaces. First, a shallow groove or pit is made at each bonding location in the affected surface of one wafer. The required depth of the groove or pit depends on the specific application and is typically of the order of 1 μm. Part or all of the recessed surface in the groove or pit is coated with a thin layer of titanium/tungsten alloy followed by a thin layer of gold; this layered metal coat is needed because it is wet by a molten eutectic alloy that is to be used as the solder. The entire affected surface of the other wafer, or at least the part of the surface that faces the metal-coated portion of the recess in the first wafer, is similarly coated so that the solder can wet both wafers at the bonding location.

In this example, the eutectic alloy is made of aluminum and germanium. A layer of aluminum 1 μm thick is deposited on part of the coated portion of the recessed surface in the groove or pit. A layer of germanium 0.6 μm thick is deposited on the aluminum. The combined thickness of the aluminum and germanium exceeds the depth of the groove so that the top of the germanium layer protrudes slightly above the wafer surface. However, the combined volumes of aluminum and germanium are chosen so that when they are subsequently melted, the volume of the resulting aluminum/germanium alloy will be less than that of the groove or pit.

The second wafer is placed like a lid on the first wafer with the bonding locations aligned. The wafers are clamped together and heated to a temperature near the eutectic melting point, causing the aluminum and germanium to diffuse into each other to form the molten eutectic aluminum/germanium alloy. Because the molten alloy wets the metal-coated surfaces of the wafers, it spreads out on those surfaces, thereby pulling the two wafers toward each other by capillary action. Because the volume of the molten alloy is less than that of the groove or pit, the spreading and pulling continues until the faying surfaces of the wafers are in intimate contact with each other.

The joined wafers are then cooled. The coefficient of thermal expansion of the eutectic alloy exceeds that of the wafers; therefore, differential thermal shrinkage of the alloy during cooling pulls the two wafers together even more tightly.

This work was done by Frank T. Hartley of Caltech and Paul M. Zavracky of Northeastern University for **NASA's Jet Propulsion Laboratory**. *Further information is contained in a TSP [see page 1].*

NPO-19477

Soldering Stacked Integrated-Circuit Chips

Connections would be made on broad surfaces and edges.

NASA's Jet Propulsion Laboratory, Pasadena, California

An advanced concept of fabrication and packaging of electronic circuitry calls for soldering and similar thermal bonding to form intimate electrical, mechanical, and thermal connections between adjacent stacked silicon and other wafers, including integrated-circuit chips. The method would provide additional options for designing and fabricating high-density electronic circuits in robust packages.

The concept is a generalization of the method described in the preceding article, "Soldering Parts Together at Precise Faying Surfaces" (NPO-19477). For example, (see figure) eutectic metal alloy bonds in grooves and pits, as described in the preceding article, could simultaneously constitute wireless electrical interconnections, high-thermal-conductance paths for dissipation of heat, and strong mechanical bonds between adjacent chip layers in a stack of chips. Optionally, a suitable plastic could be used,

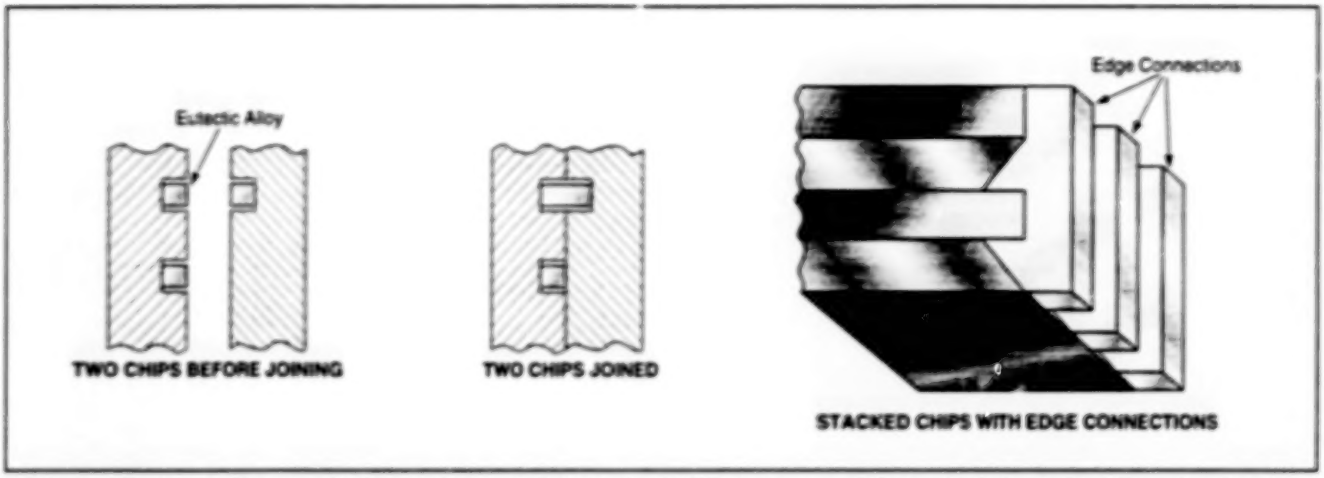

A Eutectic Alloy (e.g., solder), placed in grooves in amounts that do not quite fill the grooves, would be used to make electrical, thermal, and mechanical connections between stacked integrated-circuit chips. Electrical connections could also be formed on the edges of stacked chips.

instead of a eutectic alloy, in joints in which thermal and electrical conductance are not required.

Electrical connections through one or more chip layer(s) or through an entire stack could be made by etching holes completely through the affected chip(s) and depositing metal in the holes. Electrical connections could also be made at and across the edges of stacked chips by selective etching and metallization of the edges.

This work was done by Frank T. Hartley of Caltech for **NASA's Jet Propulsion Laboratory**. *Further information is contained in a TSP [see page 1].*
NPO-19473

Mathematics and Information Sciences

Hardware, Techniques, and Processes

BLANK PAGE

Predicting Where Terminated Unpiloted Aircraft Will Land

An algorithm updates estimated ground impact locations in real time for improved safety.

Dryden Flight Research Center, Edwards, California

An algorithm has been developed at Dryden Flight Research Center to enhance range safety during tests of unpiloted aircraft [also called "uninhabited aerial vehicles" (UAVs)]. On the basis of current information on winds and an estimate of the rate of descent of the UAV, the algorithm estimates, in real time, the location where the UAV would impinge on the ground if its test flight were suddenly terminated. The predicted location of impact is shown continuously on a range safety officer's moving-map video display so that the flightpath of the UAV can be selected to avoid ground assets (e.g., manmade structures) in the event that the flight must be terminated. The algorithm can be adapted easily to various termination techniques.

Every unpiloted aircraft operating at Dryden Flight Research Center is required to contain a flight-termination system (FTS) to ensure that the aircraft does not leave the designated airspace or range in the event that normal command and control is lost. In addition, the location where the UAV would strike the ground is of concern inasmuch as the designated airspace includes areas of high value. A means of predicting where a UAV will land is critical for real-time flightpath management.

Algorithms in use at other range facilities were designed for high-kinetic-energy aircraft. The need at Dryden Flight Research Center was for an algorithm that could account for low-speed (low-kinetic-energy) aircraft. In addition, the algorithm was required to operate in real time, to be flexible in its ability to account for a variety of termination techniques, and to provide a reasonable estimate of the location of impact.

The moving-map display (see figure) provides continuous information on the present horizontal location, altitude, speed, and heading of a UAV, plus range boundaries and other information. Additional operational boundaries can also be displayed; these boundaries can be designated as UAV keep-out zones. They are typically drawn around ground assets. During the flight, the range safety officer provides guidance to the UAV operator so that the predicted location of impact does not enter any UAV keep-out zone.

The estimate of the location of impact is based on the assumption that the aircraft descends as though under a parachute. Thus, the rate of descent is characterized by a parachute drag coefficient and reference area. The predicted location of impact is a function of the altitude of the UAV, the assumed rate of descent, and the magnitude and direction of the wind. The wind data are critical; they are used by the algorithm to predict the down-range drift during the descent. Wind data are obtained from weather balloons launched prior to and throughout the flight of the UAV. In general, the data from the balloons are available in altitude increments of 1,000 ft (305 m). The data are contained in a separate file called the "winds file."

The purpose of the FTS is to keep the UAV within the designated airspace or range. The advantage provided by the algorithm is an ability to make a termination decision with more confidence that the UAV will not drift to an impact in a sensitive area. Indeed, termination can be delayed to enable the UAV to clear a ground asset. Once the FTS has been activated, the algorithm continues to update the predicted location of impact (provided that accurate altitude data are still available).

The algorithm has been adopted by several UAV operators, who use it in their command-and-control stations; this offers the advantage of redundancy with the Dryden control room for protection against a display failure. The simplicity of the algorithm (approximately 240 lines of code) enables its incorporation with even modest equipment. The use of the algorithm greatly increases the flexibility and safety of UAV operations at Dryden Flight Research Center.

This work was done by Jeff Bauer of **Dryden Flight Research Center**. *Further information is contained in a TSP [see page 1].*

DRC-97-07

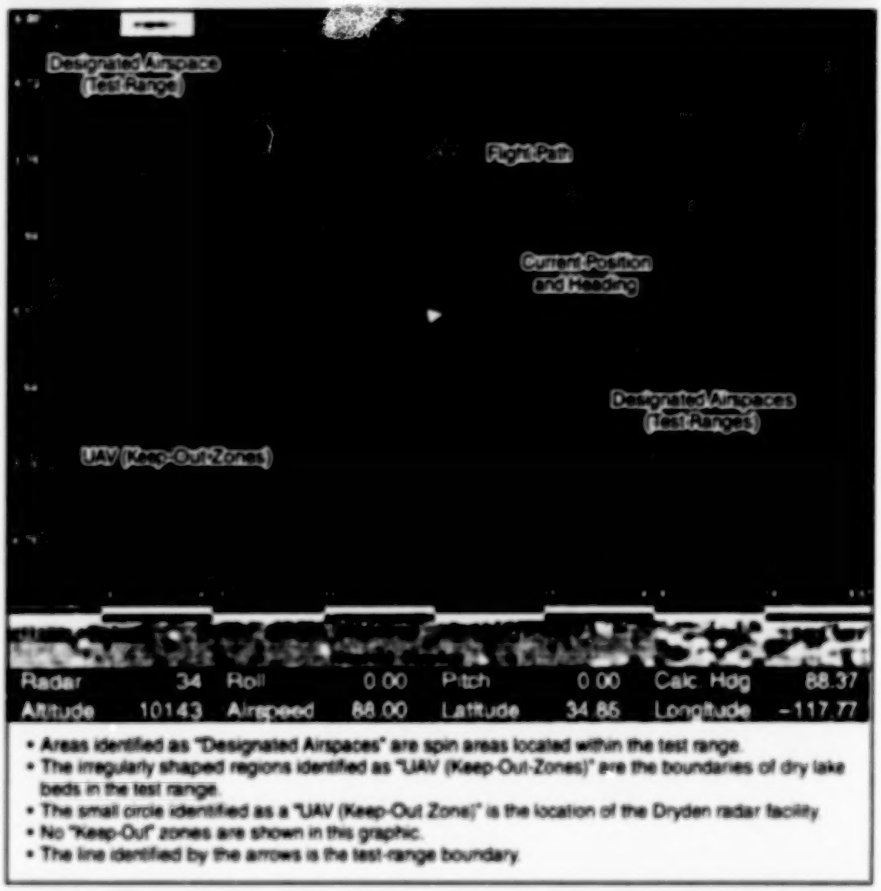

The Moving-Map Display presents continuously updated information on the present three-dimensional location, velocity, and other flight parameters, and of the estimated location of impact in the event of termination of the flight.

Reconstruction of Images From Circular-Scan Sensors

Images can be reconstructed faster than before.

NASA's Jet Propulsion Laboratory, Pasadena, California

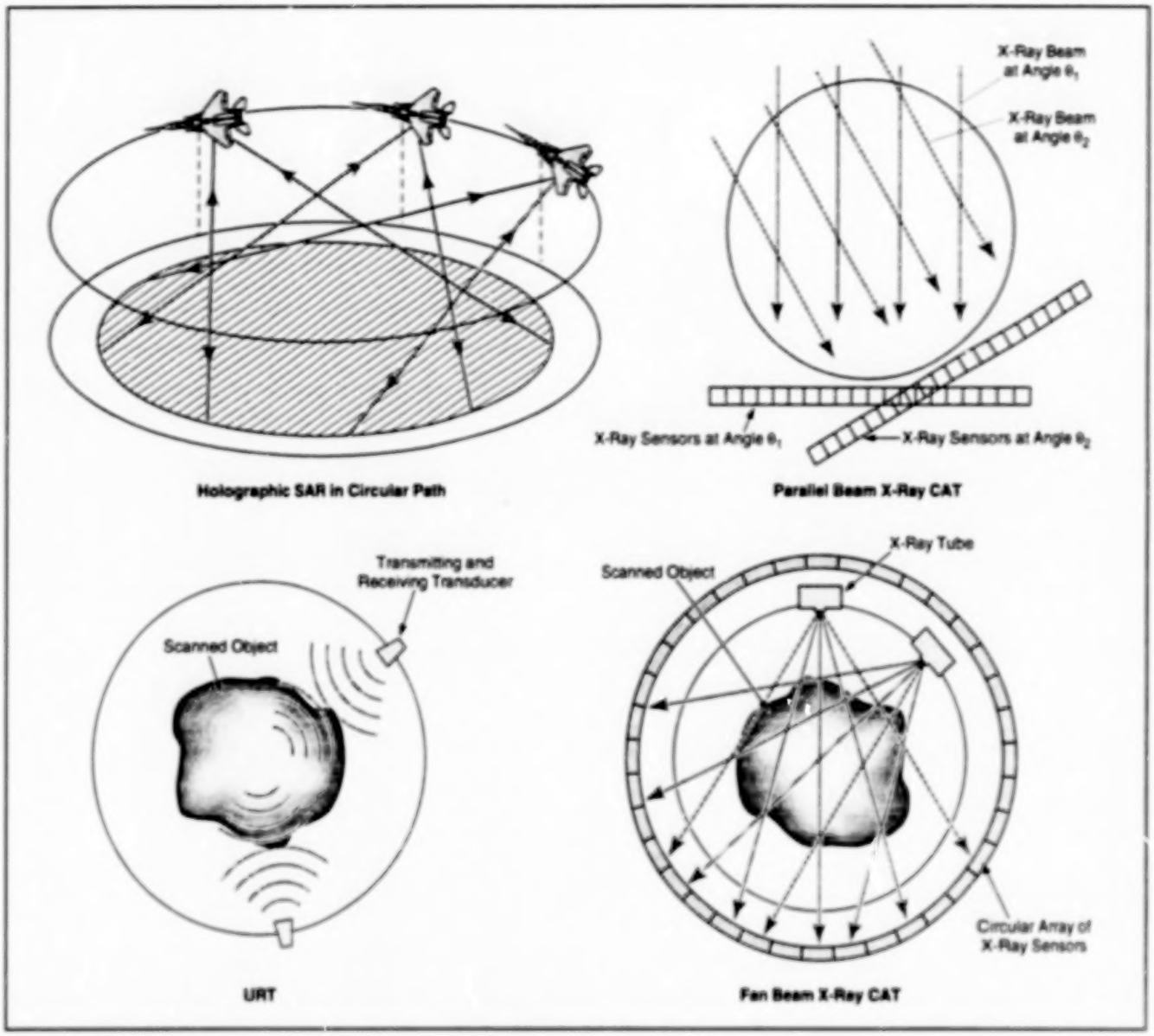

Figure 1. **Circular Scans** with various sensors generate data that can be processed to reconstruct images of the scanned scenes. The algorithm described in the text can accommodate these and other sensors and variations of the basic circular scanning geometry.

An improved algorithm for reconstructing images from the outputs of circular-scan sensors has been devised. With relatively minor variations, the algorithm is applicable to data acquired by diverse circular-scan sensors (see Figure 1), including those of holographic synthetic-aperture radar (HSAR), x-ray computer-aided tomography (CAT), magnetic-resonance imaging (MRI), positron-emission tomography (PET), and ultrasonic-reflectivity tomography (URT). It can even be applied to data acquired by sonar and seismic sensors.

One older algorithm of this type, known as the convolution back-projection algorithm, has been popular in computer-aided tomography because it offers superior image quality and ease of adaptation to fan-beam geometry. Another one, known as the direct Fourier algorithm, is highly efficient in computation, but it depends on the use of a Cartesian coordinate grid and, therefore, its image quality depends on the interpolation subalgorithm used to transform the signal spectrum into the Cartesian coordinates. Moreover, the direct Fourier algorithm applies to parallel-beam CAT only.

The improved algorithm overcomes the limitations of the direct Fourier algorithm and offers a computational efficiency between two and six times that of the convolution back-projection algorithm. Before images are formed, all computations are performed in polar coordinates. Polar-to-Cartesian transformation is finally applied to the reconstructed image for image display purpose. Based on the circular symmetry, this algorithm performs fast Fourier correlation in the azimuth dimension.

The reference functions used in the improved algorithm are the amplitude-weighted two-dimensional spectra of the point-target responses (PTRs). [A PTR can be regarded as an extended or "blurred" version of a conventional point-spread function (PSF). The PTR is the PSF-blurred-curved-line response obtained from a point target imaged by a wide-beam circular-scan system like HSAR.] A reference function is updated for each range bin to achieve exact focusing. By choosing proper weighting functions, this algorithm is capable of generating an ideal PSF like that predicted for Fraunhofer diffraction by a circular aperture (see Figure 2). Further shaping of the PSF can be achieved by use of extra weighting. The high computational efficiency of this algorithm is attributable to the characteristics of the two-dimensional spectrum of the PTR.

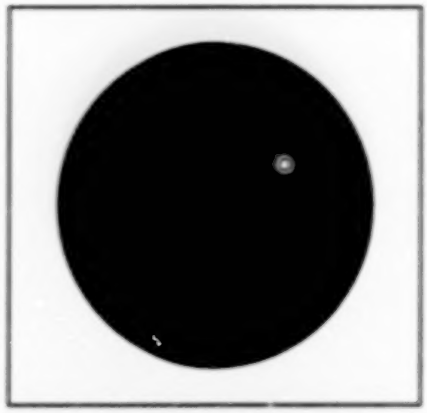

Figure 2. This Image of a Point Target was generated by applying the improved algorithm in a computer simulation of HSAR or URT, using a pulse with a bandwidth of 0.133 × its carrier frequency. The PSF in this image exactly follows that of Fraunhofer diffraction by a ring aperture.

This work was done by Michael Y. Jin of Caltech for ***NASA's Jet Propulsion Laboratory****. Further information is contained in a TSP [see page 1].*

In accordance with Public Law 96-517, the contractor has elected to retain title to this invention. Inquiries concerning rights for its commercial use should be addressed to

Technology Reporting Office
JPL
Mail Stop 122-116
4800 Oak Grove Drive
Pasadena, CA 91109
(818) 354-2240

Refer to NPO-19559, volume and number of this NASA Tech Briefs issue, and the page number.

Dynamic Routing for Networks With Random Connectivities

Throughput would be maximized by use of routing along the least populated paths.

NASA's Jet Propulsion Laboratory, Pasadena, California

A developmental algorithm for dynamic routing of messages and assignment of servers in a communication network implements a simple, stationary joint routing and service policy. Unlike a previously developed routing algorithm, the present algorithm is not based on stationarity and precise knowledge of connection probabilities; it is suitable for a network with connectivities and connection probabilities that are unknown and/or that vary with time. When fully developed, the algorithm could be used to increase the capacities of wireless-communication networks, for example.

The routing and service policy and the corresponding basic theoretical version of the algorithm were derived for a mathematical model of an N-node acyclic network with a single input node and a single output node (see figure) and the following other characteristics.

- The basic topology of the network is fixed.
- All jobs enter through the single input node, and there is at most one arrival during any given time slot.
- Each server (node) is always connected to all of its output queues.
- During each time slot, there is some probability that each server is either connected to or disconnected from each of its input queues.

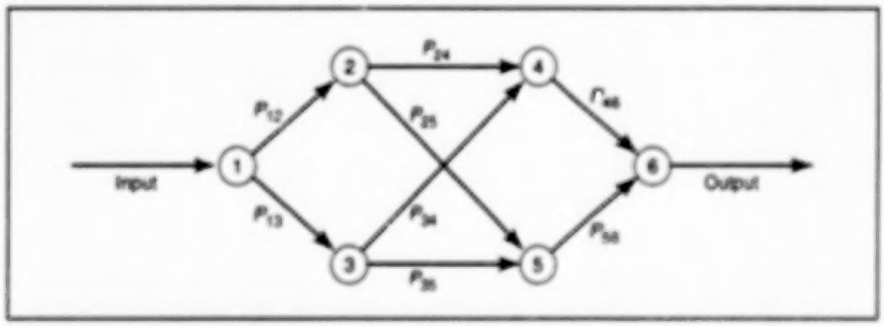

This Single-Input, Single-Output, Six-Node Network is a simple example of a network with random connectivities. Each symbol P_{ij} denotes the probability that server j is connected to the output of server i during a given time slot. Each numbered node denotes a server.

- During each time slot, each server must decide which of its connected input queues to serve and into which of its output queues it should place the completed job.

The basic policy and algorithm, implemented independently by each server, is as follows: Upon completion of each job, each server would calculate the number of jobs queued up along every path from itself to the destination and would dispatch the just-completed job along the path containing the fewest jobs. If two or more paths to the destination were equally populated, one would be chosen at random. Each server would always serve whichever of its input queues was the longest according to the most recent calculation.

In performing its routing calculations, the server would utilize queue-length information that it obtained from the rest of the network. This information could be attached, for example, to acknowledgments of receipt of packets of data. Each server must know the lengths of all the queues in the network, but knowledge of connection probabilities is not needed. Thus, the network would respond dynamically to changes in network connection probabilities.

It has been demonstrated theoretically that the foregoing policy and algorithm would maximize the network throughput and result in stabilization of the network in the sense that queue lengths at the intermediate nodes of the network would be stabilized if these lengths were

stabilizable at all. In practice, the queue-length information available to each server would not always be entirely accurate and timely; however, it has been conjectured that the stability of the network would be robust with respect to delays in queue-length information. The results of an initial simulation in software have been interpreted as signifying that the algorithm would perform well over a broad range of inputs and under partial or delayed queue-length information.

This work was done by Keith Scott of Caltech for **NASA's Jet Propulsion Laboratory**. *Further information is contained in a TSP [see page 1].*

This software is available for commercial licensing. Please contact Don Hart of the California Institute of Technology at (818) 393-3425. Refer to NPO-20188.

Life Sciences

Hardware, Techniques, and Processes

BLANK PAGE

Continuous Unidirectional Locking Orthotic Joint

New orthotic joint can help rehabilitate patients with knee and ankle injuries.

Marshall Space Flight Center, Alabama

A continuous unidirectional locking orthotic joint has been designed to help rehabilitate patients with knee and ankle injuries. In some cases, this device can also be used during recovery from wrist or elbow injury.

During rehabilitation with the unidirectional locking joint, the patient gradually stretches the damaged joint toward full extension. The orthotic joint aides in this therapy by resisting flexion of the joint, while still allowing extension.

To flex the braced limb, the patient simply releases the locking feature manually. This allows the unidirectional joint to rotate freely through the normal range of flexion. When used for knee or ankle joint recovery, this device also prevents the damaged joint from collapsing because it can bear the full weight of the patient.

This continuous unidirectional locking orthotic joint was designed using a hinge-type joint with a manually selectable continuous locking feature. Two long straps with boltholes allow it to be attached to standard orthotic brace parts. When this new joint is used in the knee area, for example, one side of the hinge joint is attached to the thigh portion of the brace, while the other is attached to the calf portion. Two identical joints are required for this type of application.

One of the principal novel features of this joint, the use of an overriding clutch as the mechanism that allows free rotation in the sense of extension but locks when rotation in the sense of flexion is attempted, can be compared with two similar previously developed orthotic joints. These two joints were discussed in *NASA Tech Briefs* articles "Automatic Locking/Unlocking Orthotic Knee Joint" (MFS-28633), Vol. 18, No. 5 (May 1994), and "Improved Automatically Locking/Unlocking Orthotic Knee Joint" (MFS-27997), Vol. 19, No. 5 (May 1996).

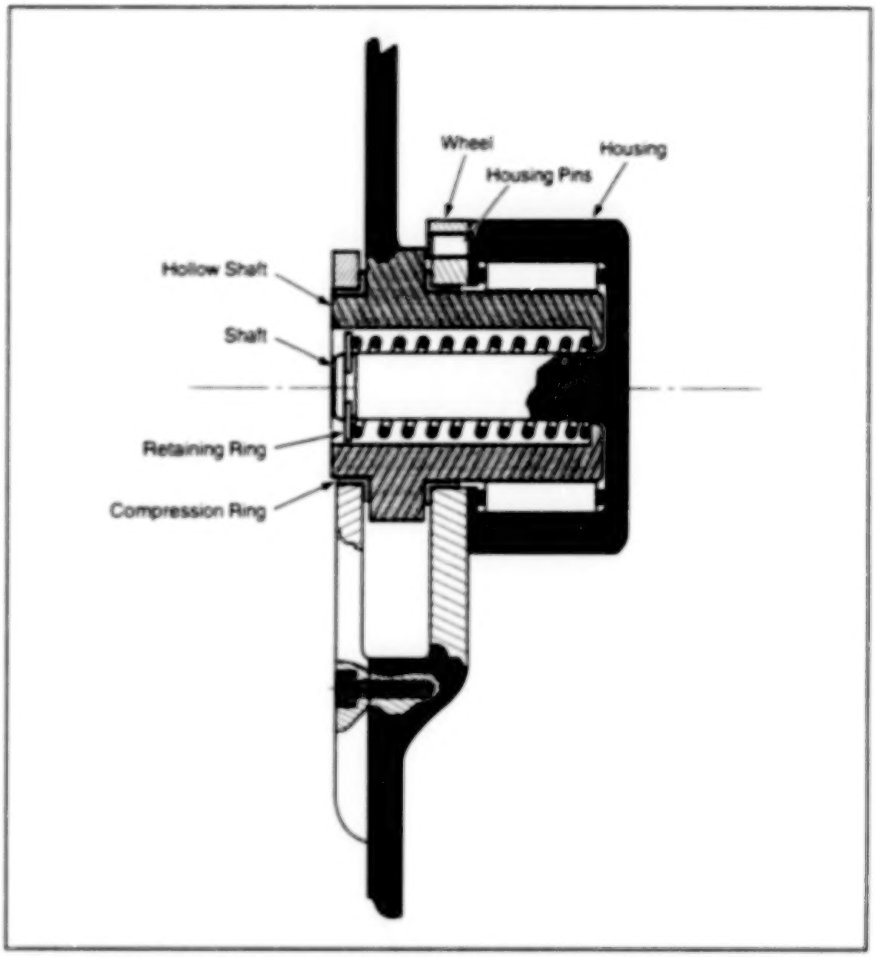

A Compression Spring operating inside a hollow shaft locks and unlocks the continuous unidirectional locking orthotic joint by urging the housing and its pins into engagement with the wheel. This spring acts through a retaining ring, which is affixed to the shaft and protrudes from the housing through the hollow shaft.

Another novel feature is the method of controlling the locking and unlocking of the joint. Like the previously developed joints, this device includes an overtravel stop to prevent hyperextension. The configuration of the joint and of the overrunning clutch affords an unprecedented capability for operation without the need for additional connecting members.

This work was done by Bruce Weddendorf of **Marshall Space Flight Center**. *Further information is contained in a TSP [see page 1].*

Inquiries concerning rights for commercial use of this invention should be addressed to the Patent Counsel, Marshall Space Flight Center: (205) 544-0021. Refer to MFS-31114.

Fiber-Optic Catheter Probe Would Measure Temperature

The probe could be used in a human artery.

NASA's Jet Propulsion Laboratory, Pasadena, California

Figure 1 schematically illustrates a proposed multiple-wavelength infrared radiometric instrument with a catheter probe that would be used to determine the temperatures of the inside walls of tubes, cavities, and the like. The instrument could be useful in a number of industrial and biomedical applications; for example, to monitor the temperature of a human arterial wall from within.

The catheter probe would consist of two optical fibers, a guide wire, and a balloon. The fiber-optic tip has a device on the end that gives a radial field of view, rather than a forward view. This allows

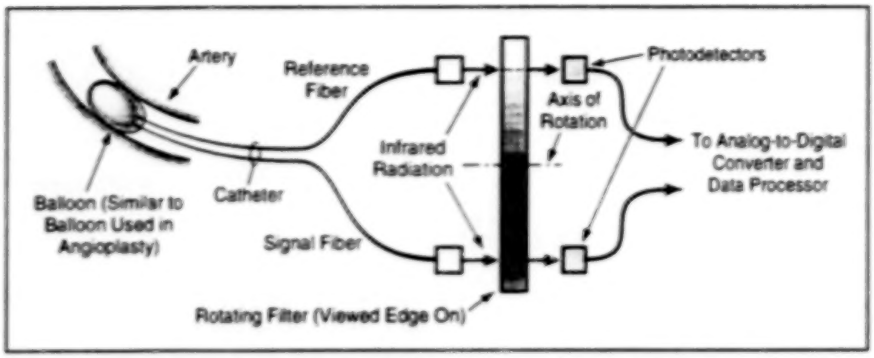

Figure 1. **Optical Fibers in the Catheter Probe** would carry infrared radiation from the probe tip to the radiometric equipment.

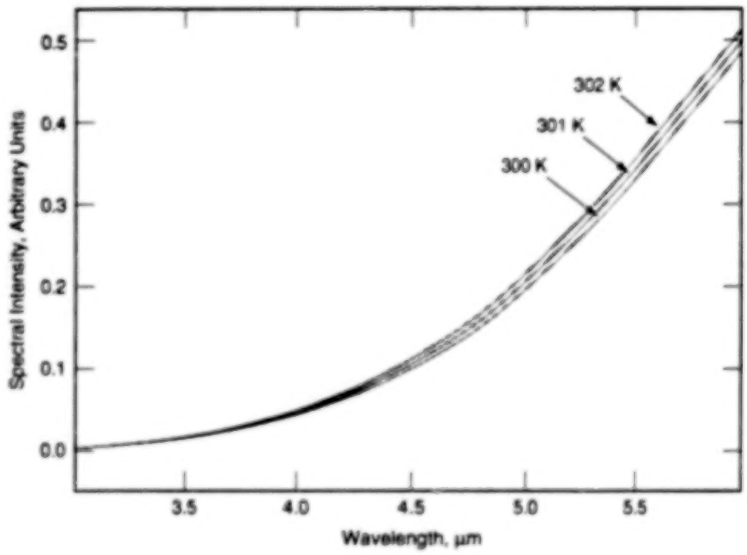

Figure 2. **To a Close Approximation**, the black-body spectra of different temperatures in the range of interest merge at a wavelength of 3 μm; this feature provides a reference for calibration.

localization of measurement. One of the optical fibers, called the "signal" fiber, would transmit infrared radiation from the surface to be monitored to the radiometric equipment. The other optical fiber, called the "reference" fiber, would be coated with a reflective material at the probing end and would provide the radiometric equipment with radiation that would be used to compensate for any gradients of temperature along the probe. In order to avoid absorption by water in the blood, as well as scattering by cellular blood components, the measurement is done from within a balloon. An expandable balloon is inflated to contact the artery walls, and the fiber-optic tip measures the balloon-wall temperature from the inside. Since the balloon is in contact with the artery wall and has a small thermal mass and conductance, it has the same temperature as the artery wall.

The radiation leaving the optical fibers would pass through a rotating circular band-pass infrared filter, the pass band of which would vary with rotation angle in a predetermined way. The filtered radiation from each fiber would be detected, then digitized as a function of time, then processed to obtain a spectrum from the known relationships among the rotation angle of the filter as a function of time, the nominal wavelength of the pass band as a function of the angle, and the sensitivity of detection as a function of wavelength.

The temperature would be taken to be that of the black-body spectrum that best fit the compensated spectrum from the signal fiber. One of the salient features of the proposed instrument is that it would automatically provide a reference for each black-body spectrum in the biological temperature range of interest (300 to 310 K). It would do this by sampling at a wavelength of 3 μm (in addition to other wavelengths). A reading at 3 μm constitutes a reference because the intensities of all black-body spectra in this temperature range at this wavelength are so nearly equal (see Figure 2) that they can be taken to be equal for the purpose of calibration. This feature "locks down" the low-wavelength side of the spectrum.

This work was done by Gregory H. Bearman, Michael L. Eastwood, and Timothy N. Krabach of Caltech for **NASA's Jet Propulsion Laboratory**. *Further information is contained in a TSP [see page 1].*

In accordance with Public Law 96-517, the contractor has elected to retain title to this invention. Inquiries concerning rights for its commercial use should be addressed to

Larry Gilbert, Director
Technology Transfer
California Institute of Technology
Mail Code 315 - 6
Pasadena, CA 91125
(818) 395-3288

Refer to NPO-19452, volume and number of this NASA Tech Briefs *issue, and the page number.*

National Aeronautics and
Space Administration

END

02\09\99